The Dissertation Committee for Puja Singh Certifies that this is the approved version of the following dissertation:

Rhodopsin Kinase Structure: Different Nucleotide-Binding States and Implications for Mechanism of Activation of a G Protein Coupled Receptor Kinase

Committee:

John J. G. Tesmer, Co-Supervisor

Marvin L. Hackert, Co-Supervisor

Makkuni Jayaram

Tanya T. Paull

Christian P. Whitman

Rhodopsin Kinase Structure: Different Nucleotide-Binding States and Implications for Mechanism of Activation of a G Protein Coupled Receptor Kinase

by

Puja Singh, B.S., M. S.

Dissertation

Presented to the Faculty of the Graduate School of

The University of Texas at Austin

in Partial Fulfillment

of the Requirements

for the Degree of

Doctor of Philosophy

The University of Texas at Austin

December, 2007

Dedication

I dedicate this work to my loving parents, without whom none of this would have happened.

Acknowledgements

I would like to thank my advisor, Dr. John Tesmer for his patience and guidance. Frankly, I could not have asked for a better mentor.

I thank Dr. Chih-chin Huang for helping me at various stages of this work. I am thankful to her for the helpful advice at times when I needed it the most.

A special thanks to all my committee members for their input.

I thank Dr. K. Palczewski who shared his expertise on GRK1 assays with me and for providing resources to conduct assays in his lab.

I also thank all my colleagues for providing a fun environment and helping me.

Finally, I would like to thank my friends and family, especially my Mom and Dad, whose constant encouragement and support kept me going.

Rhodopsin Kinase Structure: Different Nucleotide-Binding States and Implications for Mechanism of Activation of a G Protein Coupled Receptor Kinase

Publication No._____

Puja Singh, Ph.D.

The University of Texas at Austin, 2007

Co-Supervisors: John J. G. Tesmer and Marvin L. Hackert

G protein coupled receptor (GPCR) kinases (GRKs) phosphorylate activated heptahelical receptors, leading to their uncoupling from G proteins and downregulation. The desensitization of GPCRs is critical to render cells responsive to further stimuli and if not regulated can result in many pathophysiological processes including heart abnormalities and hypertension. How GRKs recognize and are activated by GPCRs are not known, in part because the critical N-terminus and the kinase C-terminal extension were not resolved in GRK2 and GRK6 structures. The long-term goal of this project was to address this question by structural analysis of rhodopsin kinase (also known as GRK1), which represents a model system for studying phosphorylation-dependent desensitization of activated GPCRs. Herein we report structures of GRK1 from six crystal forms that represent three distinct nucleotide-ligand binding states. One of the $(Mg^{2+})_2$·ADP·GRK1 structures is the most high-resolution structure (1.85 Å) of a GRK to date. In one $(Mg^{2+})_2$·ATP·GRK1 structure, almost the entire N-terminal region (residues 5-30) is observed. In addition, different segments of the kinase C-terminal extension are ordered

in the various nucleotide-bound structures. Together, these two elements form a putative receptor-docking site adjacent to the hinge of the kinase domain. Based on these structures, a model is proposed for how GRK1 interacts with activated rhodopsin and how rhodopsin binding in turn could activate the kinase. Two novel phosphorylation sites were also identified at the N-terminus. The physiological role of phosphorylation sites and the extensive dimerization interface mediated by the regulator of G protein signaling (RGS) homology domain of GRK1 was assessed using site-directed mutagenesis.

In addition to mediating interaction with activated GPCRs, the N-terminus of GRKs also forms a binding site for calcium sensing proteins. Although its physiological significance is debated, the structures of these complexes could lend further insights into the conformation of the N-terminus of GRKs. The second chapter deals with attempts to isolate Ca^{2+}·recoverin·GRK1 and Ca^{2+}·calmodulin·GRK6 complexes. Finally, the RH domain of GRK2 binds $G\alpha_q$, $G\alpha_{11}$, and $G\alpha_{14}$ subunits thereby blocking their interactions with the downstream effectors. The third chapter involves attempts to isolate a complex of GRK6 and $G\alpha_{16}$, a member of $G\alpha_q$ family.

Table of Contents

List of Tables

List of Figures

Chapter 1: Structure Determination of GRK1

INTRODUCTION

G Protein Coupled Receptor (GPCR) Signaling

G protein coupled receptors (GPCRs) are ubiquitous proteins that transduce signals to the cell interior allowing cells to respond to extracellular stimuli. The receptors are responsive to a wide-range of stimuli that range from a photon of light, pheromones and neurotransmitters, to peptide hormones. The signaling through GPCRs (Fig. 1) is mediated by activation of guanine nucleotide binding (G) protein subunits that further regulate downstream effectors that propagate the signal within the cell. The activated GPCRs must be desensitized in a regulated manner in order for cells to remain responsive to their environment. The two proteins that play a key role in this process are GPCR kinases (GRKs) and arrestins. Activated receptors are first phosphorylated by GRKs and then bound by arrestins to quench the signaling.

GPCRs form one of the largest superfamilies of membrane proteins. In humans the estimated number of GPCRs is ~950 [1], which corresponds to about 5% of the genes. GPCRs regulate diverse physiological processes that range from sensations of sight, smell and taste to endocrine function. Malfunctions associated with receptor function or regulation have been linked to diseases such as hypertension, obesity, heart abnormalities and blindness [2]. Their crucial role in regulation of cellular functions makes them a target of about 50% of drugs currently available in market [3, 4].

Figure 1: G protein coupled receptor signaling in retina.

(a) A photon of light triggers isomerization of chromophore 11-*cis*-retinal to all-*trans*-retinal, leading to a conformational change that results in activation of rhodopsin (Rho*). Rho* then activates transducin ($G\alpha_t$) by catalyzing exchange of GTP for GDP on the Gα subunit, which then dissociates from Gβγ and activates phosphodiesterase. The resulting drop in the cGMP levels results in closure of cGMP-gated cation channels causing hyperpolarization of the membrane, inhibition of the release of neurotransmittors and signaling to the brain. (b) Rhodopsin kinase initiates desensitization of Rho* by phosphorylating its cytoplasmic tail. Phosphorylated Rho* is bound by arrestin, which blocks the interaction of receptor with G proteins and quenches signaling. RGS9 hydrolyzes GTP on the Gα subunit and GDP·Gα then re-associates with the Gβγ subunits. Drop in Ca^{2+} levels in the cytoplasm (associated with closure of cGMP-gated channels) activates guanylate cyclase activating proteins, which activate guanylate cyclase resulting in resynthesis of cGMP and opening of channels.

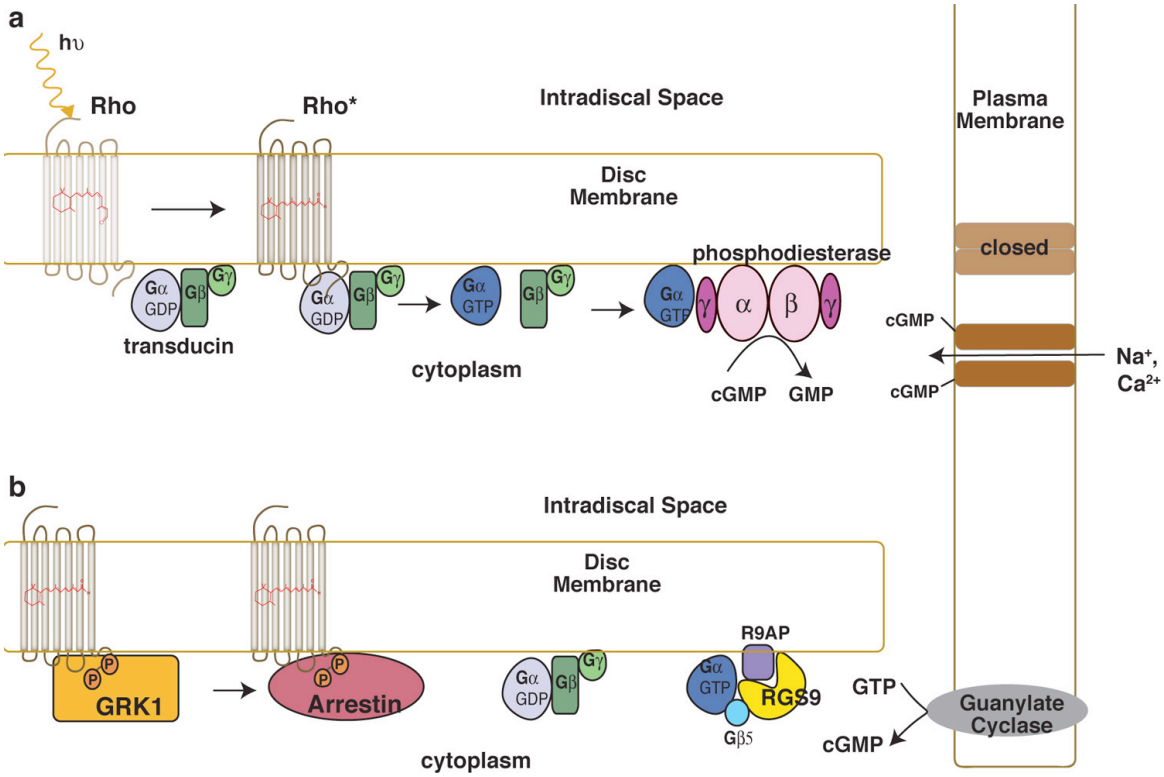

Rhodopsin Structure

GPCRs are integral membrane proteins that possess seven transmembrane helices, hence the name 7TM or heptahelical receptors. The extracellular side forms the ligand-binding surface while the cytoplasmic surface forms a binding site for the signaling proteins (Fig. 2). Its availability (~ 0.5-1 mg/eye) and relative ease of purification make rhodopsin, a retinal photoreceptor, one of the most well-studied GPCRs. Rhodopsin is the first GPCR to have its primary sequence deciphered [5, 6], to be purified to homogeneity and is the first receptor to have a crystal structure reported [7]. It is the only receptor for which crystal structures are available representing the conformations of both the active [8] and inactive [9] states. The functional unit of rhodopsin was initially characterized to be a monomer [10] but recent biophysical and biochemical studies suggest that rhodopsin can form dimers and other higher-order oligomers [11-14]. Oligomerization is seen in other GPCRs as well [14-16]. The physiological relevance of receptor dimers (or oligomers) is debated but it could play a role in receptor biosynthesis, trafficking and internalization.

Rhodopsin is composed of the apoprotein opsin, which is covalently linked to the chromophore 11-cis-retinal through Schiff's base linkage to the ε-amino group of Lys216. Upon stimulation by a photon of light, the chromophore and Lys216 become deprotonated to form the photo-activated state of rhodopsin (Rho* or metarhodopsin II or MetaII). The conformational change upon activation may not be dramatic [8]. However, in the active conformation the cytoplasmic surface of rhodopsin becomes accessible to signaling proteins. The heterotrimeric G proteins, GRKs and arrestins are protein families that can specifically recognize and bind to the activated form of receptors.

Figure 2: Crystal structure of a photoactivated intermediate of rhodopsin.

In this model (PDB code: 2I37) ribbons are colored cyan, sheets wheat and loops grey. Oxygen atoms are colored red and nitrogens blue. The helices I (αI and αI'), II (αII and αII') and the cytoplasmic helix 8 (H8 and H8'), which mediate dimer formation (~800 $Å^2$ buried surface area) are colored slate. In this model the Schiff's base linkage between the Lys296 residue and the chromophore was predicted to be deprotonated based on the analysis of the retinal content and the absorption maxima of these light-exposed crystals. Thus, the structure appears to represent a photoactivated intermediate of rhodopsin [8]. Compared to the structure of inactivated rhodopsin [9], the transmembrane helices do not undergo a dramatic conformational change. The cytoplasmic loops that are thought to interact with Gα subunits, GRKs and arrestins are also not ordered. The grey region represents the plasma membrane.

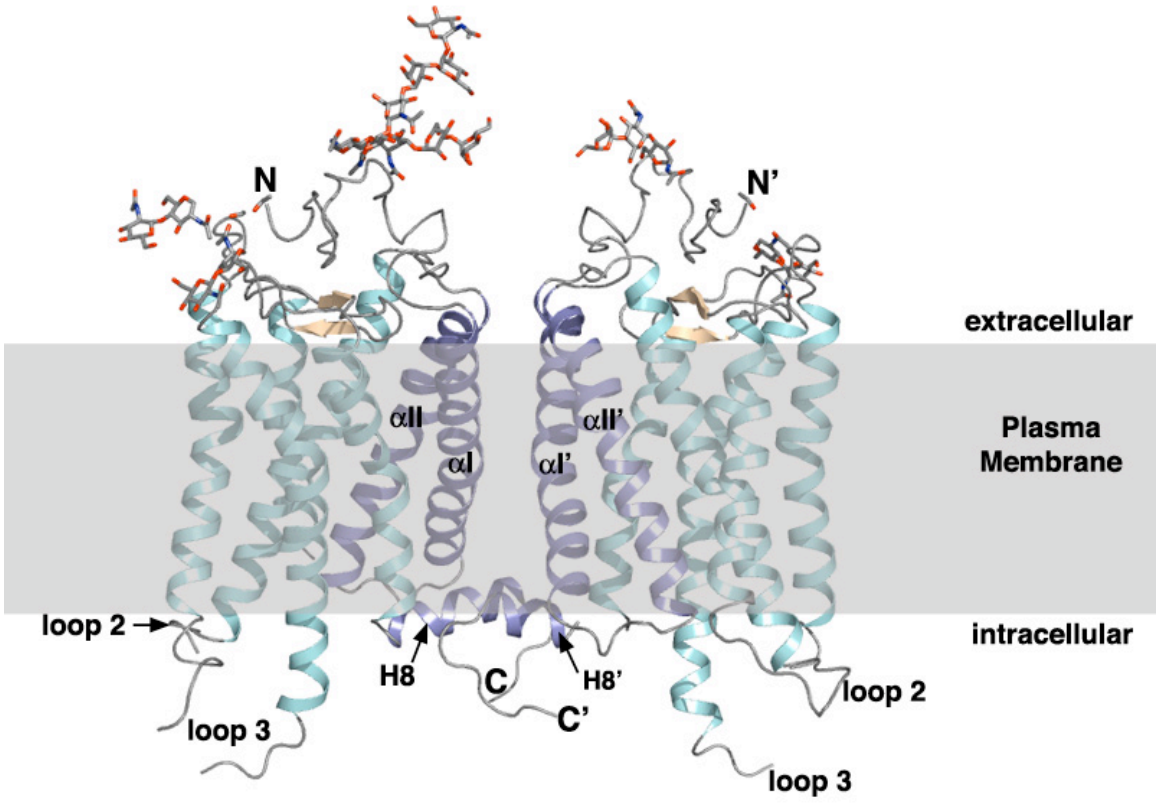

The Discovery of GRKs

The phosphorylation of rhodopsin was first described in the early 1970s when it was shown that a rod outer segment (ROS) preparation undergoes phosphorylation in the presence of radiolabeled-ATP. The incorporation of phosphates was found to be stimulated in the presence of light [17] and was later demonstrated to be occurring *in vivo* as well [18, 19]. It was suggested that light-enhanced phosphorylation was resulting from conformational changes in rhodopsin and not because of stimulation of the kinase [20]. This was followed by purification of a protein kinase from ROS that was specific for photobleached rhodopsin [21, 22]. Subsequent studies focused on understanding the affects of phosphorylation of rhodopsin, the relation of visual "excitation" to other processes such as membrane permeability and identification of the various steps involved in the pathway. The term "rhodopsin kinase" was coined owing to the specificity for rhodopsin. Over the next three decades the kinase has been extensively investigated. This includes cloning and purification of rhodopsin kinase [23-32], identification of post-translational modification such as isoprenylation [33-36], and autophosphorylation [25, 37-39] and determination of substrate specificity and regulation of activity [25, 30, 40-52]. Being the first member of the family of kinases that specifically bind to and phosphorylate the activated form of a GPCR, rhodopsin kinase (RK) is also known as GPCR kinase 1 or GRK1.

The GRK Family

GRKs are Ser/Thr protein kinases that specifically recognize and phosphorylate the activated form of GPCRs. There are seven members of the mammalian GRK family [53], which are grouped into three sub-families based on sequence homology. The GRK1 sub-family includes GRK1 and GRK7; GRK2 sub-family includes GRK2 and GRK3; and the GRK4 sub-family includes GRK4, GRK5 and GRK6. The GRK2 sub-family and

GRK6 are ubiquitously expressed. GRK1 and GRK7 are expressed in the retina and pineal gland, GRK4 in testis, brain and kidney and GRK5 in heart, lung and retina.

GRK1: Gene Structure and Localization

The gene for human GRK1 contains seven exons and is located on chromosome 13 (13q34) [24, 54]. In retina, GRK1 is a key player in phototransduction whereas the exact role of the kinase in pinealocytes is not clear [55, 56]. A number of phototransduction proteins have been identified in the pineal gland indicating an evolutionary relationship between the photoreceptors and the pineal gland. The expression of GRK1 in retinal rod and cone cells varies in a species-specific manner and has been linked to the daily activities of the species.

GRK1 Domain Architecture

Bovine GRK1 is produced as a precursor of 561 amino acids. The protein is post-translationally modified by farnesylation on Cys558 with the subsequent proteolytic cleavage of the last three residues and carboxyl-methylation of the terminal residue.

The N-terminus

The N-terminus of GRKs has been shown to be critical for receptor phosphorylation. Point mutations and truncations of the extreme N-terminus in GRKs has been shown to block receptor phosphorylation with no apparent affect on the phosphorylation of soluble substrates [49]. An antibody directed against the residues 17-34 of GRK1 was shown to block rhodopsin phosphorylation, without affecting the intrinsic kinase activity [45]. However, there is no evidence for a direct interaction between the N-terminus and the receptors. It has been predicted that the N-terminus forms an amphipathic helix that could mediate binding to the lipid bilayer [57]. The recent NMR structure of GRK1 N-terminal

peptide bound to Ca^{2+}-recoverin reveals that the residues 4-16 form an amphipathic helix and the residues 9-11, 14 and 15 were shown to bind to a hydrophobic surface on recoverin [58].

The Regulator of G protein Signaling (RGS) Homology (RH) domain

The residues 31-180 and 512-531 comprise a domain that is homologous to the catalytic domain of the RGS proteins The RH domain of GRKs is homologous to the RGS proteins sharing ~17-34 % sequence identity. In addition to the classical nine helix bundle [59], GRKs have been shown to contain two additional helices (α10 and α11). The kinase domain in GRKs is inserted in a loop between the α9 and α10 helices thus splitting the RH domain into two discontinuous segments [60] (Fig. 3).

RGS proteins function as GTPase activating proteins (GAPs) for Gα subunits of the heterotrimeric Gαβγ complex, thus adding a regulatory step to the signaling cascade. This is accomplished by stabilization of the switch regions of the Gα protein subunit in a transition state conformation [59]. The exact role of the RH domain in GRKs is not well defined. However, in GRK2 the RH domain binds the $G\alpha_q$ subunit. The binding surface was mapped to the helices α5 and α6 [61]. Thus, GRK2 sub-family can also regulate signaling via phosphorylation-independent desensitization of activated GPCRs by sequestering both $G\alpha_q$ and Gβγ (via the PH domain) subunits. The GRK1 and GRK4 sub-families have not yet been shown to interact with any of the Gα subunits.

Figure 3. RH Domains as Protein Interaction Domains.
(a) RGS4 (PDB code: AGR) was the first structure of an RGS protein and defined the RGS fold of nine α helices. These are divided into "terminal" (α1-α3, α8 and α9 helices, colored magenta) and "bundle" (α4-α7, colored slate) subdomains. The α3-α4 and α5-α6 loops as well as the α8 helix forms the $G\alpha_{i1}$ binding surface. The RH domain of axin binds adenomatous polyposis coli (APC) peptide in the cleft between the α2, α3, α4 and α7 helices [62]. (b) The RH domain of p115-RhoGEF (PDB code: 1SHZ) contains two additional helices (α10 and α11), which have been colored green as they are insertions to the core RGS fold. The N-terminal helix and the β-strand (colored orange, as they are not a part of the RGS domain) form a $G\alpha_{12/13}$ binding interface. (c) The structure of GRK6 (PDB code: 2ACX) reveals a third helix (α0) at the N-terminus of the RGS domain, in addition to α10 and α11. The kinase domain is inserted between the α9 and α10 helices in GRKs. The RH domain of GRK6 forms an extensive dimer interface in the crystals [63]. The α5-α6 helices form the $G\alpha_q$ binding surface in the GRK2 sub-family [61].

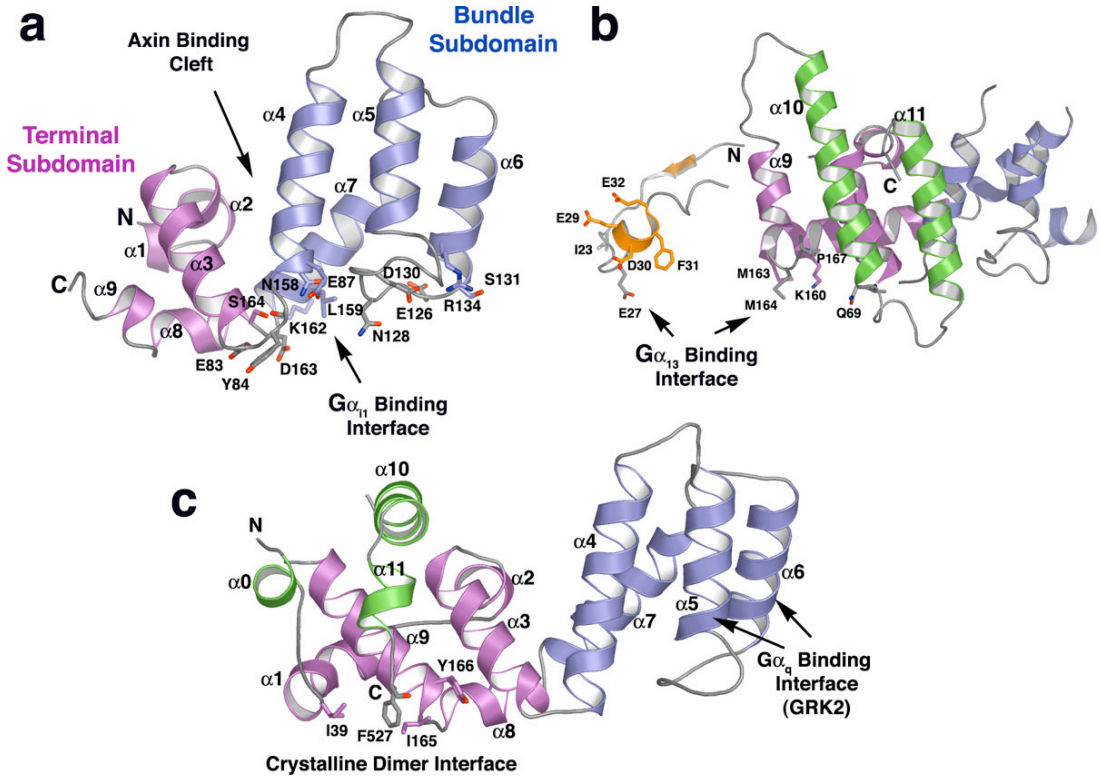

The Kinase Domain

The most conserved region of GRKs is the kinase domain (residues 181-454 in GRK1) that belongs to a Ser/Thr protein kinase family that also includes Protein Kinase A (PKA), G (PKG) and C (PKC) (the AGC kinases). GRK1 shares ~ 39-55% sequence identity to the kinase domain of other members of the GRK family and ~34 % identity to non-GRK AGC kinases. GRKs also include the "C-terminal extension" of the kinase domain (residues 455-511 in GRK1) that is characteristic of the AGC kinase family. The kinase C-terminal extension is believed to play important regulatory roles in other AGC kinases [64].

The crystal structures of various AGC kinases in different nucleotide-bound states have contributed to our current understanding of the structure of the kinase domain and their mechanisms of activation and substrate binding. The kinase domain is comprised by a "small lobe" (residues 181-268 in GRK1) and a "large lobe" (residues 269-454 in GRK1) that are linked by a hinge region (Fig. 4a). The cleft between the two lobes forms the the active site. In AGC kinases, the small and large lobes of the kinase domain "close" upon binding adenine nucleotides, enabling a proper alignment of the catalytic machinery in the active site. Thus far, there is no evidence of a similar conformational change induced in GRKs upon nucleotide binding in the crystal structures of GRK2 and GRK6.

The C-terminal extension of the kinase domain of AGC kinases contains residues required for catalysis and is a site of interaction of *cis*-acting regulatory proteins. The extension (Fig. 4A) has been divided into three structural elements. It starts with the C-lobe (large lobe) tether (CLT, residues 300-319 in PKA) that contains a conserved PxxP motif and has been suggested to be a SH3 binding site in PKB. Immediately following the CLT is the active site tether (AST), which links the NLT and CLT and contributes

residues to the nucleotide and substrate binding. The AST becomes ordered in a ligand dependent manner and is proposed to facilitate nucleotide entry and release. At the C-terminal end of the extension is the N-lobe (small lobe) tether (NLT, residues 340-350 in PKA), which contains residues that interact with the β4 strand and the αB and αC helices of the small lobe [64].

The activation of AGC kinases is also associated with multiple phosphorylation events, which occur at sites termed the "activation loop", the "turn motif", and the "hydrophobic motif". The latter two sites reside in the C-terminal extension of the kinase domain. The phosphorylation of activation loop by phosphoinositide-3 dependent kinase 1 (PDK1) facilitates nucleotide-binding and enhances the rate of catalysis [65]. The NLT contains the hydrophobic motif (HM), and phosphorylation of this site stabilizes the small lobe by securing the NLT packing against the small lobe. The HM of PKB also serves as a docking site for PDK1 (which lacks the C-terminal extension), which then phosphorylates the activation loop of PKB. The "turn motif", which is phosphorylated in PKC and PKA, stabilizes the small lobe [66]. GRKs lack equivalent serine or threonine residues in the activation loop and the hydrophobic motif. Thus, GRKs have a distinct mechanism of activation and use other structural features to compensate for the loss of these motifs. In GRK1, two major autophosphorylation sites have been identified (Ser488 and Thr489) [25, 38], and these map to the "turn motif" of the AGC kinases. GRK2 bears acidic residues at the equivalent region that could mimic a constitutively phosphorylated state.

Figure 4. "Open" and "Closed" Conformations of an AGC Kinase Domain.

(a) The kinase domain of PKA in the active "closed" conformation (PDB code: 1L3R) bound to an inhibitory peptide, PKI (salmon). The small lobe comprises of antiparallel β sheets (orange) and two prominent helices αB and αC (yellow). Large lobe is primarily α-helical. The active site is shown here bound to ADP, Mg^{2+} and AlF_3. The different segments of the kinase C-terminal extension have been colored differently for emphasis. The phosphorylation sites in the activation loop (magenta) and "turn motif" of the N lobe tether have been shown as stick models. The hinge (magenta) connecting the two lobes allows "closure" of the domain. The hydrophobic motif is not shown in this view. (b) The small lobes of the kinase domain in the "open" conformation (PDB code: 1CMK) and "closed" conformation (same model as in panel a) were aligned. (c) The molecular surface representation of the aligned kinase domain in panel b to visualize the degree of closure upon activation. The coloring scheme is the same as in panel b.

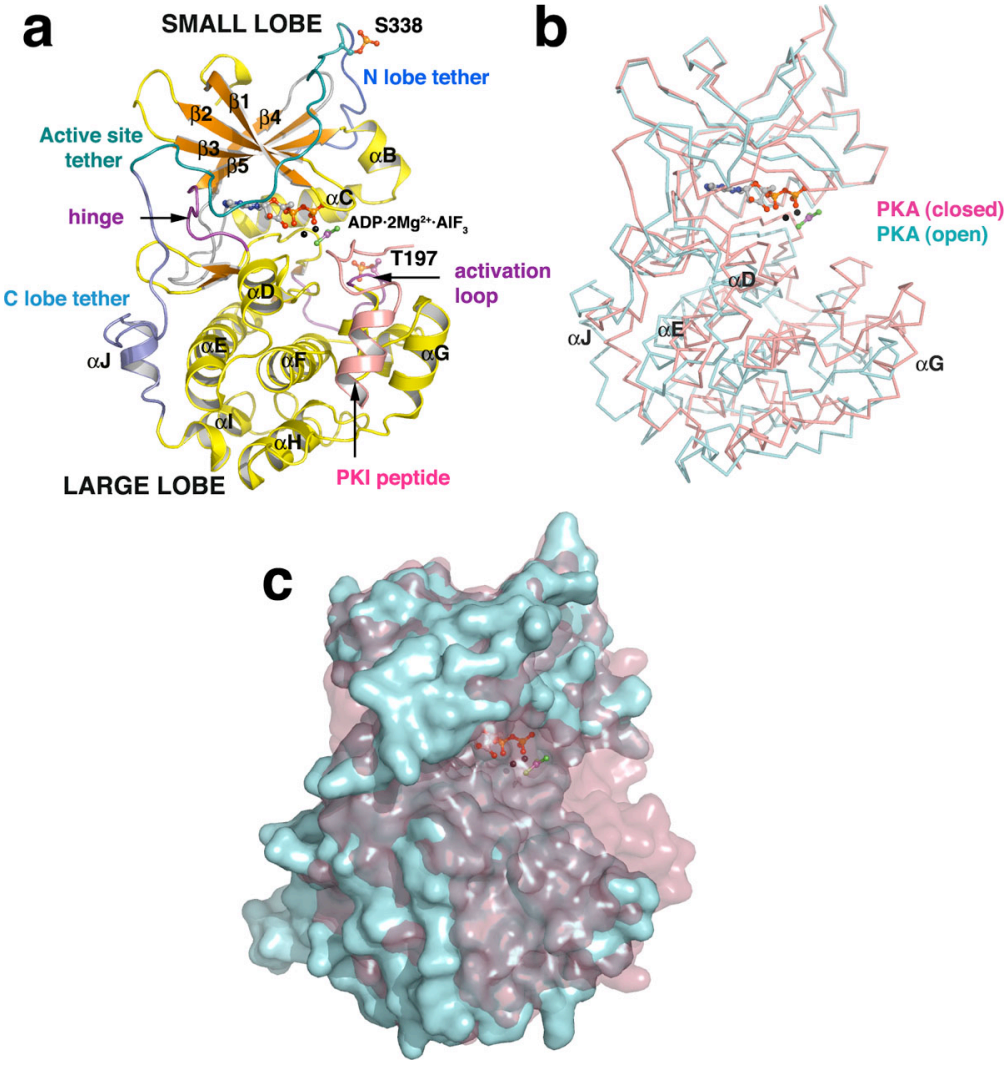

The C-terminus (membrane-targeting domain)

The conserved RH-kinase core found in all GRKs is followed by a membrane-targeting domain (residues 532-561 in GRK1) that varies in a sub-family dependent manner. GRK1 bears a consensus sequence for farnesylation with the exception of chicken GRK1, which is modified by geranylgeranylation. A GRK1 mutant lacking the lipid-modification is defective in membrane recruitment and is evidenced by a higher K_m for Rho* [34].

Photoreceptor Cells

In vertebrates, vision is mediated by highly specialized photoreceptors in the retina that serve to relay the signal from photons of light to the brain in the form of an electrical signal in a process termed phototransduction. There are about 10^8 photoreceptor cells in the mammalian retina, consisting of rods and cones. In evolutionary terms, the rods have arisen more recently than cones and are believed to have developed from cones cells [67]. Cones operate over a broad range of illumination, are responsible for color vision and are crucial for photopic (diurnal) vision. In contrast, rods function at relatively lower intensities of illumination and are responsible for scotopic (night) vision. Rod cells outnumber cones by 20-fold, and it has been argued that having an excess of rod cells enables these photoreceptors to respond to almost every photon that the retina encounters.

The photoreceptor cells consist of three major functional regions: the outer segment, inner segment and the synapse. The outer segments form the venue for phototransduction. In rods, the outer segments are composed of stacks of membranes whereas in cone cells these are simply invaginations of the plasma membrane. The discs contain the photopigment rhodopsin, which constitutes > 80% of all the proteins in the outer segment [68].

Phototransduction Cascade: Activation

*Photoisomerisation and Formation of Rho**

Phototransduction in vertebrate rod cells is initiated by the absorption of a photon by rhodopsin, isomerizing its chromophore 11-*cis*-retinal to all-*trans*-retinal (Fig. 1a) through a number of intermediates to form Rho*. These intermediates are short-lived but can be trapped at low temperature and are distinguished based on their absorption spectra. For example, the transition to the intermediate metarhodopsin I (MetaI) conformation occurs in ~100 μs (λ_{max} ~ 478 nm) and depending on the temperature, the transition from MetaI to MetaII can take 1-10 ms (λ_{max} ~ 380 nm). In the MetaII state, the covalently bound all-*trans*-retinal is deprotonated and as a result, rhodopsin looses its color and is said to have "bleached". The active MetaII form of rhodopsin activates heterotrimeric G proteins and is also phosphorylated by rhodopsin kinase.

Activation of Transducin

Rho* catalyzes nucleotide exchange on the heterotrimeric G protein transducin (G_t). The resulting GTP-bound G_t subunit dissociates from the Gβγ subunits and binds to the inhibitory subunit (γ) of membrane-associated cGMP phosphodiesterase 6 (PDE6), the "effector protein", releasing the inhibition on the catalytic α and β subunits of the enzyme (within milliseconds). The activated PDE6 hydrolyses cGMP resulting in a rapid depletion of cGMP in the intradiscal space and the subsequent closure of the cGMP-gated cation channels in the ROS plasma membrane. As a result, the flow of inward current (in the form of Na^+ and Ca^{2+} ions) is blocked. This leads to hyperpolarization of the membrane, inhibition of the release of the neurotransmitter glutamate at the synapse, and sends a signal to the brain.

An important feature of phototransduction cascade is the amplification of signal at each step. A photon of light activates rhodopsin and each activated rhodopsin further activates ~100 transducin molecules. In amphibians, the turnover of transducin activation is ~150 turnovers per second and one molecule of activated transducin in frogs causes hydrolysis of ~600 cGMP molecules per second [69]. The end result is the closure of cGMP-gated cation channels and hyperpolarization of the membrane.

Phototransduction Cascade: Inactivation

A rapid and efficient termination of the photoresponse (return to the "dark-state") is crucial for rhodopsin to remain responsive to subsequent photons and allows cells to respond to the changes in illumination. It involves an efficient termination of each amplification step of the signaling cascade (Fig. 1b). The rate of inactivation determines the time course of photoresponse.

Inactivation of Rho*

Rho* is inactivated by thermal decay but, this occurs at a very slow rate (on the order of tens of milliseconds in the retina). The ability to rapidly turn off the rhodopsin cascade is crucial for nocturnal (scotopic) vision and involves two proteins, rhodopsin kinase and arrestin. Rhodopsin kinase phosphorylates the cytoplasmic tail of Rho*. Phosphorylated Rho* is then bound by arrestin and this sterically blocks the interaction of activated receptor with G proteins (Fig. 1b). The principal sites of phosphorylation on rhodopsin have been identified as being Ser334, Ser338 and Ser343. Both MetaI and MetaII forms are phosphorylated by rhodopsin kinase. Opsin is also phosphorylated, and this is stimulated in the presence of all-*trans*-retinal [70]. *In vivo*, it has been shown that incorporation of one phosphate per Rho* leads to ~50 % reduction in transducin activation. However, there are six potential phosphorylation sites in mice and seven in

human and bovine rhodopsin. The multiple phosphorylation of rhodopsin is required for efficient arrestin binding [71] and is thought to contribute to the reproducibility of the single photon response [72].

Following the inactivation of Rho* either by thermal decay or phosphorylation by GRK1, the all-*trans*-retinal is released and recycled to regenerate all-*cis*-retinol (in the "retinoid cycle") [73]. The opsin molecule is dephosphorylated by protein phosphatase 2A (PP2A) before incorporation of the chromophore 11-*cis*-retinol, resulting in the regeneration of ground state rhodopsin.

Inactivation of Transducin and PDE

Activated transducin is able to hydrolyze bound GTP but at a very slow rate compared to the time course of photoresponse. The GTPase activity of transducin is enhanced by Regulator of G protein Signaling protein 9 (RGS9), which is bound to its obligatory subunit Gβ5 and the membrane anchor R9AP [74] (Fig. 1b). The phosphorylation of rhodopsin and inactivation of transducin terminates further activation of PDE, with the inactivation of transducin being roughly 2.5 times slower than rhodopsin deactivation [75].

Regulation by Calcium

In addition to the inactivation of the various signaling components, the restoration of cGMP levels to the dark level is crucial for the recovery of photoresponse. This is closely linked to the concentration of Ca^{2+} in the cells. The decline in the levels of cGMP in the cytoplasm is associated with the closure of the cGMP-gated cation channels. However, Ca^{2+} continues to be extruded via the $Ca^{2+}\cdot$ K^+/Na^+ exchanger and as a result the cytoplasmic levels of Ca^{2+} decline. This stimulates the synthesis of cGMP by guanylate cyclase, which restores cGMP levels, leading to the opening of the channels.

Regulation of GRK1

GRK1 activity is regulated at multiple levels. The most robust regulation of GRK1 activity is mediated by the substrate Rho*, followed by phosphorylation of serine and threonine residues within the amino terminus and the C-terminal extension of the kinase domain. GRK1 has also been reported to be regulated by Ca^{2+}·recoverin. This is however, debatable (see Chapter 2).

Regulation by Rho*

The interaction of GRK1 with Rho* stimulates the kinase activity of GRK1. Peptides derived from the C-terminal tail of rhodopsin are poor substrates (K_m values are in the mM range) but, in the presence of a C-terminally truncated rhodopsin [76], the peptide phosphorylation is enhanced [76, 77] by over 100-fold. This suggests that Rho* docks at site(s) distinct from the C-terminal phosphorylation sites and this docking allosterically regulates the kinase activity. Isolated ROS have been shown to incorporate hundred fold molar excess of phosphates per molecule of Rho* ("high-gain" rhodopsin phosphorylation). The molecular mechanism of this phenomenon is not clear, although once activated by Rho*, the kinase can transphosphorylate several nonactivated rhodopsin molecules in the vicinity [78]. This has been suggested to play a role in light-adaptation at low intensities of light.

Docking involves the cytoplasmic loops of the receptor because mutagenesis of residues in these loops reduce receptor phosphorylation by GRK1 [79]. In addition, peptides derived from the second and the third cytoplasmic loops of rhodopsin have been shown to inhibit receptor phosphorylation without affecting GRK1 autophosphorylation [41]. The sites on GRK1 responsible for receptor-mediated activation are not well established. The N-terminus is required for efficient receptor phosphorylation [45, 49, 58] however, it has been suggested that it is more important for binding lipid bilayer than

mediating a direct interaction with the receptor [57]. The C-terminal extension of the kinase domain is also implicated in receptor binding [80].

Regulation by Autophosphorylation

In addition to phosphorylating Rho*, GRK1 has been shown to autophosphorylate at 3-4 positions [25] when incubated with ATP (K_m ~ 2-4 μM). GRK1 autophosphorylation is independent of the presence of rhodopsin and the major sites have been identified as Ser488 and Thr489. Autophosphorylation lowers the K_m for ATP and is believed to promote the dissociation from phosphorylated Rho*, perhaps due to electrostatic repulsions. A third, and a minor, site was mapped to Ser21, which is now believed to be a PKA site [81]. The significance of phosphorylation at this site is not well understood. The site-directed mutagenesis studies suggest that the autophosphorylation may determine the initial site of phosphorylation on Rho* [39]. It has also been suggested that autophosphorylation lowers the affinity for Ca^{2+}·recoverin [82].

GRK1 Physiology and Disease

The pigment melanin in the iris of retina provides protection against damage by UV light. However, exposure to direct sunlight or even a continued exposure to dim light can kill the photoreceptor cells by triggering apoptosis, as demonstrated in transgenic mice lacking rhodopsin kinase [83]. The photoresponse is of higher amplitude and a longer duration in these mice. Mutagenesis studies revealed that the sensitivity to light is associated with the delayed inactivation of Rho*.

In humans, several inactivating mutations in GRK1 are known to cause Oguchi disease, a stationary form of night-blindness that is characterized by a substantial delay in dark recovery after photobleaching. Oguchi disease was first described in 1907 and is characterized by golden-brown discoloration of the fundus of retina upon light adaptation

that disappears after prolonged dark adaptation (Mizuo-Nakamura phenomenon). Oguchi causing mutations in GRK1 have been reported in patients of European ancestry [84]. All these patients suffer abnormal recovery kinetics of rod cells. One case involves heterozygous mutations in the two alleles bearing a point mutation V380D in exon 5 (residue in the catalytic domain) of one allele and a frameshift mutation Ser-536 (4-bp del) in exon 7 of the second allele that results in premature termination of the protein. The unaffected family members of the patient were found to be carriers of one of the two mutations and were normal. Another patient was found to be homozygous for deletion of residues 357-398 (within the catalytic domain) in the exon 5. In addition, a frameshift mutation was predicted that would result in premature termination 18 codons downstream resulting in a non-functional kinase. A variant form of Oguchi disease was recently found in a Pakistani family encompassing a deletion of exon 3 resulting in a non-functional protein [85]. The recently reported missense mutation P391H in two Japanese siblings in a consanguineous family with reduced cone cell responses [86] suggests a role of GRK1 in recovery of cone photoreceptors as well.

Project Goals

The crystal structures of GRK2 (PDB code: 1OMW) [60] and GRK6 (PDB code: 2ACX) [63] defined the structures of two sub-families of GRKs. These structures resolved the common domain organization of GRKs and enabled us to predict the orientation of GRKs at the membrane surface. However, it is still not well established as to how GRKs recognize activated GPCRs and how this interaction in turn activates the kinase. These questions remain unanswered in part because critical structural elements were disordered in all the prior structures of GRKs. This includes the extreme amino terminus and the kinase C-terminal extension of GRKs. The aim of this project was to crystallize bovine GRK1. This would be the first structure of the vertebrate-specific subfamily of GRKs. In addition, relatively higher affinity of GRK1 (2-4 μM) for ATP compared to GRK2 and GRK6 (~35 μM) makes GRK1 an ideal system for studying nucleotide-ligand complexes [87].

Structural Analysis of GRK1

The structural analysis of GRK1 has been hindered owing to the poor yields and the apparent instability of the purified protein. The first step to determine the atomic structure of GRK1 was thus the purification of sufficient amounts of homogenous and catalytically active GRK1. We designed a soluble variant of GRK1 lacking the C-terminal 26 residues for expression in insect cells. The next step was finding the conditions under which GRK1 crystallized followed by collection of X-ray diffraction data and structural analysis.

Functional Analysis of GRK1

The N-terminus of GRK1 was revealed in one of the Mg^{2+}·ATP·GRK1 structures and mass spectral analysis provided evidence of phosphorylation at two previously unidentified sites (Ser5 and Thr8). In addition, the RH domain mediates dimerization in all the crystal forms of GRK1, similar to that observed for GRK6. The functional roles of the phosphorylation sites and the residues at the dimer interface was assessed using steady-state kinetics of site-directed mutants.

METHODS

Generation of pFastBac Dual-His_6 Vector

The pFastBac Dual vector (Invitrogen) was re-engineered to introduce a hexahistidine tag followed by a stop codon after the SalI site (downstream of the polyhedrin promoter, PH). Two oligonucleotides (SalIH6stop and revSalIH6stop) containing the hexahistidine sequence and a stop codon were designed such that the ends were complementary to the overhangs generated in the pFastBac Dual vector after SalI and SpeI digestion (Table 1).

The 5′ end of the oligos was phosphorylated using T4 polynucleotide kinase (Promega) followed by incubation of their equimolar mixture at 95 °C for 5 minutes. To facilitate annealing of oligos, the mixture was then gradually cooled to room temperature. The hybridized oligos were ligated into the SalI/SpeI sites of pFastBac Dual vector. The ligation mixture was transformed into DH5α cells and an ampicillin-resistant (100 μg/ml) positive clone was confirmed by DNA sequencing (DNA core facility, ICMB, University of Texas at Austin). The modified vector will be henceforth referred to as the pFastBac Dual-His_6 vector (Fig. 5) and lacks the SstI site.

Figure 5. Schematic representation of pFastBac Dual-His$_6$ vector.

pFastBac Dual vector (Invitrogen) was re-engineered to replace the SstI site at the PH promoter with a hexahistidine tag followed by a stop codon (shown in red). The unique restriction sites have been labeled and the arrows (black) indicate the directionality of the multiple cloning sites downstream of the respective promoters. The graphic map was created using PlasMapper (http://wishart.biology.ualberta.ca/PlasMapper/).

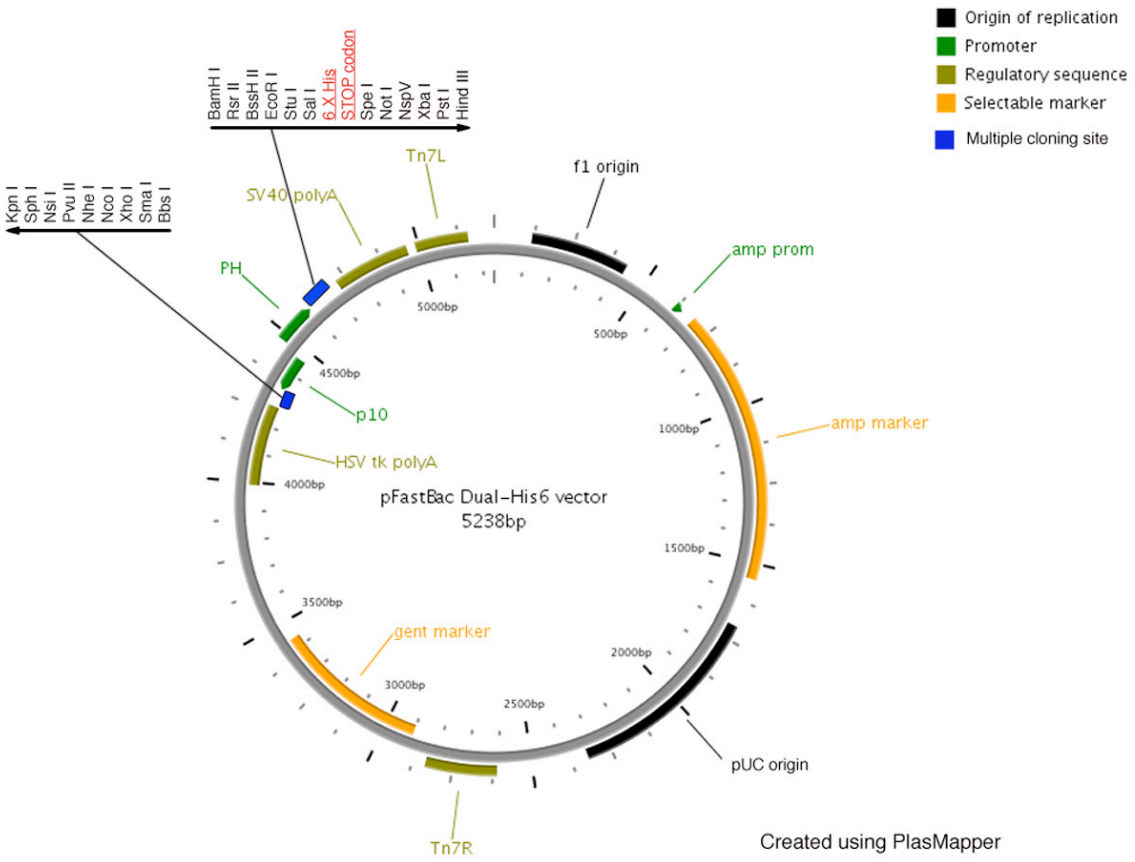

Cloning of Bovine $GRK1_{535}$ into pFastBac Dual-His_6 Vector

A soluble variant of bovine GRK1 (residues 1-535, $GRK1_{535}$) was amplified from GRK1 cDNA in pRK5 vector (a gift from Dr. Robert Lefkowitz, Howard Hughes Medical Center, Duke University, North Carolina) using Pfu Polymerase (Stratagene). The PCR amplification was carried out using Grk1fBamHI and rGrk1short535 primers (Table 1) with an annealing temperature of 63 °C.

The $GRK1_{535}$ PCR fragment was ligated into the BamHI/SalI sites of pFastBac Dual-His_6 vector, downstream of the polyhedrin promoter. The ligation reaction was transformed into DH5α cells, ampicillin-resistant (100 μg/ml) transformants were picked and a positive clone was confirmed by DNA sequencing (DNA core facility, ICMB, University of Texas at Austin). Recombinant protein expressed using this vector construct will contain exogenous valine and aspartate residues (from SalI restriction site) followed by a non-cleavable hexahistidine tag at the C-terminus (Fig. 6).

Cloning of Bovine GRK1 and Mutants into a pcDNA3.1 Vector

PCR fragment encoding wild-type bovine GRK1 was amplified from the GRK1 cDNA vector in pRK5 (a gift from Dr. R. Lefkowitz) using Grk1fBamHI and Grk1rXhoI primers (Table 1). 30 cycles of amplification with the annealing temperature 59 °C were carried out using Pfu Turbo polymerase (Stratagene). The PCR fragment was then ligated into the BamHI/XhoI sites of the pcDNA3 vector (Fig. 7). Ligation mixture was transformed into DH5α cells and transformants were selected based on resistance to ampicillin (100 μg/ml). Plasmid DNA was purified and positive clones were confirmed by DNA sequencing (DNA sequencing facility, University of Michigan). The pcDNA3-GRK1 vector was used as a template to generate dimer-interface mutants (D164A, L166K, W531A, D164A/L166K, D164A/W531A, L166K/W531A) and amino-terminal

mutants (T8A, T8E, T8D, S5A, S5D) using the QuikChange Mutagenesis Kit (Stratagene). Refer Table 2 for the list of GRK1 mutagenesis primers.

Cloning of Bovine GRK1 and Mutants into pFastBac HTB Vector

GRK1 in pcDNA3.1 vector was sub-cloned into the pFastBac HTB vector for expression in High Five cells. The fragment encoding bovine GRK1 or a mutant in pcDNA3.1 was excised with BamHI and XhoI enzymes and ligated into pFastBac HTB vector downstream of polyhedrin promoter (Fig. 8). Ampicillin-resistant clones (100 μg/ml) were picked and DNA sequence was verified (DNA sequencing facility, University of Michigan, Ann Arbor). The fusion protein expressed bears a TEV cleavable His_6 sequence at the N-terminus. Digestion with TEV protease results in five exogenous residues at the N-terminus (gly-ala-met-gly-ser) of GRK1.

Figure 6: $GRK1_{535}$ construct cloned into pFastBac Dual-His_6 vector.

A PCR fragment encoding residues 1-535 of bovine GRK1 was cloned at the BamHI/SalI sites (blue and italicized) downstream of the Polyhedrin (PH) promoter. The vector sequence is in lower case. The numbers (top panel) indicate the start of the restriction site sequence. The 6 x His tag and the stop codon (underlined) in the vector sequence are colored red.

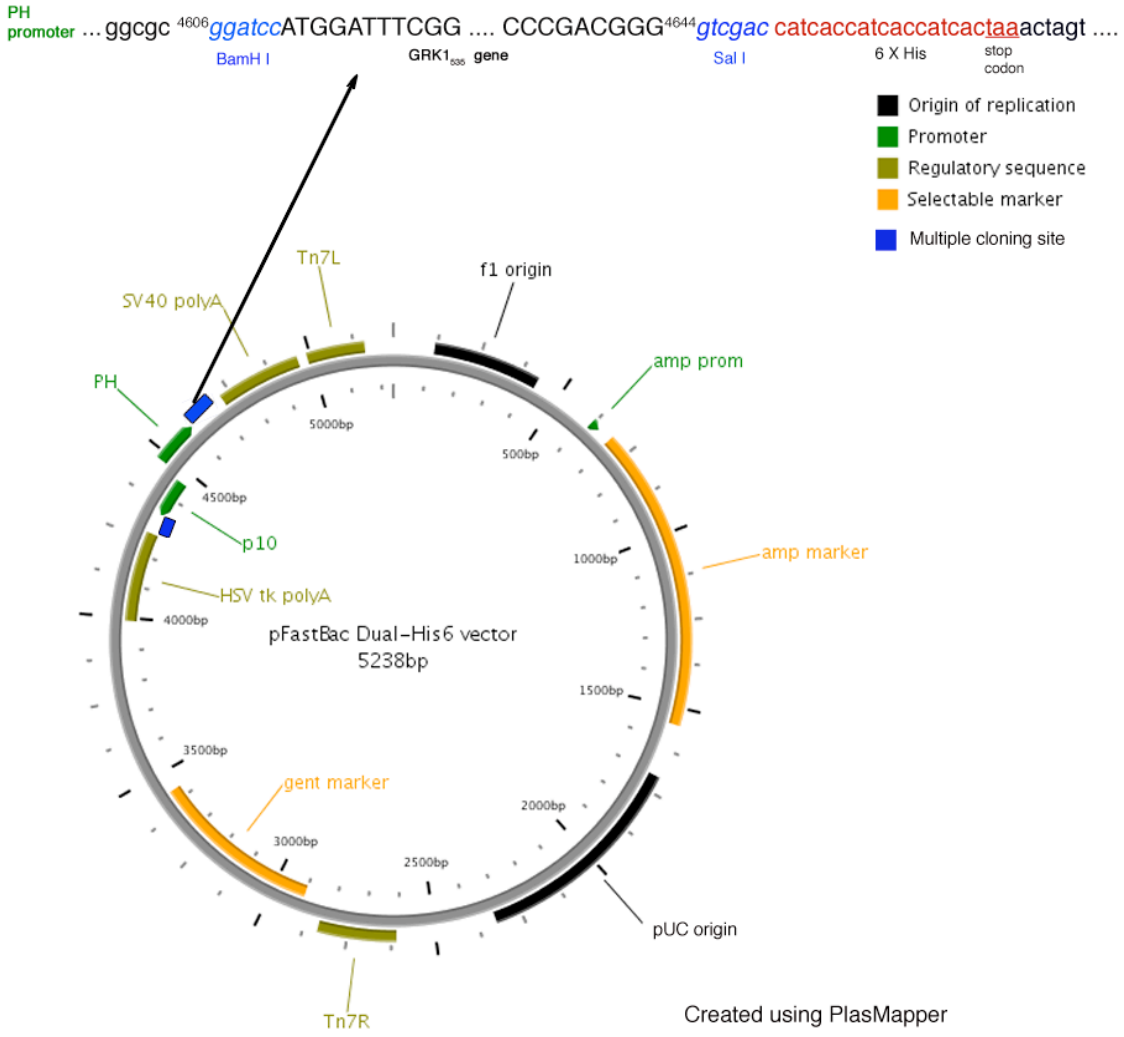

Table 1. List of primers used for cloning.

Restriction enzymes sites are underlined and the stop codon is in bold text and italicized. The glycine to alanine mutation (to prevent myristoylation) at position 2 in $G\alpha_{i1}$ sequence is in red in the primer sequence.

Name	Sequence	Restriction enzyme site
SalIH6stop	5'-TCGACCACCATCACCATCACCAT***TAA***A-3'	Sal I
revSalIH6stop	5'-CTAGT***TTA***ATGGTGATGGTGATGGTGG-3'	Spe I
Grk1fBamHI	5'-GTAGTAGGATCCATGGATTTCGGGTCCCTGGAGA-3'	BamH I
Grk1rXhoI	5'-CAAGTACTCGAG***TTA***CTAGGAAAGCACACACATGC-3'	Xho I
rGrk1short535	5'-CAAGTAGTCGACCCCGTCGGGCCGCCACACG-3'	Sal I
Gbeta1for	5'-GTAGTAGTCGACATGAGTGAACTTGACCAGTTACGGC-3'	Sal I
revGbeta1	5'-CAAGTAAAGCTT***TTA***GTTCCAGATTTTGAGGAAGCTGT-3'	Hind III
mutGi1forXmaI	5'-GTAGTACCCGGGATGGCCTGCACACTGAGCGCTGAGG-3'	Xma I
rev28Gi1BglII	5'-CAAGTAAGATCTCTCTCCGTCCTCCCGGAGGTTA-3'	Bgl II
G16for40BglII	5'-GTAGTAAGATCTCGCGGGGAGCTGAAGCTGCTGCTTT-3'	Bgl II
revG16KpnI	5'-CAAGTAGGTACC***TCA***CAGCAGGTTGATCTCGTCCA-3'	Kpn I

Table 2. GRK1 mutagenesis primers.

The mutations in the primer sequences are in red.

Mutant	Primer	Sequence	Template (in pcDNA3)
D164A	Grk1D164Af	5' -CTTCCAGGAGTTCCTGGCCAGCCTCTACTTCCTGC- 3'	GRK1
	Grk1D164Ar	5' - GCAGGAAGTAGAGGCTGGCCAGGAACTCCTGGAAG - 3'	
L166K	mL166Kf	5' - CCAGGAGTTCCTGGACAGCAAGTACTTC - 3'	GRK1
	mL166Kr	5' - GAAGTACTTGCTGTCCAGGAACTCCTGG - 3'	
W531A	mW531Af	5' - ACTTGAACGTGGCGCGGCCCGACGGGCAGAT - 3'	GRK1
	mW531Ar	5' - ATCTGCCCGTCGGGCCGCGCCACGTTCAAGT - 3	
D164A/L166K	mDLf	5' - CCAGGAGTTCCTGGCCAGCAAGTACTTC - 3'	GRK1
	mDLr	5' - GAAGTACTTGCTGGCCAGGAACTCCTGG - 3'	
D164A/W531A	mW531Af	5' - ACTTGAACGTGGCGCGGCCCGACGGGCAGA - 3'	GRK1 D164A
	mW531Ar	5' - ATCTGCCCGTCGGGCCGCGCCACGTTCAAGT - 3	
L166K/W531A	mW531Af	5' - ACTTGAACGTGGCGCGGCCCGACGGGCAGAT - 3'	GRK1 L166K
	mW531Ar	5' - ATCTGCCCGTCGGGCCGCGCCACGTTCAAGT - 3	
T8A	TPO8f	5' - GATTTCGGGTCCCTGGAGGCGGTGGTGGCCAATTCAGCC - 3'	GRK1
	TPO8r	5' - GGCTGAATTGGCCACCACCGCCTCCAGGGACCCGAAATC - 3'	
T8E	TPO8Ef	5' - GATTTCGGGTCCCTGGAGGAGGTGGTGGCCAATTCAGCC - 3'	GRK1
	TPO8Er	5' - GGCTGAATTGGCCACCACCTCCTCCAGGGACCCGAAATC - 3'	
T8D	GRK1 T8D forward primer	5'-CGGGTCCCTGGAGGACGTGGTGGCCAATTCAGC-3'	GRK1
	GRK1 T8D reverse primer	5'-GCTGAATTGGCCACCACGTCCTCCAGGGACCCG-3'	
S5A	GRK1 S5A forward primer	5'- GATGGATTTCGGGGCCCTGGAGACGGTG-3'	GRK1
	GRK1 S5A reverse primer	5'-CACCGTCTCCAGGGCCCCGAAATCCATC-3'	
S5D	GRK1 S5D forward primer	5'-GGGATGGATTTCGGGGACCTGGAGACGGTGG-3'	GRK1
	GRK1 S5D reverse primer	5'-CCACCGTCTCCAGGTCCCCGAAATCCATCCC-3'	

Figure 7: Schematic representation of GRK1 and mutants cloned into pcDNA3.1 vector.

Bovine GRK1 gene was cloned at BamH I/Xho I sites (in blue) downstream of T7 promoter. The numbers (bottom panel) indicate the start of the restriction sequence. Vector sequence is in lower case. The vector encodes resistance to ampicillin and neomycin (NTP_II marker).

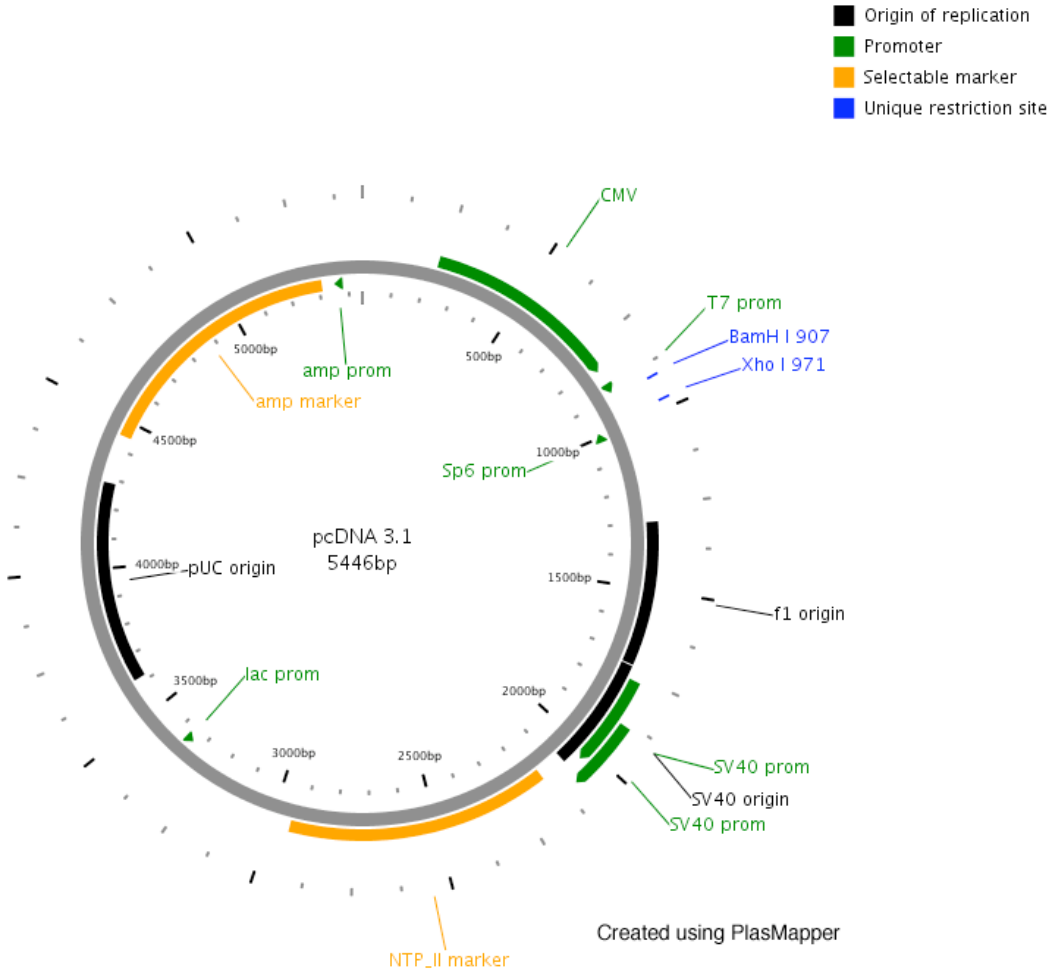

T7 promoter . . . gagctc 907 ggatcc ATGGATTTCGGGT . . . GTGTGCTTTCCTAG 971 ctcgag catgca . . .
BamH I GRK1 gene stop codon Xho I

Figure 8. GRK1 and mutants cloned into pFastBac HTB expression vector.

Fragment encoding bovine GRK1 and mutants was excised from the pcDNA3.1 construct and sub-cloned into the BamHI/Xho I sites (in blue) of pFastBac HTB vector. The vector sequence is in lower case.

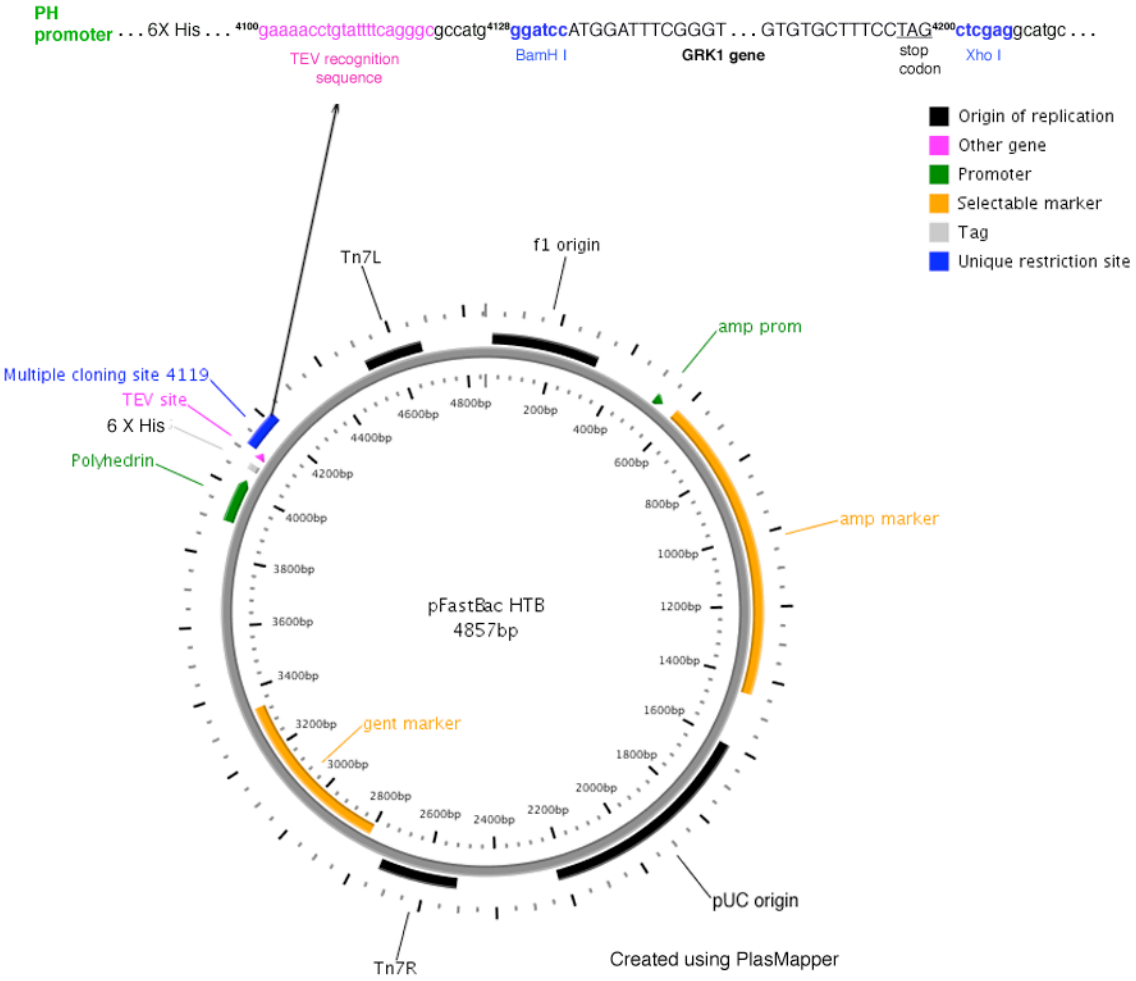

Generation of Recombinant Baculoviruses

Recombinant baculoviruses were generated using the Bac-to-Bac Baculovirus Expression System (Invitrogen). A range of 1-5 ng of pFastBac construct ($GRK1_{535}$-His_6 or GRK1 or a mutant) was used for transformation of 10 µl MAX Efficiency DH10Bac (Invitrogen) chemically competent *E. coli* cells (instead of 5 pg per 100 µl cells) as this yielded a reasonable number of colonies for blue/white colony screening. The cells were incubated on ice for 30 minutes and then heat-shocked for 45 seconds at 42 ºC. The tubes were chilled on ice for about two minutes before adding 90 µl of room temperature S.O.C. medium (Invitrogen). The cells were then transferred to a 14 ml polypropylene round-bottom tube (Becton Dickinson) and incubated in a shaker at 37 ºC for four hours (225 rpm) to allow cells to recover from heat-shock. During this incubation site-specific transposition occurs thus incorporating the expression cassette into the bacmid DNA. Next, 100 µl of a 1:10 and 1:20 dilution of cells in the S.O.C. medium was plated on TKG plates, [Luria-Bertini (Miller's) broth (ISC Bioexpress) agar plates containing 50 µg/ml kanamycin, 10 µg/ml tetracycline, 7 µg/ml gentamicin, 40 µg/ml IPTG and 100 µg/ml X-gal (was added fresh)]. The plates were incubated for 48 hours at 37 °C. A few large and isolated white colonies were picked and restreaked on fresh TKG plates. A clone that had a white phenotype on restreaked plate and no longer grew on LB plates (100 µg/ml ampicillin) was used to inoculate a 5 ml overnight culture containing 50 µg/ml kanamycin, 10 µg/ml tetracycline and 7 µg/ml gentamicin. A glycerol stock of bacmid was stored at –80 °C. Recombinant bacmid DNA was prepared fresh by the ethanol precipitation method (protocol from Bac-to-Bac Baculovirus expression system user manual). Wide-bore pipette tips were used to avoid shearing of the large bacmid DNA. Purified bacmid DNA in 1X TE buffer (10 mM Tris-HCl pH 8.0, 1 mM EDTA) was used to transfect High Five insect cells using cationic transfection agent FuGENE 6

(Roche). Approximately 2 x 10^6 High Five cells grown in Insect Xpress medium (Cambrex) supplemented with 100 units/ml penicillin (Gibco) and 100 μg/ml streptomycin (Gibco) were plated in a T-25 flask (Corning) in a total volume of 5 ml. Cells were allowed to attach to the surface for one hour at 28 ºC. In a sterile 1.5 ml eppendorf tube, 3 μl FuGENE6 was mixed with 97 μl of room temperature Dulbecco's modified Eagle's medium (DMEM, Gibco), which does not contain serum or antibiotics. The tube was flicked to mix the contents and incubated at room temperature for 5 minutes. Approximately 2 μg bacmid DNA (in TE buffer, pH 8.0) was added to the diluted FuGENE6 and mixed by tapping the tube. The DNA:lipid mixture was incubated at room temperature for 15-30 minutes and then added to the cells. The flask was swirled to mix and incubated in 28 ºC humidified incubator for 3-5 days.

Clarified supernatant containing the virus was harvested by centrifugation (3000 X g for 5 minutes) and labeled the "P_1 virus". Virus was stored at 4 °C in the dark and an aliquot was also kept at –80 °C for long-term storage. To generate a high-titer virus, 100 ml culture of High Five cells at a density close to 2 x 10^6 cells/ml in a 1 L baffled flask was infected with 100 μl of P_1 virus. The cell culture was incubated in a shaker (140 rpm) at 28 °C. Cells were harvested 72-96 hours post viral addition when >90% cells were lysed. Virus thus amplified was labeled "P_2". "P_3" virus made by infecting 250 ml cells (2 x 10^6 cells/ml) with 300 μl of P_2 virus was used for infecting six liters of High Five cells for protein expression.

Expression and Purification of Recombinant $GRK1_{535}$-His_6

For protein expression, six liters (8 x 750 ml in 2 L baffled flasks) of High Five cells were grown in Insect Xpress medium containing 100 units/ml penicillin and 100 μg/ml streptomycin in a 28 ºC shaker at 140 rpm. When the cell density was close to 2 x 10^6 cells/ml, 30 ml of "P_3 virus" was added per 750 ml cell culture. Approximately 40

hours post viral addition cells were harvested by centrifugation at 1500 X g for 15 minutes in Beckman JLA 8.100 rotor. The pellet was flash-frozen in liquid nitrogen and stored at –80 °C.

Thawed High Five cell pellet was resuspended in approximately 100-150 ml of cold lysis buffer (Buffer A) containing 20 mM Na-HEPES pH 7.5, 300 mM NaCl, 10 mM β-mercaptoethanol and fresh EDTA-free protease inhibitor cocktail (Roche). When using the dounce homogenizer (40 ml capacity, Wheaton) cells were lysed with 10 passes of loose pestle followed by 10 passes of tight pestle. An additional step was 40 pulses (one second each) of a sonicator (VirSonic 60, VirTis). Alternatively, cells were lysed by one or two passes through Emulsiflex-C3 (Avestin) high pressure homogenizer at 10,000 psi. Samples were checked for lysis under a light microscope and then spun at 40,000 rpm for 45 minutes (4 °C) in a Beckman Ti-45 rotor. The supernatant was filtered using a combination of 1.2 μ filter (Millipore) and a glass filter (Fisherbrand) and diluted to a final protein concentration of 5 mg/ml with Buffer A. All the purification steps were carried out at 4 °C. The diluted supernatant was loaded onto a 5 ml Ni^{2+}-NTA drip column (Qiagen) pre-equilibrated with Buffer A. After washing with 10 column volumes (CVs) of Buffer A and 20 CVs of Buffer B (Buffer A containing 20 m*M* imidazole pH 8.0) the bound protein was eluted in 2-3 ml fractions with Buffer C (Buffer A with 150 m*M* imidazole pH 8.0). (Fig. 9A) The low imidazole wash (Buffer B) elutes appreciable amount of $GRK1_{535}$-His_6, and using a 10 ml Ni^{2+}-NTA column solved the problem.

Fractions containing $GRK1_{535}$-His_6 (in Buffer C) were pooled and diluted six-fold with a buffer containing 20 m*M* Na-HEPES pH 7.5 and 1 m*M* DTT to lower the final ionic strength of the solution to ≤50 m*M* NaCl. Diluted and filtered $GRK1_{535}$-His_6 was loaded onto an 8 ml Source 15S column (Pharmacia) pre-equilibrated with ion exchange buffer A (20 m*M* Na-HEPES, 50 m*M* NaCl and 1 m*M* DTT) at a flow rate of 2 ml/min.

Protein was eluted in an 80 ml gradient of 0-40% ion exchange Buffer B (20 m*M* Na-HEPES pH 7.5, 1*M* NaCl and 1 m*M* DTT). $GRK1_{535}$-His_6 elutes in five peaks. A better separation of different peak fractions was observed using a shallow gradient of 0-30% Buffer B (80 ml). The Source 15S fractions (0.6 ml each) were pooled and labeled as: Pool A (peak 1), Pool B (peaks 2-3) and Pool C (peak 4) (Fig. 9B). A fifth peak (Pool D), which elutes in high salt wash (1M NaCl) appears to contain aggregated protein as it clogs the filter when the pooled fractions are concentrated. This peak fraction was discarded. The Pool A fractions elute at NaCl concentration ranging from 140 to 175 m*M*, Pool B elutes at 180-210 m*M* NaCl whereas Pool C elutes at an approximate NaCl concentration of 220 m*M*. The various pooled peak samples were concentrated to 10-15 mg/ml using a 50 kDa molecular weight cutoff centriprep (Millipore), and flash-frozen as 50 µl pellets in liquid nitrogen. Protein at this stage was ~95% pure (estimated by SDS-PAGE) and hence not purified further. Yield of pure $GRK1_{535}$-His_6 (Pool A) varies from 7-10 mg/L of cell culture.

Figure 9: Purification of recombinant $GRK1_{535}$-His_6.

A. **Ni^{2+}-NTA affinity purification**. The hexahistidine tag at the C-terminus of $GRK1_{535}$-His_6 enables affinity purification on a Ni^{2+}-NTA column. Samples have been labeled, from left to right: (M) protein standards, (1) pellet fraction after cell lysis, (2) supernatant fraction containing soluble protein after ultracentrifugation run, (3) flow-through of supernatant loaded onto the Ni^{2+}-NTA column, (4) column wash with Buffer A, (5) column wash with Buffer B, and (6)-(19) protein eluted with Buffer C. The fractions containing $GRK1_{535}$-His_6 (lanes labeled 6-18) were pooled and further purified on a cation exchange column.

B. **SDS-PAGE and chromatogram of elution from Source 15S column.** Samples have been labeled (from left to right), (M) protein standards, (L) diluted $GRK1_{535}$-His_6 (from nickel affinity purification step) loaded onto Source 15S column. The fractions eluted with an increasing NaCl gradient have been pooled as: fractions 14C-2C (peak 1) were pooled as Pool A, fractions 1B-8B (peaks 2-3) as Pool B, fractions 10B-14B (peak 3) were pooled as Pool C. Fraction 8B represents the peak fraction of Pool D (fractions 5B-12B). The fractions pooled as Pool A, B, C and D have been marked on the gels and the chromatograms in four different colors. (FT) is the flow-through of protein loaded on the column.

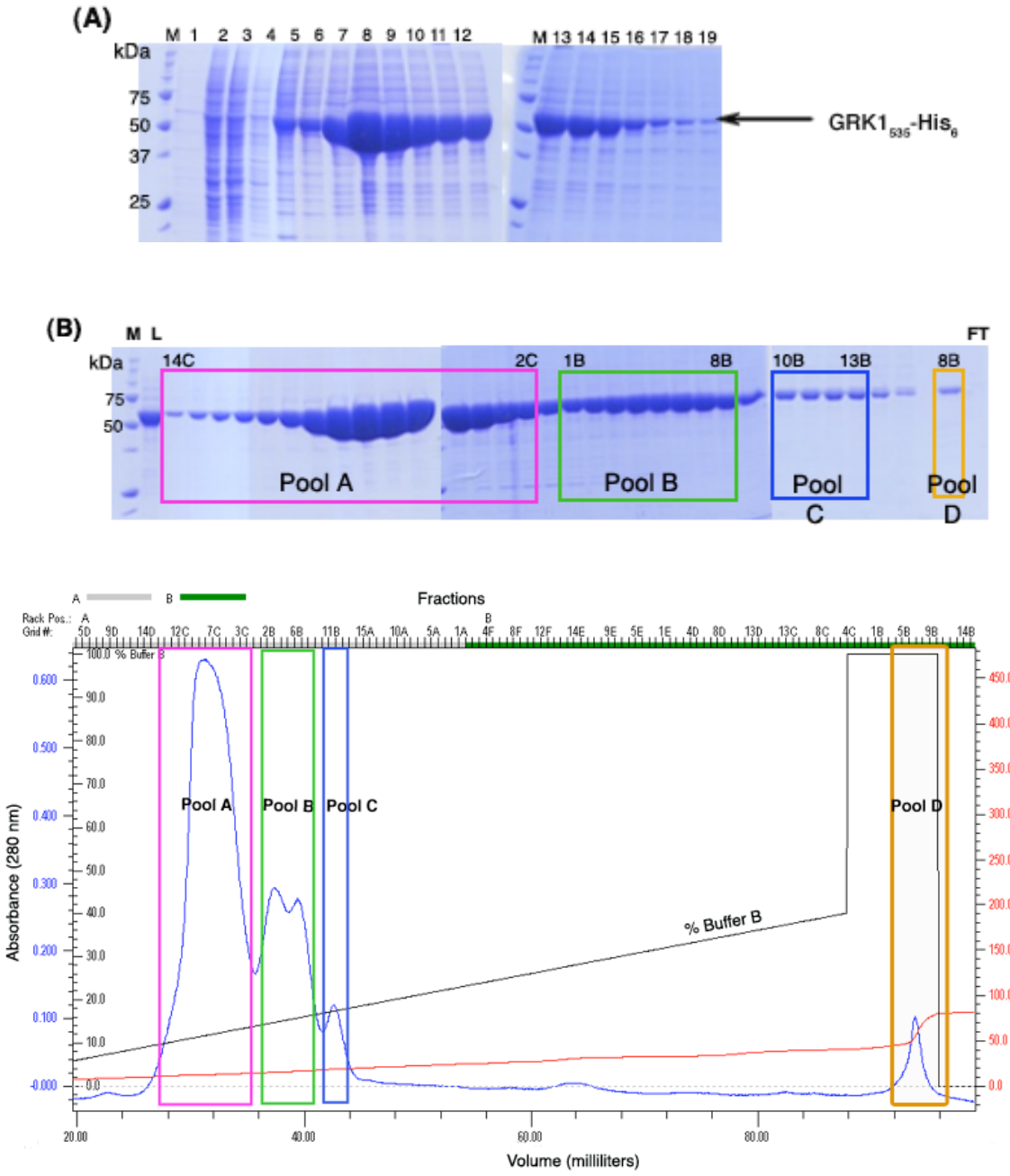
(A)
M 1 2 3 4 5 6 7 8 9 10 11 12
M 13 14 15 16 17 18 19
kDa
75
50
37
25
GRK1535-His6
(B)
M L
FT
kDa
14C
2C
1B
8B
10B
13B
8B
75
50
Pool A
Pool B
Pool C
Pool D
A
B
Fractions
Rack Pos.:
Grid #:
% Buffer B
Pool A
Pool B
Pool C
Pool D
% Buffer B
Absorbance (280 nm)
Conductivity (mS/cm)
Volume (milliliters)
20.00
40.00
60.00
80.00

Expression of GRK1 and Mutants in COS-1 Cells

COS-1 cells grown to about 50% confluency in 100 mm dishes were transiently transfected with either wild-type bovine GRK1-pcDNA3 or a mutant in vector. Transfection was carried out based on manufacturer's protocol (Roche) using 18 μl of FuGENE 6 (Roche) and 6 μg plasmid DNA (a ratio of 3:1). Cells were harvested approximately 44 hours post transfection. Cell pellets were partially purified using SP-Sepharose FF resin (Pharmacia) as described earlier [88]. GRK1 was eluted with 300 mM NaCl. The eluate was analyzed (10 μl) by immunoblotting using either an antibody directed against residues 17-34 of GRK1 (rabbit GS-19 or GS-20, a gift from Dr. K. Palczewski) or an antibody that recognizes the C-terminal 20 residues of GRK1 (rabbit polyclonal C-20, Santa Cruz). The empty pcDNA3.1 vector was processed in a similar manner. The yield of purified protein was too little and not homogenous, which would not allow us to assess the mutants using steady state kinetics. Hence, GRK1 and mutants were expressed in baculovirus infected Five cells.

Expression and Purification of His_6-GRK1 and Mutants in High Five Cells

GRK1 and mutants were expressed in High Five cells similarly to the expression of $GRK1_{535}$-His_6. Following lysis and ultracentrifugation run the pellet fraction (containing membrane-bound protein) was resuspended in the lysis buffer containing 300 mM NaCl and slowly poured in liquid nitrogen. Popcorn-like residues formed were stored at –80 ºC. The soluble fraction of the protein was purified on a 5 ml Ni^{2+}-NTA column as described for $GRK1_{535}$-His_6 (Fig. 10A). Fractions containing His_6-GRK1 fusion protein (calculated mass is ~66.3 kDa) were pooled and dialyzed overnight at 4º C against a buffer containing 20 mM Na-HEPES pH 7.5, 300 mM NaCl and 10 mM β-mercaptoethanol in the presence of 2-3 % (w/w) TEV protease. Digestion with TEV

protease cleaves the His_6 tag, and as a result of which GRK1 does not bind to a Ni^{2+}-NTA column and thus can be purified from the uncut His_6-tagged fusion protein. The final purification step was cation exchange chromatography on a 8 ml Source 15S column (Pharmacia) and was carried out similarly to the $GRK1_{535}$-His_6 purification (Fig. 10B).

The purification of membrane-bound His_6-GRK1 (the fraction of protein that is expected to be farnesylated at the C-terminus) was carried out the following day. Thawed membrane resuspension was solubilized in 1% (v/v) Triton X-100 (Amresco) and stirred on ice-bath for an hour. The solubilized protein was separated from cell debris by ultracentrifugation and purified similarly to the method used for the purification of soluble fraction with the only difference that all the buffers used were supplemented with 0.02% (w/v) dodecyl maltoside, DDM (Dojindo). The soluble and membrane-bound proteins also were purified as a mixture from homogenized cells in the presence of 0.02% DDM.

Figure 10. Purification of wild-type GRK1.

The purification profile of soluble fraction of GRK1 wild-type protein is shown here, The purification of GRK1 and mutants and the membrane fraction of each protein differs at the Source S purification step, where the elution of protein is observed in multiple peaks. The number of peaks and the ionic strength at which they elute varies slightly.

A. **Ni^{2+}-NTA affinity purification.** GRK1 and mutants are expressed as His-tagged proteins, which can be cleaved by TEV protease. The samples have been labeled from left to right as; (M) protein standards, (1) pellet fraction after lysis and ultracentrifugation, (2) supernatant fraction after ultracentrifugation containing soluble fraction of protein, (3) Flow-through of loading protein on nickel column, (4) wash with the lysis buffer, (5) wash with buffer B containing 20 m*M* imidazole, (6) GRK1 containing fractions eluted from nickel column were pooled based on Bradford analysis and, (7) GRK1 containing pooled fractions (in lane labeled 6) were dialyzed overnight in the presence of 3 % w/w TEV protease.

B. **Purification on Source S column.** After overnight dialysis in the presence of TEV protease, GRK1 was purified on a second Ni^{2+}-NTA column to separate it from the uncut-fusion protein. The dialyzed protein was loaded on nickel column and the flow-through that contains the cut protein was collected. The flow-through was diluted five times to lower the ionic strength and purified on a Source 15S column. The samples have been labeled from left to right as; (M) protein standards and, (3C) – (3A) fractions eluted with a salt gradient. Protein at this stage elutes in multiple peaks (upto four/five) and the peak fractions containing pure GRK1 (Peak 2) that were pooled have been marked on the gel. The first peak usually contains fusion protein or a mixture of fusion and TEV-cleaved protein and these fractions were not pooled.

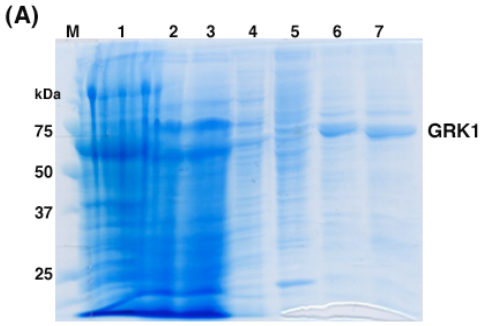
(A)
M 1 2 3 4 5 6 7
kDa
75
50
37
25
GRK1

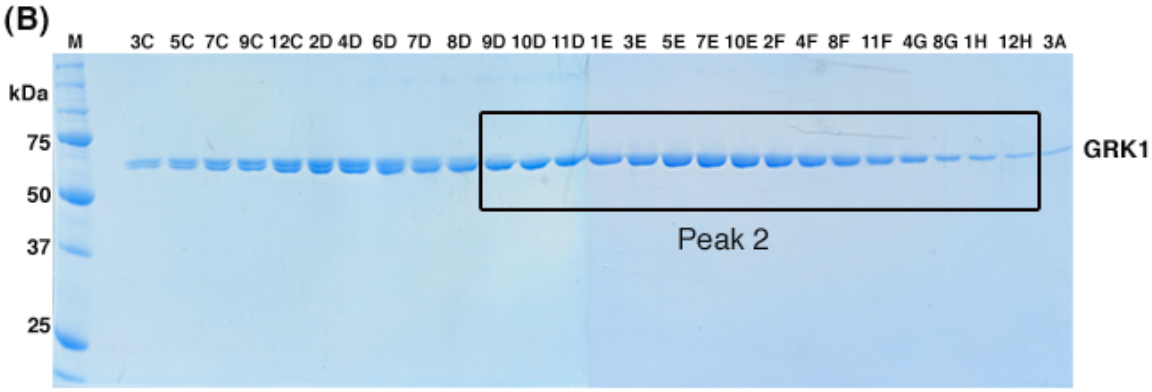
(B)
M 3C 5C 7C 9C 12C 2D 4D 6D 7D 8D 9D 10D 11D 1E 3E 5E 7E 10E 2F 4F 8F 11F 4G 8G 1H 12H 3A
kDa
75
50
37
25
GRK1
Peak 2

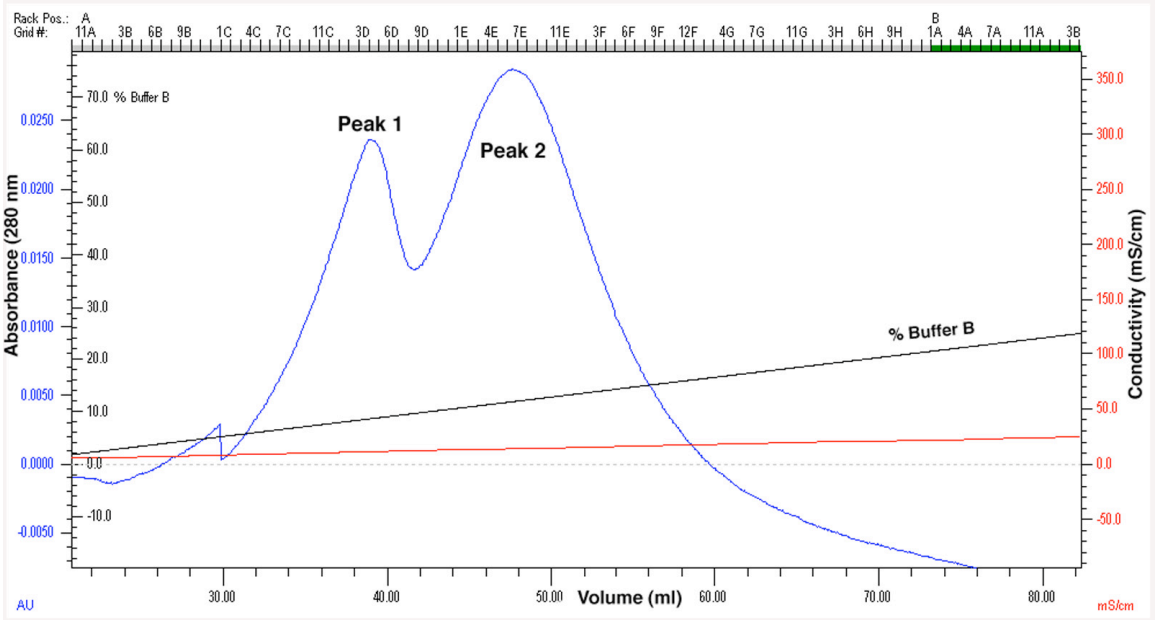
Peak 1
Peak 2
% Buffer B
Absorbance (280 nm
Conductivity (mS/cm)
Volume (ml)
AU
mS/cm

Western Blot Analysis of $GRK1_{535}$-His_6

$GRK1_{535}$-His_6 samples (10, 30 and 100 ng) or GRK1 and mutants (10 μl each) expressed in COS-1 cells were separated by 10% SDS-PAGE. A prestained kaleidoscope marker (Bio-Rad) was loaded in one well to help assess the extent of transfer. A PVDF membrane (Millipore) was prepared by submerging it in the transfer buffer (20% methanol, 48 m*M* Tris base, 39 m*M* glycine and 1.3 m*M* SDS) for about 1-2 minutes. The left-hand corner of the membrane was trimmed to help orient the membrane. Two blotting pads (VWR) were prepared by soaking them in 20% methanol. The assembly process was carried out in the following order: a wet blotting pad was laid down first on the anode plate followed by a wet PVDF membrane, protein gel and then the second wet blotting pad was placed on top. A small glass tube was rolled over to remove all the air bubbles before assembling the cathode plate. Transfer was carried out at 10 V for an hour on a semi-dry transfer cell (Bio-Rad).

The membrane after transfer was blocked using 5% milk in 1X PBS for 30 minutes at room temperature. The blot was probed with a 1:1000 dilution (in blocking buffer) of a rabbit GS-19 or GS-20 antibody, which recognizes residues 17-34 of GRK1 (gifts from Dr. K. Palczewski, Case Western Reserve University, Cleveland, Ohio) or a C-terminal antibody, C-20 from Santa Cruz. The incubation with the primary antibody was carried out for an hour either at room temperature or overnight at 4 ºC. The secondary antibody was HRP goat anti-rabbit IgG (H+L) (Zymed) used at 1:3000 dilution in blocking buffer for an hour at room temperature. The blot was washed thrice (for five minutes each), both after the transfer and after incubation with the two antibodies. To determine if the C-terminus of $GRK1_{535}$-His_6 was intact, Penta-His HRP conjugate (Qiagen) was used as per manufacturer's instructions. In either case, the blot was developed using the LumiGLO chemiluminescent substrate system (KPL) and then

scanned with a Typhoon 9410 Imager (Amersham). The bands were quantified using ImageQuant software version 5.2 (Molecular Dynamics).

Incubation With ATP

To assess if the different pooled peaks of $GRK1_{535}$-His_6 (Source 15S purification step) correspond to different phosphorylation forms or if they were the truncated protein products, Pool A and C samples of $GRK1_{535}$-His_6 were incubated with a final concentration of 4 m*M* ATP pH 7.5 and 2 m*M* $MgCl_2$, both at 4 ºC (to mimic crystallization conditions) and room temperature. An aliquot of protein sample was taken after two hours and overnight incubation. SDS-PAGE was carried out at a low voltage (~50 V) under ice-cold conditions. The gel was either stained with Bio-safe Coomasie (Bio-Rad) or analyzed by western blotting.

Recoverin Binding Assay

Nonacylated-recoverin (NA-recoverin) was coupled to CNBR-activated Sepharose CL-4B beads [30]. Approximately 50 μg $GRK1_{535}$-His_6 from Pool A, B and C were incubated with 30 μl recoverin resin (in binding buffer containing 20 m*M* Na-HEPES pH 7.5, 100 m*M* NaCl, 2 m*M* $MgCl_2$, 1 m*M* $CaCl_2$, 1 m*M* DTT and 200 μ*M* PMSF) for an hour at 4 °C. The unbound protein was collected by centrifugation and the resin was washed twice with binding buffer containing 500 m*M* NaCl. Bound-GRK1 was eluted with a buffer (binding buffer without 1 m*M* $CaCl_2$) containing 5 m*M* EGTA and analyzed by SDS-PAGE or immunoblotting.

N-terminal Sequencing of $GRK1_{535}$-His_6

The N-terminal amino acid sequence analysis was accomplished by Edman degradation using a protein sequencer from Applied Biosystems Model 494HT (Applied

Biosystems, Foster City, CA, USA) at University of Michigan Protein Structure Facility, Ann Arbor. The protein was blotted onto a PVDF membrane (Millipore) and stained with Biosafe Coomasie (Bio-Rad). The protein bands were excised and washed three times with water after wetting with methanol. The PVDF bands were air dried and placed into the sequencer cartridge (Applied Biosystems). Sequence analysis was performed using the manufacturer's method for proteins in gas phase mode. Detection of PTH (Phenylthiohydantoin)-amino acids was at 269 nm by an Applied Biosystems 140C LC-system. Data analysis was performed using the Applied Biosystems Model 610A data analysis software™ (Version 2.1). Amino acids were assigned in comparison to a standard mixture containing 19 PTH-amino acids as supplied by the instrument manufacturer.

Phosphoaminoacid Analysis

Dr. Benlian Wang (Center for Proteomics and Mass Spectrometry, Case Western Reserve University) conducted these experiments. $GRK1_{535}$-His_6 (20 μg) in 20 μl of 1 *M* pH 8.0 Tris-HCl buffer consisting of 8 *M* Urea was reduced by dithiothreitol (DTT) for 2 hrs at 30 ºC. An S-alkylation treatment was then done by adjusting the solution to 2.5 m*M* idoacetamide and reacting for 30 min at 25 ºC in dark. After about 10- fold dilution with water, sequencing grade modified trypsin (Promega, Madison, WI) was added at an enzyme to protein ratio of 1:50 (w/w). The digestion was carried out for 16 hrs at 37 ºC. In case of endogenous rhodopsin kinase (a gift from Dr. K. Palczewski, Case Western Reserve University, Ohio), digestion was performed in the gel. The band containing RK was first excised from the SDS-PAGE gel and then destained with 50% acetonitrile in 100 m*M* ammonium bicarbonate, and 100% acetonitrile. The protein was reduced and alkylated using 20 m*M* DTT and 50 m*M* idoacetamide respectively, for 30 minutes each in dark. The reaction reagents were removed and the gel pieces were washed with 100

m*M* ammonium bicarbonate, dehydrated in acetonitrile. The dried gel pieces were reswelled in 50 m*M* ammonium bicarbonate containing sequencing grade modified trypsin for overnight digestion. Tryptic peptides were extracted from the gel with 50% acetonitrile in 5% formic acid.

MonoTip TiO (GL Sciences Inc, Tokyo, Japan) was used to enrich phosphopeptides according to the manufacture's protocol. The Tip was first conditioned with 100% acetonitrile, 0.2 *M* phosphate buffer (pH 7.0) and equilibrated with 50% acetonitrile in 0.1% formic acid. Samples were loaded and rinsed with 30% acetonitrile in 0.1% formic acid and 0.1 *M* potassium chloride. Phosphopeptides were eluted from the column with 2.5% aqueous ammonia in 20% acetonitrile and concentrated by vacuum centrifuge followed by resuspension in 0.1% formic acid. LC-MS/MS analysis of the tryptic digests were performed using a quadrupole ion trap mass spectrometer (model LTQ) from Thermo-Finnigan (San Jose, CA) coupled with an Ettan MDLC system (GE Healthcare, Piscataway, NJ). Phosphopeptides were acquired in positive ion mode, and automatic data-dependent neutral loss scan method. That is, when a specific neutral loss (-49 Da and -32.7 Da for the doubly and triply charged ions) on fragment ions (MS2) was detected, MS3 was automatically triggered. The obtained data were submitted to Bioworks by searching the phosphorylation on serine, threonine and tyrosine residues. The sites of phosphorylation were confirmed by tandem MS2 and/or MS3.

Intact mass Analysis

$GRK1_{535}$-His_6 samples were desalted using Vydac C4 ultramicrospin column (The Nest Group) according to the manufacturer's protocol and then reconstituted in a solution containing 50% acetonitrile-0.1% formic acid. The samples were infused to QSTAR XL mass spectrometer (Applied Biosystems) through a syringe pump at 0.5 μl/min. The

intact protein mass was analyzed by Bayesian protein Reconstruct using Analyst QS 1.1 software.

Rhodopsin Phosphorylation Assays

Urea-stripped bovine rod outer segments (uROS) used in the assays were either a gift from Dr. Rachel Sterne-Marr, Siena College or were prepared in the laboratory following the method described elsewhere [52] . Rhodopsin phosphorylation assays were carried out following the protocol described earlier [88]. Briefly, an assay mixture was prepared containing 2.5 μ*M* uROS, 20 m*M* Tris-HCl pH 7.5, 2 m*M* EDTA, 5 m*M* $MgCl_2$, 0.1 m*M* ATP pH 7.5 and ~10 μCi [γ-^{32}P]ATP (MP Biomedicals). The assay mixture tube was covered with aluminium foil to protect it from light. Reaction was initiated by adding 1 μl of $GRK1_{535}$-His_6 (from Source 15S purification step) per 9 μl assay mixture followed by exposing the samples to room light at 30 ºC.

Concentration dependent assay

The amount of $GRK1_{535}$-His_6 protein (Pool A, B and C) used in a 10 μl reaction was 10 ng (16.3 n*M*), 30 ng (50 n*M*) or 100 ng (166.7 n*M*). Reaction was quenched after 10 minutes by addition of 10 μl of 2X SDS-loading buffer. Half of the sample was loaded on a SDS-PAGE gel and the gel was run until the dye front ran out of the gel (contains unincorporated [γ^{32}-P]ATP). The gel was dried and exposed to a phosphorimager screen. The screen was scanned after overnight exposure using a Typhoon 9410 Imager (Amersham) and the ImageQuant software version 5.2 (Molecular Dynamics) was used to analyze the data. For a control, 10 ng bovine GRK2 was used.

Time course experiment

Pool A and C samples of $GRK1_{535}$-His_6 (30 ng or 50 n*M* each) were used to assay the time course of rhodopsin phosphorylation in uROS. Reactions were terminated by addition of 10 µl of 2X SDS-loading buffer 1, 3, 5, 7.5, 15, 20, 30 and 40 minutes after the addition of kinase.

Rhodopsin: K_m and V_{max} measurements

To monitor the time course of rhodopsin phosphorylation, a 100 µl assay mixture was prepared containing 20 µM ROS, 2 mM $MgCl_2$, 20 mM Bis-tris propane, pH 7.5, 40 nM soluble fraction of GRK1, and 100 µM [γ-^{33}P]ATP mix (100-1000 cpm/pmol, Perkin Elmer). Reactions were initiated by illuminating the samples at 30 °C. Reactions were quenched after 0, 1, 2.5, 5, 7.5, 10, 15 and 20 minutes by addition of 1 ml of 10% trichloroacetic acid, TCA (Sigma). The assay was carried out with each measurement in duplicate. Samples were pelleted by centrifugation at maximum speed for 2 minutes and the supernatant containing unincorporated ^{33}P was discarded. The pellet was washed 3-4 times with 1 ml of 10% TCA until the counts in the washes were <500. After extensive washing, the pellet was dissolved in 88-97% formic acid and mixed with 5 ml scintillation fluid (Opti-Fluor, Packard Bioscience). The radioactivity was measured using a scintillation counter.

For kinase titrations, a 100 µl assay mixture was prepared the same way except that the amount of kinase was varied from 0-245 ng (0-39 nM) of soluble fraction of GRK1 and 0-125 ng (0-20 nM) of membrane fraction or mixture of both. The reactions were initiated by addition of 100 µM [γ-^{33}P]ATP mix (100-1000 cpm/pmol) and illumination at 30 °C. Reactions were quenched after 10 minutes (based on the time course assays) by addition of 1 ml of 10 % TCA. Samples were processed and analyzed similarly to the time course experiment.

For K_m and V_{max} measurements, assay mixtures (100 μl) were prepared as described above containing either 8 n*M* membrane fraction or 18 n*M* soluble fraction of GRK1 (concentrations used were based on kinase titrations). The amount of uROS was varied from 1-40 μM. Reactions were initiated by addition of 0.1 mM [γ-^{32}P]ATP mix (100-1000 cpm/pmol, Amersham) and illumination at 30 °C. Two measurements were made for each concentration of uROS in 2-3 independent assays. Reactions were quenched and processed as described above. Similar assays for $GRK1_{535}$-His_6 were carried out using 18 nM Pool A and B (10 min) and 65 nM Pool C (20 min). Protein amounts were normalized by SDS-PAGE and A280 measurements (>95% homogenous). The data were analyzed by non-linear analyses and curve-fitting programs of GraphPad Prism version 4.0a for Macintosh. The kinase activity was expressed as nanomoles of ^{33}P or ^{32}P incorporated per minute per milligram of kinase. The linearity of the reaction was confirmed using the double-reciprocal plot.

Size Exclusion Chromatography

$GRK1_{535}$-His_6 (~75 μM) was loaded onto two tandem Superdex 200 HR 10/30 preparative columns (Pharmacia) pre-equilibrated with 20 mM Na-HEPES pH 7.5, 100 mM NaCl and 1 mM DTT at a flow rate of 0.3 ml/min. $GRK1_{535}$-His_6 elutes in one peak and the molecular weight corresponds to 69,438 Da (calculated mass is 63,348 kDa), based on the standard curve using proteins of known molecular weight (Bio-Rad). $GRK1_{535}$-His_6 containing fractions were pooled and concentrated to 2.54 mg/ml in a 50 kDa MWCO centricon (Millipore) and used for sedimentation equilibrium analysis.

Sedimentation Equilibrium

Sedimentation equilibrium analysis was carried out in Beckman Optima XL-1 analytical ultracentrifuge. A six-channel centerpiece was set up as per manufacturer's

instructions. $GRK1_{535}$-His_6 (100 μl) at three different concentrations corresponding to an A_{280} of 0.3 (4.9 μM), 0.5 (8.1 μM) and 0.7 (11.4 μM) was loaded in the sample chamber while 120 μl of $GRK1_{535}$-His_6 gel filtration buffer was loaded in the reference chamber of the centerpiece. The optimal speed for sedimentation equilibrium run was estimated to be 8,000 rpm based on the plot of rpm/ sedimentation coefficient versus molecular weight [89], assuming that the protein exists as a monomer in solution (calculated molecular weight of $GRK1_{535}$-His_6 is 61,348 Da). Protein was sedimented to equilibrium in an An-50Ti rotor at 4° C under vacuum at 7,000, 10,000 and 15,000 rpm. The three rotor speeds were selected following the instructions in the Beckman manual. A fourth rotor speed (25,000 rpm) was selected, in case oligomerization occurred in solution. Three absorbance scans were recorded for each rotor speed at the three protein concentrations used in order to ascertain that equilibrium had been attained, starting with the lowest speed first. Data was analyzed using Ultrascan 7.2 software.

Crystallization of $GRK1_{535}$-His_6

$GRK1_{535}$-His_6 Pool A (7-12 mg/ml) was used for crystallization by hanging drop vapor diffusion method, either at 4 or 20 °C. Protein solution (0.8-1.0 μl) solution was mixed with an equal volume of the well solution. Drops set up with nucleotide ligands contained protein pre-mixed with a final concentration of 2 m*M* $MgCl_2$ and either 4 mM ATP, ADP or AMPPNP, pH 7.5 (the concentrations are based on the crystallization conditions of GRK6).

Three peptides derived from bovine rhodopsin sequence were synthesized at the Protein Structure Facility, University of Michigan, Ann Arbor. Peptide P1 contains one phosphorylation site whereas peptide P3 contains three (phosphorylation sites have been underlined). A third peptide used was labeled L5-6 (loop 5-6, residues 236-249), which inhibits rhodopsin phosphorylation by about 62±10% without affecting GRK1

autophosphorylation. It is also not a substrate for GRK1. All the three lyophilized peptides (~90% pure) were resuspended in a buffer containing 20 m*M* Na-HEPES pH 7.5 and 100 m*M* NaCl. The pH of the final solution was adjusted to ~7.0 with NaOH. $GRK1_{535}$-His_6 was pre-mixed with either one or a mixture of the peptides (at a final concentration of 10 m*M*). The crystals that grew were not dependent on the presence of peptide(s). However, presence of nucleotide (4 m*M* ADP or ATP at pH 7.5 and 2 m*M* $MgCl_2$) was essential. Another approach was to soak crystals for an hour in a cryoprotectant containing 10 m*M* final concentration of peptide(s) (either at 4 or 20 ºC) before flash-freezing them.

P1: KTETS^{343}QVAPA [46]

P3: DDEAS^{334}TTVS^{338}KTETS^{343}QVA [76]

L5-6: ^{236}QQQESATTQKAEKE^{249} [41]

Crystals of GRK1·$(Mg^{2+})_2$·ATP appeared under two different conditions at 4 °C (Fig. 11A, B). Well solution consisted of 11% PEG 6000, 200 m*M* NaCl, 5% glycerol, 100 m*M* Na-tartarate pH 4.35 (crystal form I), and 12% PEG 3350, 200 m*M* NaCl, 5% glycerol, 100 m*M* Na-citrate, pH 4.3 (crystal form II). These crystals appeared in 1-2 days and grew to a maximum dimension of 0.6 x 0.02 x 0.06 mm in one week as clusters of rods. Harvesting solution (the respective well solutions with 20 mM Na-HEPES, pH 7.5, 2 mM DTT, 4 mM ATP, pH 7.5, 2 mM $MgCl_2$, and 5% glycerol) was slowly added (1µl at a time) to the drops containing the crystals and individual rods were removed using a cryoloop (Hampton Research) or excised with a scalpel/eye knife (Beaver). Crystals were then transferred to 50 µl cryoprotectant solution (respective harvesting solutions with 25% glycerol) and were flash-frozen in liquid nitrogen until data collection. Crystals did not show any sign of damage even though they were harvested without a step-wise equilibration to the final harvesting condition.

Apo-GRK1 grew as hexagonal plates (crystal form III) to a dimension of 0.36 x 0.04 x 0.04 mm at 4 °C (Fig. 11C). These crystals took the longest to nucleate (~2 weeks). The well solution contained 11% PEG 3350, 200 m*M* NaCl, and 100 m*M* MES, pH 6.4. Crystals were harvested similarly to the crystal forms I and II and the cryoprotectant consisted of the well solution with 20 mM Na-HEPES, pH 7.5, 2 mM DTT, and 25% glycerol.

Crystals of GRK1·$(Mg^{2+})_2$·ADP were grown under three different conditions (crystal forms IV-VI). Crystal form IV grew at 20 °C using well solution containing 22% PEG 6000, 1 M NaCl, 5% glycerol, and 100 mM MES pH 6.25. Rod-shaped crystals appeared in 1-2 days and grew to maximum dimension of 0.2 x 0.12 x 0.08 mm over the course of one week (Fig. 11D). To prevent damage to the crystals, 1 µl harvesting solution (24% PEG 6000, 1.2 M NaCl, 100 mM MES, pH 6.25, 20 mM Na-HEPES, pH 7.5, 2 mM DTT, 4 mM ADP, pH 7.5, 2 mM $MgCl_2$, and 5% glycerol) was added at a time to the crystal containing drops. The crystal was then serially transferred through 50 µl drops of cryoprotectant (harvesting solution) containing glycerol at 6.25%, 12.5% and 25% glycerol. The crystal was soaked in the harvesting solution for two hours at 20 °C in the presence of 10 mM final concentration each of P1 and L5-6 peptides and was flash-frozen in the cryostream at the synchrotron. Crystal form V grew to maximum dimension of 0.2 x 0.05 x 0.02 mm over the course of one week at 4 °C using well solution containing 15% PEG 8000, 900 mM NaCl, 100 mM MES, pH 6.25, and 5% glycerol (Fig. 11E). The crystals were harvested similarly to the crystal form IV. The cryoprotectant consisted of 17% PEG 8000, 1.3 M NaCl, 100 mM MES, pH 6.25, 20 mM Na-HEPES, pH 7.5, 4 mM ADP, pH 7.5, 2 mM $MgCl_2$, 2 mM DTT, 25% glycerol, and 10 mM P1 peptide. The crystals were soaked for one hour at 4 °C in the peptide containing cryoprotectant before freezing them in liquid nitrogen. The crystal form VI

grew as clusters of rod-like plates at 4 °C using the well solution containing 15% PEG 8000, 800 mM NaBr, 100 mM MES, pH 6.25, and 5% glycerol. The crystals grew to maximum dimensions of 0.32 x 0.28 x 0.04 mm over the course of two weeks (Fig. 11F). Individual rods were excised using a cryoloop (Hampton Research) or a scalpel/eye knife (Beaver) and were harvested in a cryoprotectant solution containing 20 mM Na-HEPES, pH 7.5, 2 mM DTT, 4 mM ADP, 2 mM $MgCl_2$, 17% PEG 8000, 1 M NaBr, 100 mM MES, pH 7.5, and 25% glycerol.

The longest crystals grown using protein pre-mixed with 4 mM AMPPNP, pH 7.5, and 2 mM $MgCl_2$ appeared using the well solution containing 12% PEG 8000, 1 M NaCl, 100 mM Na-citrate pH 5.92 (Fig. 11G). These were clusters of needles and nucleated in 3-4 days at 4 °C. Tiny crystals were also grown with 12-15% PEG 8000, and 1-1.2 M NaCl; 16% PEG 3350, and 1-1.2 M NaCl; and 14% PEG 6000, and 1 M NaCl, all containing 100 mM Na-citrate buffer pH 5.92. None of these crystals were of diffraction quality and were not harvested. The conditions need to be optimized to grow thicker and single crystals.

Figure 11. Different crystal forms of $GRK1_{535}$-His_6.

(A) Clusters of rod shaped plates were grown in the presence of 4 mM ATP and 2 mM $MgCl_2$ at 4 °C. These crystals belong to the space group C2 and diffracted to 2.7 Å. (B) Rod shaped crystals were also grown in the presence of 4 mM ATP and 2 mM $MgCl_2$ at 4°C and belong to $P2_12_12_1$ space group and diffracted to 2.9 Å. (C) Hexagonal plates were grown at 4°C without any nucleotide added to the protein solution. The crystals diffracted to ~8 Å. (D - F) Crystals were grown in the presence of 4 mM ADP and 2 mM $MgCl_2$ either at 20 °C (panel D) or 4 °C (E - F) and diffracted to 1.85 Å (panel D), 2.63 Å (panel E) and 3.62 Å (panel F). (G) Sea-urchin shaped crystals were grown at 4 °C with 4 mM AMPPNP and 2 mM $MgCl_2$ added to the protein solution. These crystals were not of diffraction quality.

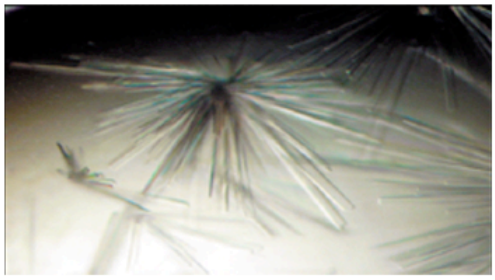

(A) Crystal Form I

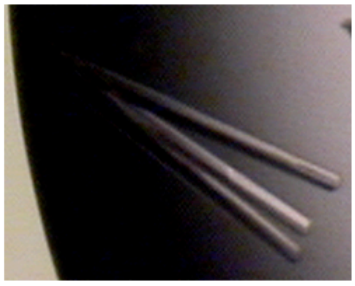

(B) Crystal Form II

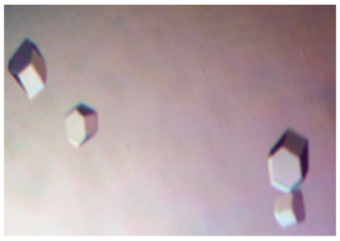

(C) Crystal Form III

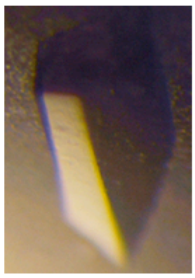

(D) Crystal Form IV

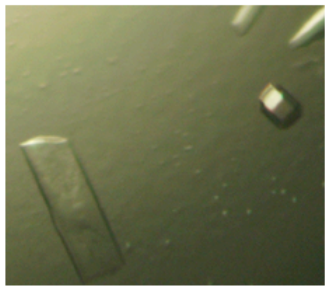

(E) Crystal Form V

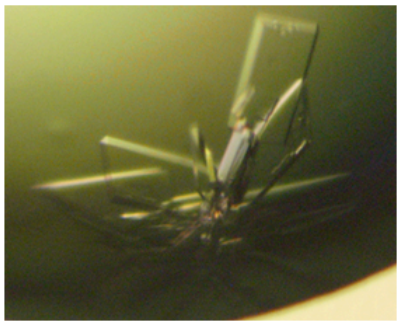

(F) Crystal Form VI

(G) Crystals grown in the presence of 4 mM AMPPNP (pH 7.5) and 2 mM $MgCl_2$

X-ray Data Collection

Diffraction maxima were collected from crystals labeled crystal form I-III at the SBC 19ID (λ = 0.97967 Å) on an ADSC Q315 detector. For crystal forms IV-VI, data were collected at the GM/CA-CAT 23ID-D beamline at the APS (Argonne National Laboratory) on a MAR300 CCD detector (λ = 0.97934 Å). The crystals were cooled in a cryostream at 100 K. The data was indexed, integrated and scaled using the *HKL2000* software package [90]. The refined values of the unit cell and the mosaic spread are summarized in Table 3.

Structure Determination and Refinement

Initial structure of GRK1 was determined using crystal form I. The data harvesting program *TRUNCATE* [91] was used to generate structure factor amplitudes from intensities. Matthew's coefficient (V_m) was estimated to be 2.74 $Å^3$/Da [92] implying that there are two molecules in each asymmetric unit with a solvent content of 55.16 %. The Wilson B-factor was estimated to be 43.4 $Å^2$.

The initial phase problem was solved by molecular replacement using the program *PHASER* [91] in the *CCP4* suite using GRK6 (PDB code: 2ACX) as a search model. All the ligands were omitted from the search model. The r.m.s. deviation of model with respect to the final structure was 0.8 Å with no clashes between trace atoms. The unique solution at the end of each search was refined and an electron density map was calculated. The Log-likelihood gain (LLG) score of the final solution was 1081.42. The initial R-factor values of the structure were 34.6% (R_{work}) and 41% (R_{free}). The coordinates were refined using TLS (Translation, Liberation and Screw-rotation) and restrained refinement in *REFMAC5* [91], alternating with rounds of manual rebuilding using the program *O* [93]. Non-crystallographic restraints (NCS) were set up for the different domains (excluding the N- and C-termini and the C-terminal extension of the kinase domain) for both the monomers in the asymmetric unit. The coordinates for Mg^{2+}

and AMPPNP were taken from GRK6 and the atom name N3B in AMPPNP was changed to O3B converting it to ATP. The ligands were manually fitted in the active site with $|F_o-F_c|$ map contoured at 3σ (Fig. 20). Electron density revealed phosphorylation of Thr8 residue, which was modeled as a phosphothreonine (TPO). Water molecules were added using the *O* macro wat_add once the R-factors were close to 20 %. The water molecules that were kept after refinement had the correct hydrogen-bonding stereochemistry and B-factor values < 50 $Å^2$. After R_{free} converged, all reflections were used for the last few rounds of refinement. The stereochemistry of the refined model was validated using *PROCHECK* [91].

The phase problem for the other crystal forms was solved using either crystal form I or IV as a search model, depending on whether ADP or ATP state was expected. The data collection and final refinement statistics are summarized in Table 3.

Table 3. Data collection and refinement statistics.

Crystal Form	I	II	III	IV	V	VI
Ligand	$(Mg^{2+})_{1 \text{ or } 2}$·ATP	$(Mg^{2+})_{1 \text{ or } 2}$·ATP	Apo	$(Mg^{2+})_2$·ADP	$(Mg^{2+})_2$·ADP	$(Mg^{2+})_2$·ADP
Data collection						
Crystal-to-detector distance (mm)	370	371.2	628.8	252	350	400
Oscillation range (°)	360	130	130	360	180	360
Oscillation angle (°)	0.75	0.75	1	1	1	1
Exposure time (sec)	1	1	1	3	3	1
Mosaicity (°)	0.2-0.42	0.12-0.42	0.56-0.8	0.53-0.71	0.35-0.8	0.22-0.4
D_{min} (Å)	2.7	2.9	7.51	1.84	2.60	3.55
R_{sym} [b]	9.6 (64.7) [a]	8.2 (43.7)	8.4 (79.1)	5.5 (49.5)	8.9 (51.2)	9.6 (47.9)
I/σ_I	22.9 (3.1)	10 (1.6)	24 (2.7)	35.1 (3.0)	19.8 (2.7)	17.4 (2.2)
Completeness (%)	99.7 (100)	96.2 (94.2)	100 (100)	99.4 (99.2)	99.8 (99.9)	97.6 (94.2)
Redundancy	6.8 (6.6)	2.2 (2.2)	7.2 (7.6)	4.2 (4.2)	5.8 (5.9)	3.6 (3.6)
Refinement						
Resolution (Å)	20 - 2.7	20 - 2.9	20 - 7.51	20 - 1.84	20 - 2.60	20 - 3.55
No. reflections	36,930 (2,668)[c]	26,552 (1,822)	2,230 (156)	49,141 (3,591)	43,677 (3,124)	17,300 (1,185)
R_{work} [d]	19.1 (27.7)	19.2 (29.5)	18.8 (42.8)	19.1 (24.3)	19.0 (27.9)	30.7 (35.8)
R_{free} [e]	24.6 (31.9)	25.6 (35.0)	27.4 (44.4)	21.7 (26.7)	23.8 (32.9)	36.7 (37.8)
R_{final} [f]	19.2 (26.9)	19.2 (27.5)	18.2 (40.0)	18.9 (23.7)	19.0 (27.0)	28.7 (36.6)
Protein atoms	8156	7841	7629	4017	8,056	7841
Non-protein atoms	234	126	0	366	381	64
Wilson B factor (Å^2)	64.2	72.9	ND	30.8	53.0	ND
Average B factor (Å^2)						
Protein atoms	46.88	44.28	239.5	37.90	40.73	132.9
Ligands	36.16	42.24	0	32.12	41.10	132.2
Solvent	36.07	23.81	0	42.75	36.73	0
R.m.s deviations						
Bond length (Å)	.011	.010	.007	.009	.010	.008
Bond angles (°)	1.3	1.28	1.0	1.2	1.25	1.1
Ramachandran plot						
most favored (%)	92.5	90.8	79.5	92.3	90.0	83.5
disallowed (%)	0.0	0.0	0.2	0.0	0.0	0.0

[a] Numbers in parentheses correspond to the highest resolution shell of data; Crystal Form I: 2.8-2.7 Å; Crystal Form II: 3.0-2.9 Å; Crystal Form III: 7.77-7.5 Å; Crystal form IV: 1.91-1.84 Å; Crystal form V: 2.69-2.60 Å; Crystal form VI: 3.68-3.55

[b] $R_{sym} = \sum_{hkl}\sum_i |I(hkl)_i - I(hkl)| / \sum_{hkl} I(hkl)_i$, where $I(hkl)$ is the mean intensity of i reflections after rejections.

[c] Numbers in parentheses correspond to the highest resolution shell of data; Crystal Form I: 2.77-2.7 Å; Crystal Form II: 2.97-2.90 Å; Crystal Form III: 7.68-7.51 Å; Crystal form IV: 1.89-1.84 Å; Crystal form V: 2.67-2.60 Å; Crystal form VI: 3.64-3.55

[d] $R_{work} = \sum_{hkl}||F_{obs}(hkl)| - |F_{calc}(hkl)|| / \sum_{hkl} |F_{obs}(hkl)|$; no I/σ cutoff was used during refinement.

[e] 5% of reflections were excluded from refinement to calculate R_{free}.

[f] All reflections were used during the last rounds of refinement.

ND = Not determined. Wilson B factors are not applicable for low resolution data sets.

RESULTS

AIM 1: STRUCTURAL ANALYSIS OF GRK1

Production of functional $GRK1_{535}$

The soluble GRK1 (labeled $GRK1_{535}$-His_6) elutes from Source S column in 4-5 major peaks (Fig. 12a) with each migrating to a different molecular weight on a SDS-PAGE gel, even after incubation with ATP (Fig. 12 inset). The LC-MS/MS analysis revealed that the mass of the major peak Pool A (Peak 1) corresponds to a full-length acetylated $GRK1_{535}$-His_6 phosphorylated at one or two sites. The masses of Pool B (Peaks 2-3) and Pool C (Peak 4) were 820 Da and 1.7 kDa respectively smaller than Pool A, suggesting that these result from proteolysis of Pool A (Table 4). The N-terminal sequencing identified the truncation sites as residues Thr8 (Pool B) and Ala17 (Pool C) in $GRK1_{535}$-His_6 (Table 4). Similar N-terminal truncations have not been reported for wild-type GRK1 purified from retina [26, 94], baculovirus-infected insect cells [28] and mammalian cells [27]. The loss of the C-terminal residues thus appears to render the amino-terminus of GRK1 more accessible to proteases. In the wild-type enzyme, the N-terminus could be protected either by direct interaction of its amphipathic helix with the lipid-bilayer/detergent micelle, or with elements of the C-terminus that are missing in our $GRK1_{535}$ protein, or by the fact that membrane localization of wild-type GRK1 hinders the approach of proteases.

The effect of the N-terminal truncations was assessed in ROS phosphorylation assays. While Pool A was the most active (Fig. 13a) Pool C, which is the most N-terminally truncated, phosphorylated rhodopsin poorly (Fig. 13c). Interestingly, Pool B had significant activity, suggesting that the first seven residues were not critical but

clearly facilitate the phosphorylation of activated receptors (Fig. 13b). The autophosphorylation activity was similar for all pools (Fig. 13c) in agreement with a role in receptor recognition for N-terminus. Steady state kinetics revealed that compared to wild-type GRK1, Pool A phosphorylates ROS with a 6-fold higher K_m (12 μM) and a 2-fold lower V_{max}, possibly because of defects in membrane targeting resulting from the loss of its C-terminal farnesylation site (Table 6). These truncated proteins were also tested for their ability to bind Ca^{2+}·recoverin. Pool B exhibited reduced recoverin binding whereas Pool C did not retain any observable affinity (Fig. 13d). Thus, our data is consistent with residues 8-17 containing elements that are implicated in both receptor function and recoverin binding. These residues span the most highly conserved region of the GRK N-terminus.

Figure 12. Analysis of different peak fractions of $GRK1_{535}$-His_6.

(**a**) Source 15S elution profile of $GRK1_{535}$-His_6. Pool A (peak 1) elutes at NaCl concentration of 140-175 mM, Pool B (peaks 2-3) at 180-210 mM NaCl, and Pool C (peak 4) at ~220 mM. A fifth peak (Pool D) corresponds to aggregated protein. The inset shows that Pool A and C fractions migrate differently on a SDS-PAGE, even after incubation with Mg^{2+}·ATP. Pool A corresponds to full-length acetylated $GRK1_{535}$-His_6 with potentially one or two phosphorylations. (**b**) N-terminal immunoblot analysis. Monoclonal rabbit GS19 antibody, which recognizes the residues 17-34 as epitope reveals that atleast this region is intact in all the samples. (**c**) C-terminal immunoblot analysis. $GRK1_{535}$ construct was expressed as a His_6 tagged protein at the C-terminus. Western using Penta-His antibody (Qiagen) revealed that the C-terminus is intact in all the three pooled peak fractions.

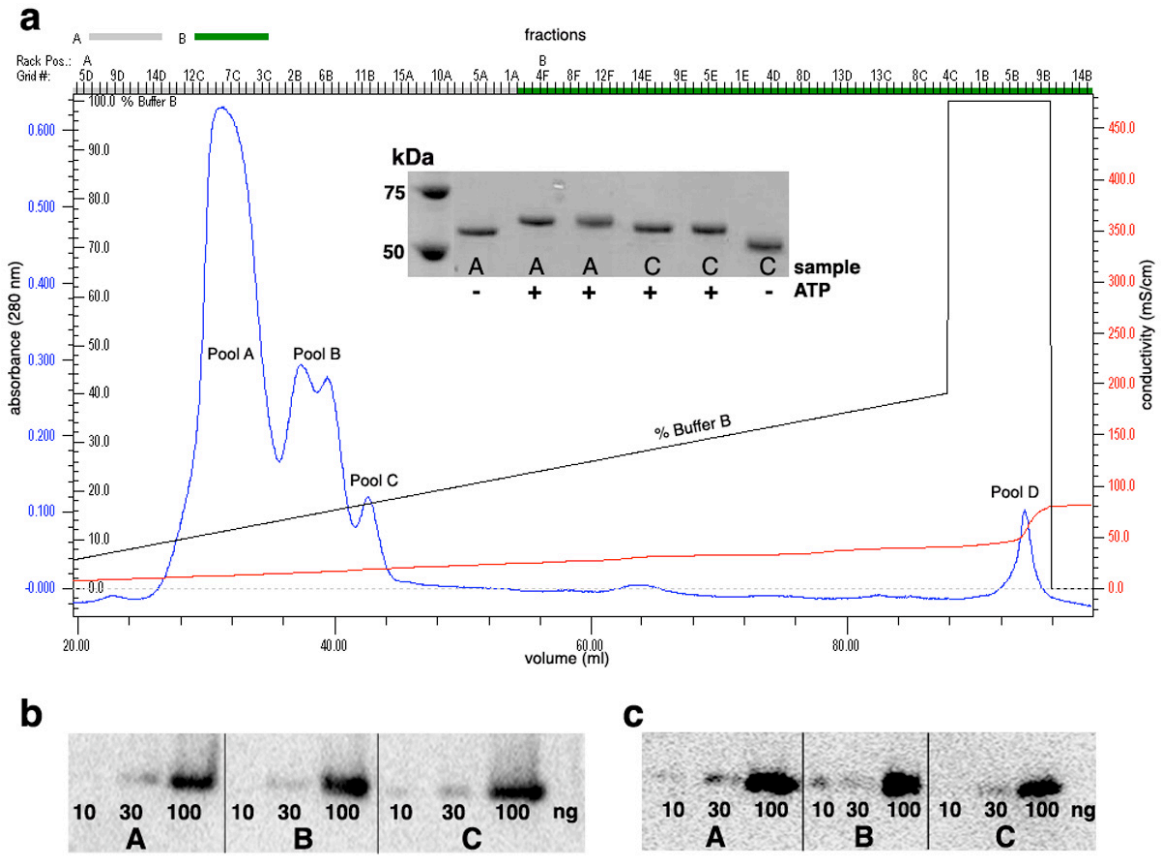

Table 4. N-terminal sequencing and MS analysis of $GRK1_{535}$-His_6.

Sample	N-terminus*	Intact Mass# (Da)	Expected Mass‖ (Da)
Pool A	Acetylated (blocked)	61,390 and 61,488	61,390
Pool B	Thr8	60,659 and 60,567	60,568
Pool C	Ala17	59,672	59,665

* N-terminal sequence analysis was performed on protein from two different purifications. The analysis of Pool A failed because the N-terminus is blocked by acetylation. The analysis revealed that Pool B and C are missing seven and 16 residues respectively from the N-terminus.

The masses corresponding to the major peaks in each sample are reported.

‖ Expected masses were calculated based on the primary sequence of $GRK1_{535}$-His_6 after taking into account the N-terminal acetylation (for Pool A) or N-terminal truncations (for Pool B and C).

Figure 13. Effects of N-terminal truncations on the activity of $GRK1_{535}$-His_6.

Protein amounts were normalized by SDS-PAGE and A_{280} measurements (>95% homogenous). (**a**) ROS phosphorylation assays using 18 nM Pool A. The reactions were initiated by addition of 100 μM [γ-^{32}P]ATP mixture (100-1000 cpm/pmol) and illumination at 30 °C. After 10 minutes reactions were quenched using 10 % TCA. The K_m for Rho* was estimated to be ~12 μM (see Table 6). The values plotted are representative of 2-3 independent experiments, with two measurements for each concentration of ROS. The data was analyzed using non-linear analysis and curve-fitting programs of GraphPad Prism version 4.0a for Macintosh. **(b)** Similar assays using 18 nM Pool B in 100 μl reactions. Pool C (not shown here) phosphorylated Rho* poorly and the steady state kinetic parameters could not be estimated under similar assay conditions. (**c**) Pool A, B and C were analyzed at three different concentrations in 10 μl reactions, with 30 ng kinase being equivalent to 50 nM. The reactions were set up the same way as in panel (a) or (b) using 2.5 μM ROS and were quenched after 10 minutes by addition of SDS running buffer. The dried gel was scanned and the bands were quantified using the ImageQuant software version 5.2 (Molecular Dynamics). Assays with no kinase added were used (lane labeled "Bl") to check the background signal from endogenous kinase contamination in the ROS sample. 10 ng GRK2 was used as a control. The autophosphorylation activity is, however, similar. **(d)** Effect of N-terminal truncations on the efficiency to bind Ca^{2+}·recoverin. Approximately 50 μg $GRK1_{535}$ samples (LOAD) were incubated with unmyristoylated-recoverin coupled to Sepharose CL-4B beads. The bound protein was eluted (BOUND) with a buffer lacking $CaCl_2$. The unbound protein is in the flow-through (FREE). Compared with Pool A, Pool B displays reduced binding whereas Pool C has no detectable affinity for the column. The experiment was repeated twice, each with the binding reactions performed in triplicate, as shown.

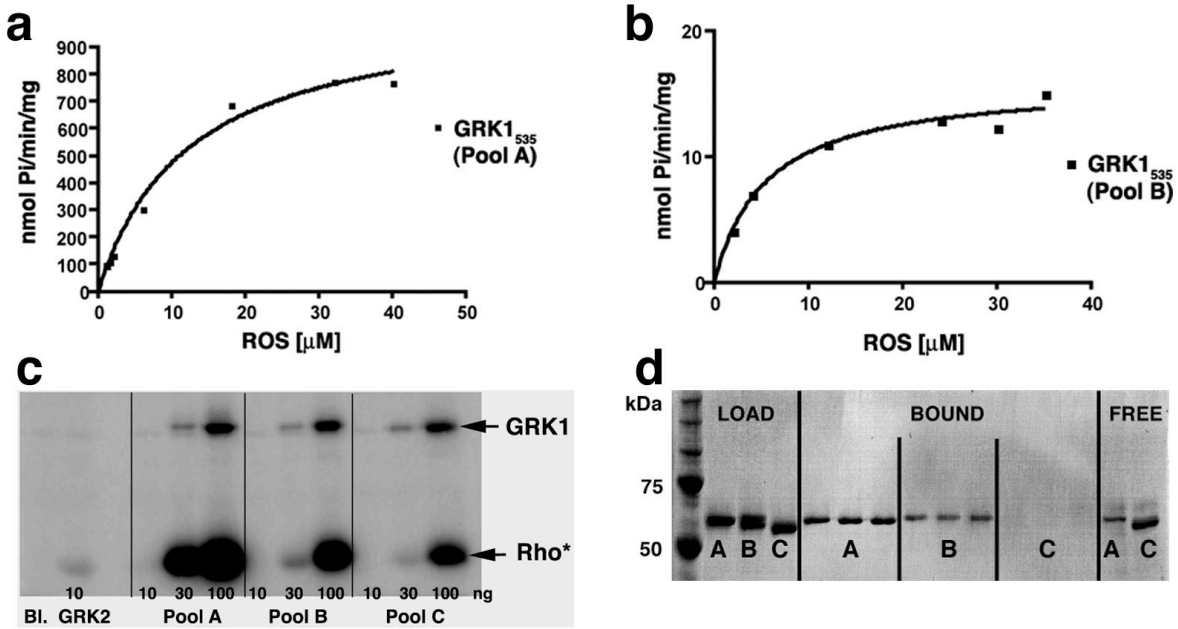

Being the most active and abundant form, $GRK1_{535}$ construct (Pool A) was co-crystallized with different nucleotide ligands to yield five crystal forms, with two bound to $(Mg^{2+})_2$·ATP and three to $(Mg^{2+})_2$·ADP. A sixth crystal form was grown in the absence of any nucleotide ligands (Table 3). Together these allow us to compare three nucleotide-ligand binding states of GRK1, represented by $(Mg^{2+})_2$·ATP·GRK1 (substrate-bound), $(Mg^{2+})_2$·ADP·GRK1 (product-bound) and the apo-form. In five crystal forms, two molecules of GRK1 are found in the asymmetric unit (Fig. 14a). In the highest resolution crystal form (IV), only one subunit is found in the asymmetric unit yielding a total of 11 independent structures. In all crystal forms, GRK1 forms a dimer, with the interface mediated by the RGS homology (RH) domain, as it was in GRK6 [63]. Although the dimer interface is conserved in all crystal forms, the relative orientation of the dimer subunits differ among the crystal forms. For example, the chain B of crystal form V needs to be rotated by ~12° to align with that of crystal form I when their A chains are first superimposed (Fig. 14b).

The overall quaternary structure of GRK1 (Fig. 14a) is similar to GRK2 and GRK6. The RH-kinase core of GRK1 is comprised of bipartite interactions between the RH and the kinase domain that are analogous to the contacts made by the SH2 and SH3 domains of inactive Src [95]. The total buried surface area is ~2,075 $Å^2$ between the two domains. The largest portion of the interface (1,360 $Å^2$) is formed between the α0, α9 and α10 helices of the RH terminal subdomain and the α9-β1, β2-β3 and αC-β4 loops of the small lobe of the kinase domain (Fig 14c). The interdomain interactions could represent stabilizing interactions between the RH and kinase domains. The α10 helix forms extensive contacts with the αC-β4 loop, which could help orient the αC helix of small lobe that contributes residues to the nucleotide-binding pocket. The second, smaller interface is formed between the α4-α5 loop of the RH bundle subdomain and the αJ

helix, the first element of the kinase C-terminal extension (Fig. 14d). The role of this interface is not known, but it could represent a stabilizing interaction for the C-terminal extension of the kinase domain. This latter interface is maintained in all crystal forms except in apo-GRK1, where it appears altered or disrupted as a direct consequence of the distinct kinase domain conformations observed in this crystal form. Otherwise, the RH-kinase core of the 9 nucleotide-bound structures of GRK1 are quite similar (0.4-0.9 Å for equivalent Cα atoms), with the regions of greatest conformational variability being the α6-α7 loops of the RH domain and portions of the kinase C-terminal extension, in agreement with their relatively high B-factors (Fig. 15).

Figure 14. The RH-Kinase Core of GRK1.

(a) The dimer of GRK1 observed in all the crystal forms. The dimerization is mediated by a conserved interface of the RH domain. The dimer shown here is of the most complete structure of GRK1 (crystal form I). The terminal subdomain of the RH domain (helices α0-α3 and α8-α11) is colored violet while the bundle subdomain (α4-α7) is colored slate. The small lobe of kinase domain (yellow) is composed of 6 β-strands (orange) and 2 α-helices (αB and αC), while the large lobe is primarily α-helical. The ligand $(Mg^{2+})_2$·ATP is drawn as spheres. Magnesium atoms are colored black, carbons white, nitrogens blue, oxygens red, phosphates orange and chloride ions cyan. The extreme N-terminal region and the C-terminal extension of the kinase domain are colored green for emphasis, as these were not previously observed in GRK2 and GRK6 crystal structures [60, 61, 63]. **(b)** The dimer-related kinase domains differ by 12° between the crystal forms I and V, revealing the flexibility of the dimer interface. Crystal form I is colored yellow and crystal form V is orange. The orientation is the same as in panel (a). The grey line and the arrow indicate the direction of the rotation axis. **(c)** The RH-small lobe interface as seen in the crystal form I (chain B). The symmetry-related residues 24-32 form extensive crystal contacts (brown) that appear to stabilize the conformation of the N-terminus in this crystal form. **(d)** The RH-large lobe interface consists of a salt-bridge between Arg458 (αJ helix) and Asp100 and hydrogen bonds with the backbone of the α4-α5 loop of the bundle subdomain. The side chains shown are conserved in all GRKs except GRK2 and GRK3 (Fig. 19).

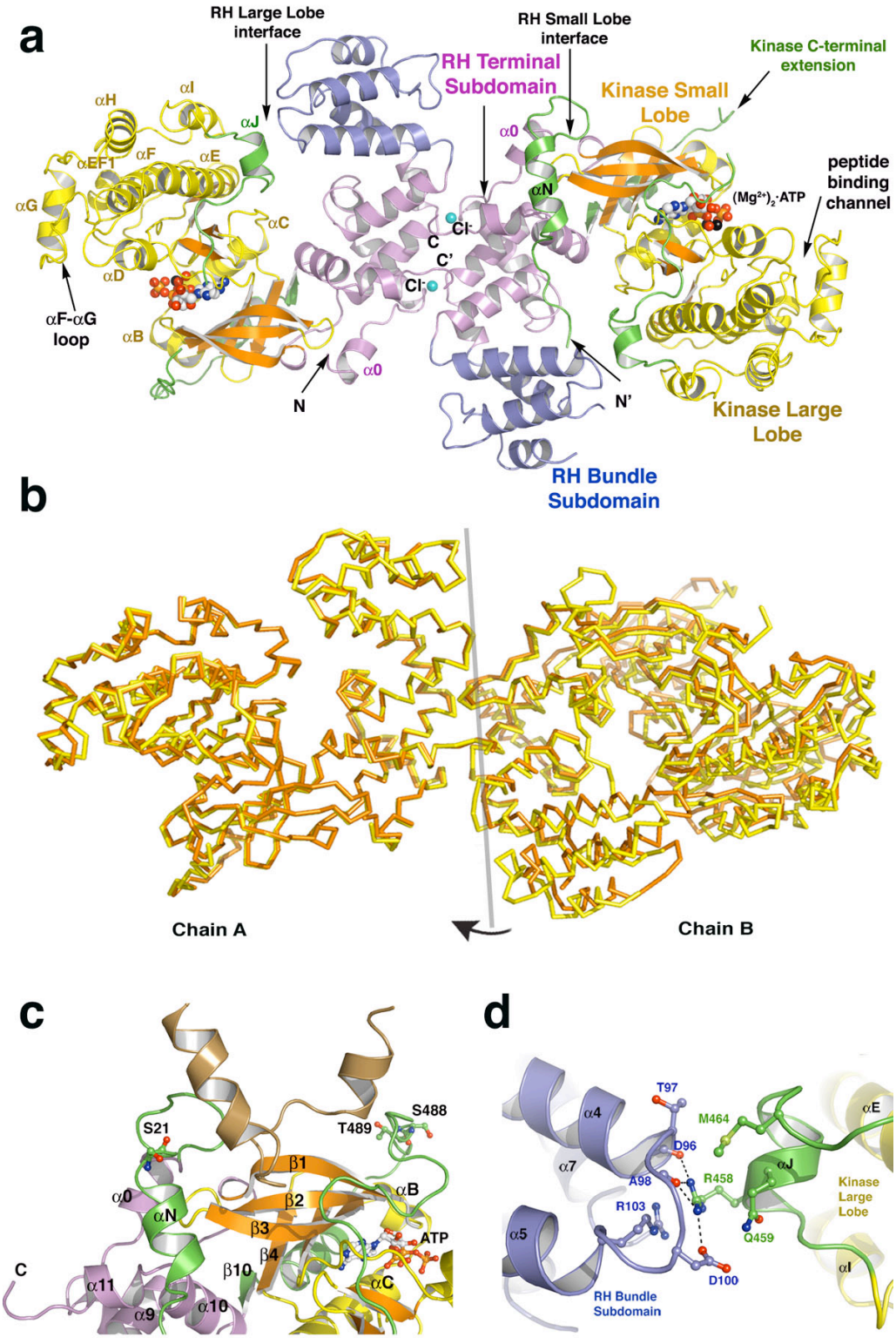
a
RH Large Lobe interface
RH Small Lobe interface
Kinase C-terminal extension
RH Terminal Subdomain
Kinase Small Lobe
αH
αI
αJ
αF
αE
αEF1
αG
αC
αD
αF-αG loop
αB
α0
αN
peptide binding channel
(Mg2+)2·ATP
Cl-
C
C'
N
N'
Kinase Large Lobe
RH Bundle Subdomain
b
Chain A
Chain B
c
S21
T489
S488
β1
β2
β3
β4
αB
α0
αN
ATP
C
α11
α9
α10
β10
αC
d
T97
α4
M464
αE
D96
α7
A98
R458
αJ
Kinase Large Lobe
R103
Q459
α5
D100
αI
RH Bundle Subdomain

Figure 15. Average backbone B factors.

The average main chain B factors for crystal form IV and chain B of crystal forms I and V are shown as a plot of the average main chain B factors as a function of residue number, with gaps corresponding to disordered residues. Regions of interest with relatively high conformational flexibility have been labeled.

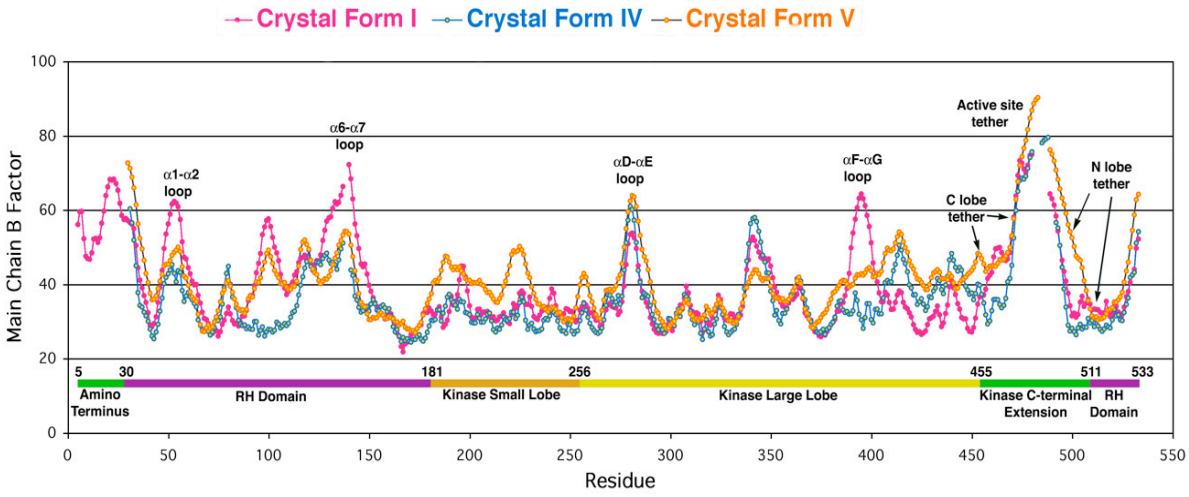

N-terminus of GRK1

The amino-termini of GRKs have been shown to contain residues that regulate receptor phosphorylation [45, 49, 57]. Up until now, this critical region (residues 1-30) has been disordered in each GRK structure determination [60, 61, 63]. One of the $(Mg^{2+})_2$·ATP·GRK1 crystal forms (chain B of crystal form I) reveals residues 5-30 (Fig. 16a and c). However, the structure is disordered in the other 10 structures of GRK1, wherein the electron density can be traced starting at either Ala29 or Ser30 or Arg31. The N-terminus forms extensive contacts with the two RH sub-domains with a total buried surface area of ~1,200 Å^2. The residues 1-4 are not ordered and appear to thread the hole formed by the bipartite interface between the RH and kinase domains. Residues 5-12 wander through the cleft formed between the bundle and terminal lobes of the RH domain. This cleft is used to bind adenomatous polyposis coli (APC) peptide in the RH domain of axin (Fig. 3) [62]. The electron density maps reveal that Thr8 residue is phosphorylated (Fig. 16b) and the side chain of phosphothreonine residue is coordinated by Gln73 and Glu93 residues (residues in the α4 helix). The hydrogen bond formation will be favored as the crystals were grown at a pH of ~4.35 when the carboxyl groups and the phosphate ion could be protonated. In addition, the two lysine residues (Lys69 and Lys93) in the vicinity could complement the charge on the phosphate. Residues 13-23 form a helix (αN) whose side chains interact primarily with backbone atoms in the RH terminal subdomain. Based on the electron density maps the Ser21 residue, one of the known phosphorylation sites in GRK1 [38, 81], does not appear to be phosphorylated. Residues 24-32 form a loop that is engaged in an extensive crystal contact. This loop region is variant in GRKs and links the N-terminus to the α0 helix of the RH domain.

The observed N-terminal structure is not dependent on phosphorylation of the N-terminus, but appears to be stabilized by the crystal contacts (Fig. 16c). Analogous crystal

contacts are lacking in the other crystal forms, including crystal form II (grown in the presence of ATP) wherein the N-terminus is not ordered. The phosphorylation at Thr8 residue led us to analyze the site by phosphoamino acid analysis of trypsinized N-terminal fragments. Phosphorylation of Thr8 was detected in $GRK1_{535}$-His_6 pre-treated with ATP but not in GRK1 isolated directly from bovine retinas, suggesting that the phosphorylation results from incubation with ATP. Ser21 residue which, is now believed to be a PKA site [81], had detectable phosphorylation in both the samples. Unexpectedly, the analysis detected phosphorylation of Ser5 in both the endogenous and *in vitro* samples (Fig. 17). The physiological role of these novel sites (Ser5 and Thr8) was assessed by steady-state kinetics (see Specific Aim 2).

Figure 16. The Most Complete Structure of GRK1.

(**a**) The RH-kinase core of GRK1 (represented by crystal form I). For this figure, the coordinates of all the GRK1 crystal forms were merged to generate a structure that spans residues 5-533 (out of 558), and the large lobe was rotated to generate the expected closed, active state analogous to that of PKA [96]. The Ser5, Thr8, Ser21, Ser488 and Thr489 phosphorylation sites are drawn as stick models. The expected position of the membrane plane is indicated. The red arrows indicate the N-terminal truncation sites mapped on the structure (refer to Table 4). The coloring scheme is as in Fig. 14a**. Top inset.** The Ser488 and Thr489 phosphorylation sites correspond to the AGC kinase "turn motif" and although not observed in the structure are expected to form electrostatic interactions with the charged residues in the αB helix of the kinase domain. **Bottom inset.** Interaction of phospho-Thr8 with the RH domain. Gln73 and Glu93 form direct hydrogen bonds, while Lys69 and Lys90 complement the charge of the phosphate moiety. (**b**) A σ_A-weighted $|F_o|-|F_c|$ map contoured at 3 σ at the N-terminus. The N-terminal residues 5-30 were excluded from refinement. The polypeptide backbone representing the first six residues is shown here for clarity, highlighting the density of phospho-Thr8. The carbon atoms colored green, oxygens red, nitrogens blue and phosphorus orange. **(c)** The structural alignment of the N-termini of GRKs. The numbers on top indicate the residue number in GRK1 sequence. The accession codes for the protein sequences are: GRK1, P28327; GRK2, NP_777135.1; GRK3, P26818; GRK4, AAI17321.1; GRK5, P43249; GRK6, P43250; GRK7, NP_776757.1.

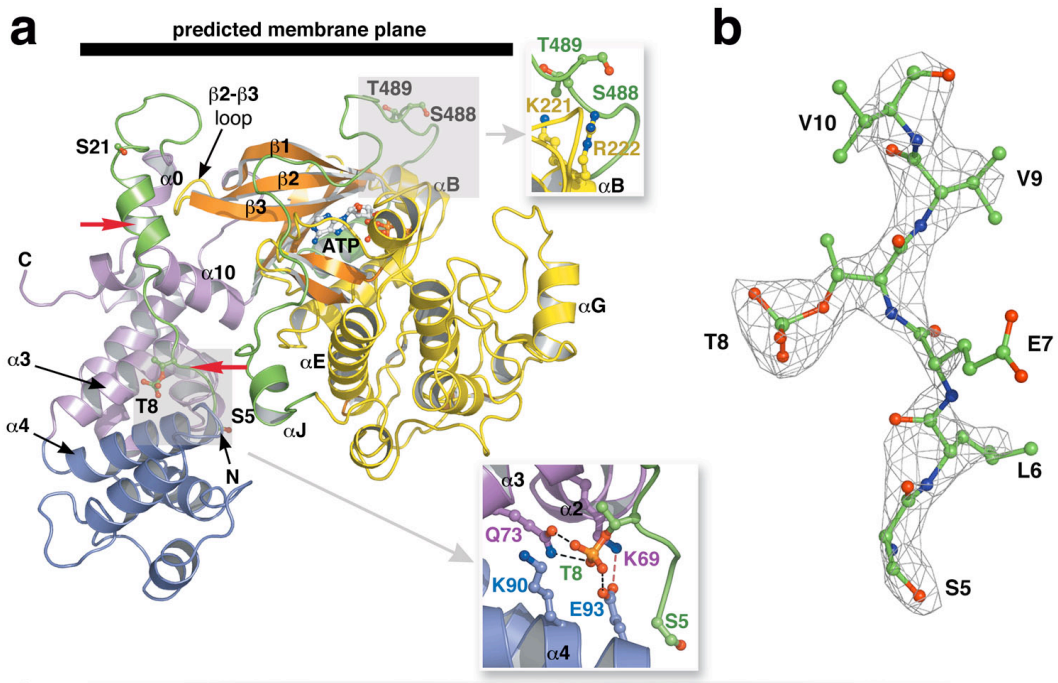

c


```
          1         10        20        30        40
GRK1   -MDFGSLETVVANSAFIAARGSFDASSGPASRDRKYLARLK 40
GRK7   MVDMGGLDNLIANTAYLQARKSSDADSKELQRRRR---SLM 38
GRK5   ----MELENIVANTVLLKAREG--GGGKRKGKSKKWKEILK 35
GRK6   ----MELENIVANTVLLKAREG--GGGNRKGKSKKWRQMLQ 35
GRK4   ----MELENIVANSLLLKARQG--GYGKKSGRSKKWKEILT 35
GRK2   ---MADLEAVLADVSYLMAMEK--SKATPAARASKKILLPE 36
GRK3   ---MADLEAVLADVSYLMAMEK--SKATPAARASKKIVLPE 36
```

Figure 17. Phosphorylation sites identified by LC-MS/MS analysis.

(a) Ser5 is phosphorylated in bovine GRK1 isolated from retinas. **(b)** Ser5 and Thr8 are phosphorylated in $GRK1_{535}$ pre-incubated with 4 mM ATP and 2 mM $MgCl_2$. **(c)** Ser21 and **(d)** Ser488 and Thr489 were identified in both endogenous and $GRK1_{535}$ samples.

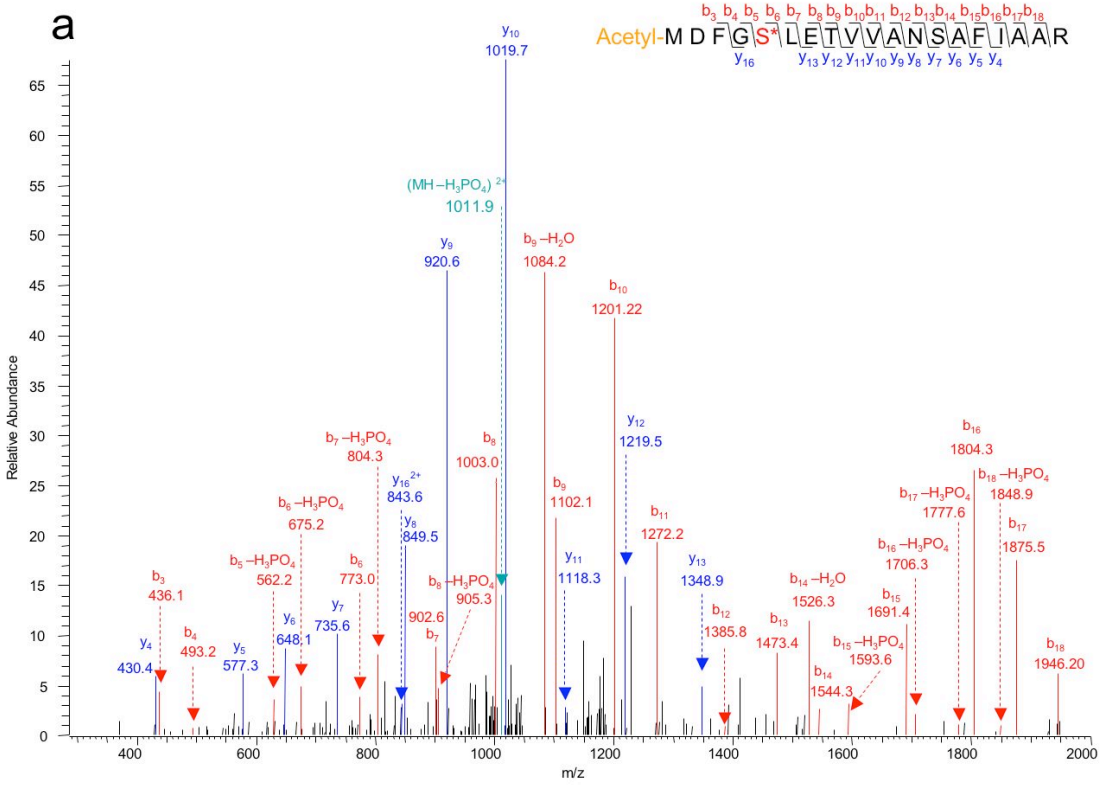

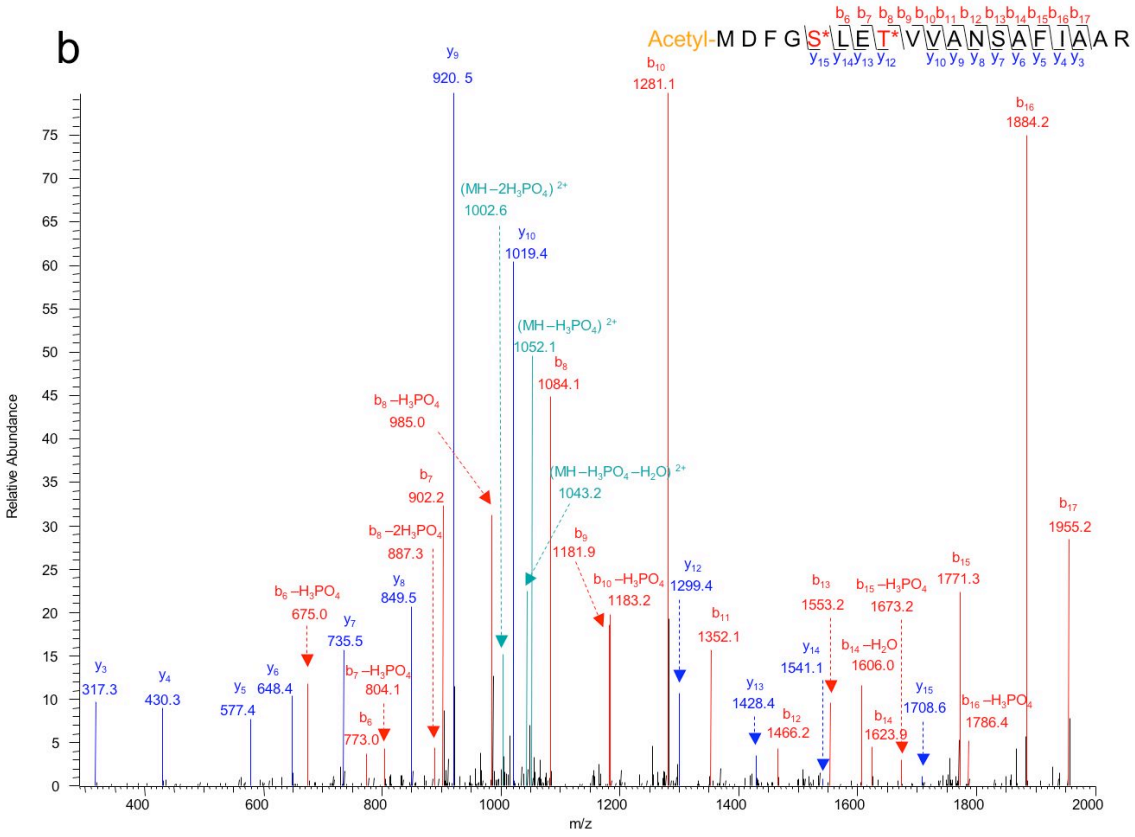
b
Acetyl-M D F G S* L E T* V V A N S A F I A A R
Relative Abundance
m/z
y9 920. 5
b10 1281.1
b16 1884.2
(MH−2H3PO4) 2+ 1002.6
y10 1019.4
(MH−H3PO4) 2+ 1052.1
b8 1084.1
b8 −H3PO4 985.0
(MH−H3PO4−H2O) 2+ 1043.2
b7 902.2
b8 −2H3PO4 887.3
b9 1181.9
b17 1955.2
y12 1299.4
b15 1771.3
b6 −H3PO4 675.0
y8 849.5
b10 −H3PO4 1183.2
b13 1553.2
b15 −H3PO4 1673.2
y7 735.5
b11 1352.1
y14 1541.1
b14 −H2O 1606.0
y3 317.3
y4 430.3
y6 648.4
b7 −H3PO4 804.1
y13 1428.4
y15 1708.6
y5 577.4
b6 773.0
b12 1466.2
b14 1623.9
b16 −H3PO4 1786.4

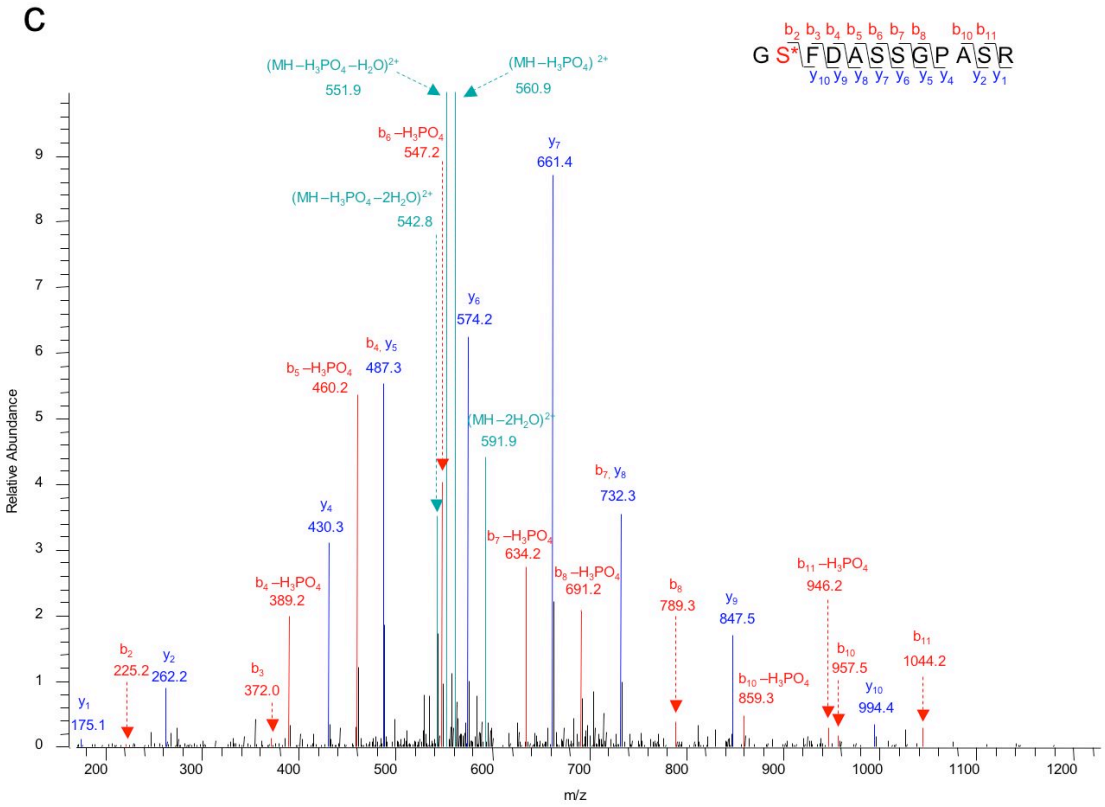
C
G S* F D A S S G P A S R
Relative Abundance
m/z
(MH−H3PO4−H2O)2+ 551.9
(MH−H3PO4) 2+ 560.9
b6 −H3PO4 547.2
y7 661.4
(MH−H3PO4−2H2O)2+ 542.8
y6 574.2
b4, y5 487.3
b5 −H3PO4 460.2
(MH−2H2O)2+ 591.9
b7, y8 732.3
y4 430.3
b7 −H3PO4 634.2
b4 −H3PO4 389.2
b8 −H3PO4 691.2
b8 789.3
y9 847.5
b11 −H3PO4 946.2
b2 225.2
y2 262.2
b3 372.0
b10 957.5
b11 1044.2
b10 −H3PO4 859.3
y10 994.4
y1 175.1

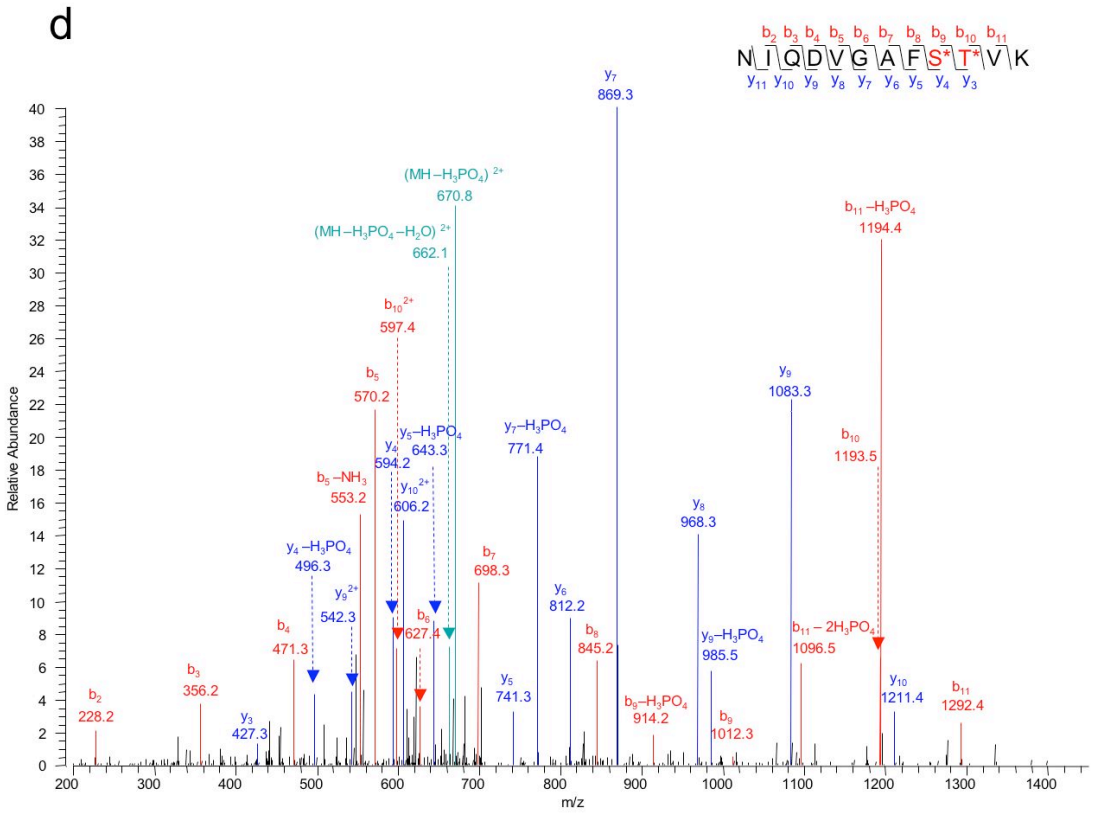
d
N I Q D V G A F S* T* V K
Relative Abundance
m/z
y7 869.3
(MH–H3PO4) 2+ 670.8
(MH–H3PO4–H2O) 2+ 662.1
b11–H3PO4 1194.4
b10 2+ 597.4
b5 570.2
y9 1083.3
y5–H3PO4 643.3
y7–H3PO4 771.4
b10 1193.5
y4 594.2
b5–NH3 553.2
y10 2+ 606.2
y8 968.3
y4–H3PO4 496.3
b7 698.3
y9 2+ 542.3
y6 812.2
b6 627.4
b8 845.2
b4 471.3
y9–H3PO4 985.5
b11 – 2H3PO4 1096.5
b3 356.2
y5 741.3
y10 1211.4
b2 228.2
b9–H3PO4 914.2
b11 1292.4
y3 427.3
b9 1012.3

RGS Homology Domain of GRK1

The conformation of RH domain is maintained in all the crystal forms with r.m.s.d. of 0.4-0.9 Å (Fig. 18a). Similar to GRK6, the RH domain of GRK1 contains a α0 helix at the N-terminus [63] that mediates contacts with both the RH and the kinase domains but does not contribute to the hydrophobic core of either domain (Fig. 18b). Unlike GRK2 and GRK6, the α6-α7 loop is not well-ordered in GRK1. The superposition of the kinase domains of GRK1, GRK2 and GRK6 reveals that the RH domains of GRK1 and GRK6 are deported similarly with respect to the kinase domain (r.m.s.d. of 1.04 Å for equivalent Cα atoms), consistent with their closer sequence homology to each other than to GRK2 (GRK1 and GRK6 share ~34 % sequence identity as opposed to 24% to GRK2). The RH domain of GRK2 is rotated ~11˚ with respect to that of GRK1, with the axis of rotation running along the RH-small lobe and the RH-large lobe interfaces (Fig. 18c).

The RH domain of GRK2 (α5 and α6 helices) makes "effector" like contacts with the $G\alpha_q$ subunit [61]. The RH domain in other GRK sub-families has not been reported to bind any Gα subunit. The structural comparison suggests that this could be because the α5 helix is ~ 2 turns shorter in GRK1 (Fig. 18c) and hence lacks the residues critical for binding $G\alpha_q$ subunit in GRK2. However, the RH domain of GRK1 forms an extensive dimer interface with a buried accessible surface area of ~2,800 $Å^2$ (Fig. 18d). The interface is seen in five crystal forms and a similar dimer exists in the ADP-bound crystal form IV along the crystallographic 2-fold axis. The residues contributing to the dimer interface are conserved in GRK1 and GRK4 sub-families (Fig. 19) and the interface could mediate protein-protein interactions *in vivo*. Preliminary investigations into the physiological role of this interface were performed by steady-state kinetic assays (see Specific Aim 2).

Figure 18. GRK1 RH Domain.

(a) Superposition of RH domains from different crystal forms of GRK1. The kinase domain (yellow) is shown for reference. **(b)** The RH domain of crystal form I (chain B) in the same orientation as in panel a. **(c)** The kinase domains of GRK1 (slate) and GRK2 (red) were aligned in this figure to highlight the differences in the orientation of the RH domain in these two GRK sub-families. The kinase domain of GRK2 is not shown for clarity. Note that the α5 helix is extended in GRK2. **(d)** The dimerization interface mediated by the RH terminal subdomain. The terminal subdomains have been colored slate and magenta to represent the two monomers. The side chains of Trp531 and Tyr167 form stacking interactions with their dimer equivalents, and Asp164 forms a hydrogen bond with the backbone of the opposing monomer. The Leu166 and Leu44 side chains also contribute to the hydrophobic core of the interface. The residues contributing to the interface are conserved in GRK1 and GRK4 sub-families, but not in GRK2, which lacks this interface.

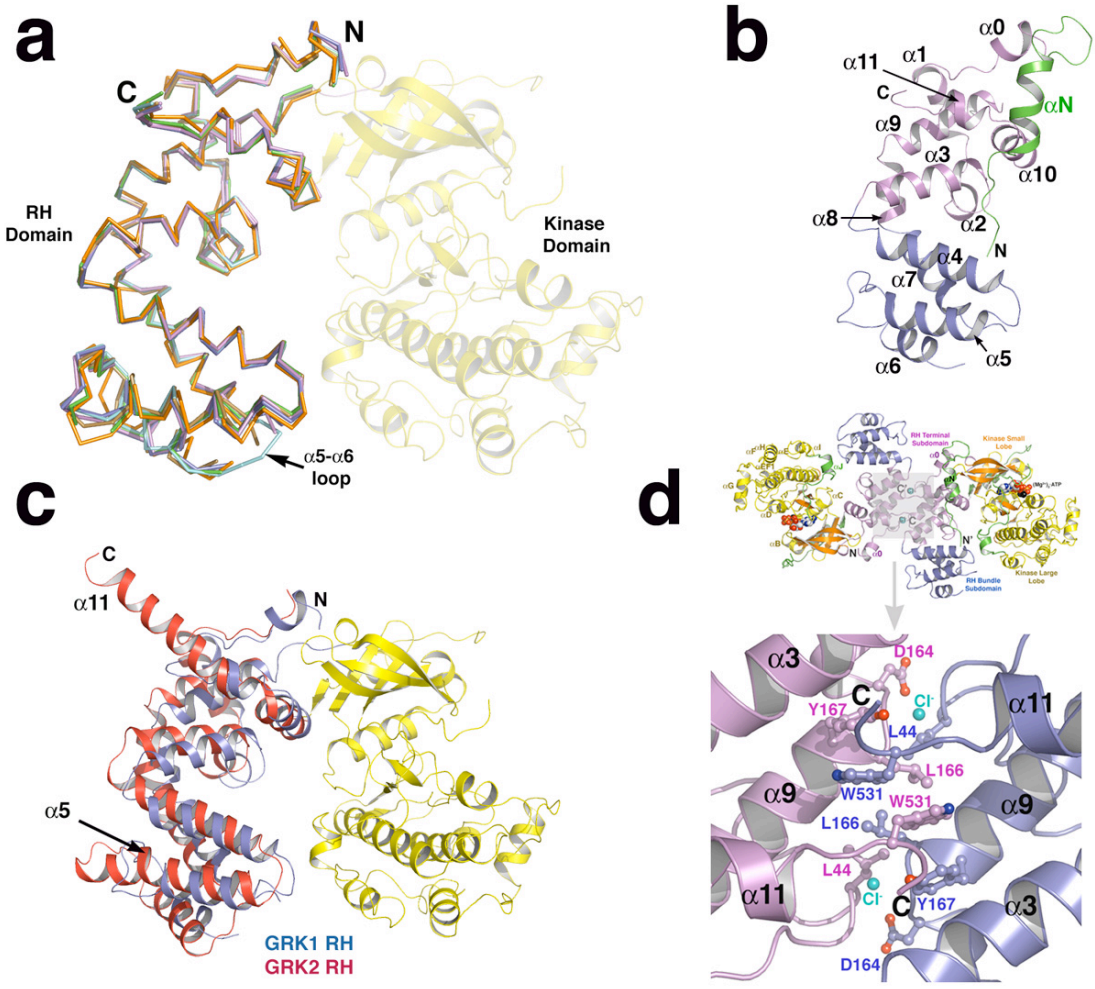

Figure 19. The structural alignment of RH domains of GRKs.

The numbers above the sequence alignment indicate the residue number in GRK1. The terminal and bundle subdomains are colored magenta and slate respectively. The sequence corresponding to the kinase domain (sandwiched between the α9-α10 helices) is not shown in this alignment and is represented by the dots. The α5 helix that is extended in GRK2 [61] with respect to GRK1 and GRK6 [63] is indicated with a translucent helix. The α6-α7 loop is not well-ordered in the GRK1 structures (colored brown). The residues that are structurally variant are colored grey. The residues that form the crystalline dimer interface are colored orange. The green asterisks below the sequence alignment indicate positions of the residues that form the bundle-large lobe interface. All the GRK sequences are bovine, except GRK4 and GRK6. The accession codes for the protein sequences are: GRK1, P28327; GRK2, NP_777135.1; GRK3, P26818; GRK4, AAI17321.1; GRK5, P43249; GRK6, P43250; GRK7, NP_776757.1.

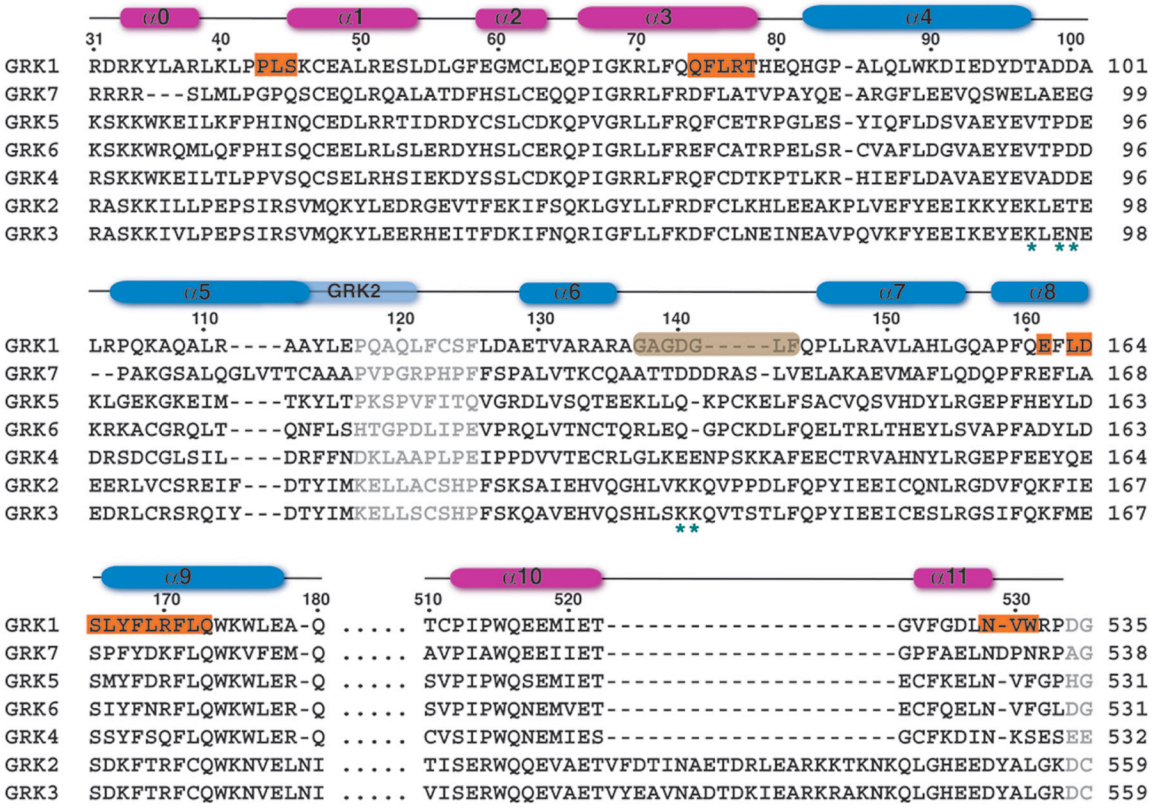

GRK1 Kinase Domain

The kinase domain of GRK1 shares 39-55% identity with the other 6 members of the GRK family and ~34 % sequence identity to those of other AGC kinases such as PKA and PKB. The kinase domain is comprised by a "small lobe" (residues 181-268) and a "large lobe" (residues 269-454) with the active site situated in the cleft between the two lobes. Even though GRK2 and GRK6 were co-crystallized with nucleotides or their analogs, the nucleotide was not well ordered [60, 61, 63, 97] and their kinase domain crystallized in an "open" conformation similar to the "open" inactive structures of PKA [98].

Nucleotide Binding and Conformational Changes

In all the nucleotide-bound structures of GRK1 both ATP and ADP are well ordered and the binding is analogous to that of AGC kinases wherein the conserved catalytic Lys216 residue (β3 sheet) coordinates with the phosphates of nucleotide. The active site of the nucleotide-bound structures is characterized by the presence of two Mg^{2+} ions except in the chain A of crystal form I and II wherein the Nζ atom of Lys497 residue from a symmetry-related molecule displaces one of the Mg^{2+} ions inducing an unusual C2'-endo conformation of the purine ring (Fig. 20a). In the ATP complex, the first metal ion coordinates the β and γ, and the second metal ion the α and γ phosphates (Fig. 20b). In the ADP complex, the metal ions coordinate the β, and the α and β phosphates, respectively (Fig. 20c). Thus, the active site of the $(Mg^{2+})_2$·ATP complex of GRK1 closely resembles that of the PKA·$(Mn^{2+})_2$·ATP complex [99], while the ADP complex resembles the Aurora-A·$(Mg^{2+})_2$·ADP complex [100].

Figure 20. Electron density omit maps of the nucleotide binding site.

(a) The substrate complex of GRK1 contoured at 4σ, wherein ATP, Mg^{2+} (black) and associated waters (green) were excluded from refinement (chain A, crystal form I). Lys216 (β1 sheet, orange carbons) coordinates the α- and β-phosphates of ATP and ADP. Glu332 (yellow carbons) coordinates both Mg^{2+} atoms close to the phosphates of the nucleotide. In this ATP·GRK1 structure, the structural Mg^{2+} ion in the active site is displaced by the Nζ atom of Lys497 (green carbons) donated by a crystal contact. As a consequence, the ribose sugar of ATP displays the C2'-endo conformation as opposed to the C3'-endo conformation observed in the other GRK1 nucleotide complexes (b and c). **(b)** The substrate complex of GRK1 contoured at 4σ (chain B, crystal form I). Asn319, which coordinates the structural Mg^{2+}, was omitted for clarity. **(c)** Product complex of GRK1. A σ_A-weighted $|F_o|-|F_c|$ omit map contoured at 5σ, wherein ADP, Mg^{2+} and associated waters were excluded from refinement (crystal form IV).

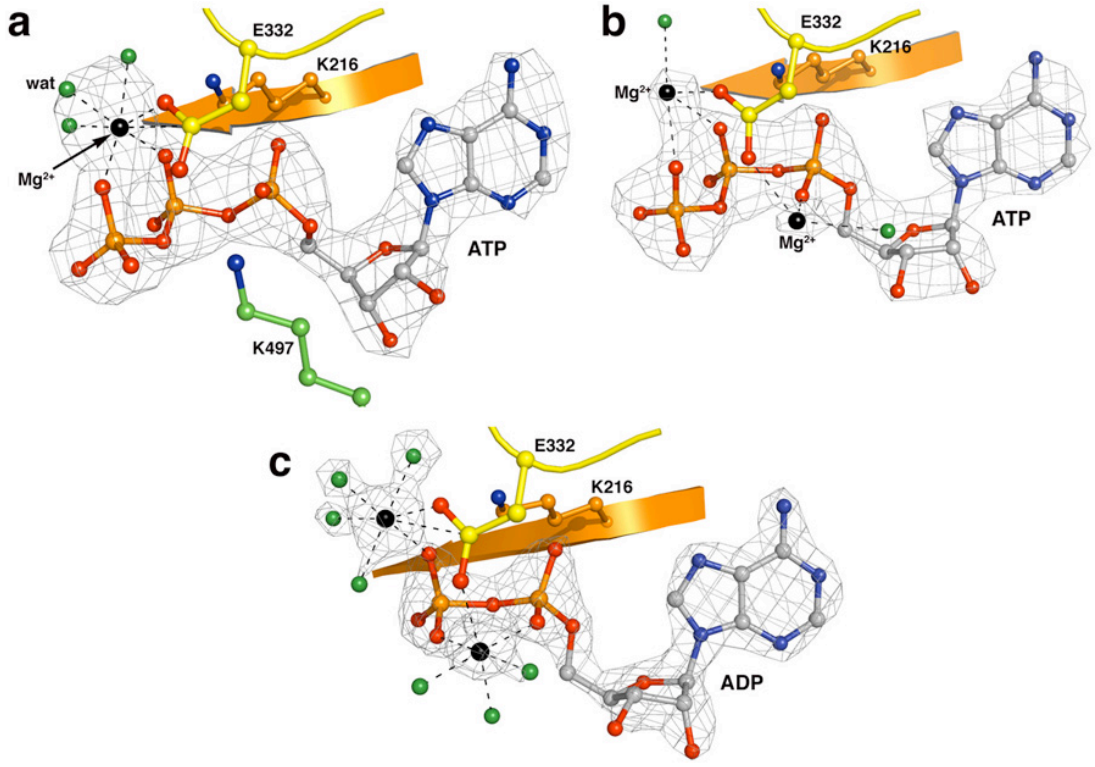

In AGC kinases, the β1-β2 loop (small lobe) contains the glycine-rich conserved GxGxFG motif (residue 194-199 in GRK1) that forms the phosphate-binding loop ("P-loop"). Nucleotide binding is associated kinase domain "closure" that involves reorientation of the Gly-rich P-loop and the active site residues that make contacts with the ribose moiety and the phosphate group of ATP. Although the substrate binding site is preformed, "closure" of the kinase domain is associated with exclusion of water molecules from the active site and orientation of residues in the αD helix and the αF-αG loop that are implicated in substrate binding. The tip of the P-loop is still dynamic and moves closer to the catalytic site when peptide substrate docks onto the large lobe and mediates contacts with the small lobe [96, 98, 99, 101]. Comparison with the "active" structure of PKA reveals that in GRK1 the P-loop is shifted by ~2.3 Å away from the nucleotide binding site. The conformation of this loop in the different nucleotide-bound structures of GRK1 is similar to that in nucleotide-free GRK2 and AMPPNP-bound GRK6 structures [60, 61, 63, 97]. The structural difference in GRKs could result from GRK-specific substitutions in the adjacent αB helix. In GRKs there is a conserved glycine residue (Gly228 in GRK1), which is substituted by a bulkier residue in other AGC kinases (Gln84 and Glu193 in PKA and PKB respectively). The presence of a smaller residue would allow the Phe198 residue (in the P-loop) to pack against the αB helix. Thus, there is no evidence of a conformational change in the P-loop in GRKs upon binding to nucleotide substrates. Since the "regulatory" kinase C-terminal extension packs near this region it is possible that this site could be involved in mediating interaction of GRKs with the activated GPCRs. In the receptor-docked kinase, the P-loop may adopt a conformation similar to that in the "active" transition-state PKA structure [96].

In case of GRK1, the various nucleotide bound kinase domains adopt a similar conformation with r.m.s.d. values of 0.3-0.71 Å for equivalent Cα atoms. Interestingly, the kinase domains of apo-GRK1 have a distinct conformation from each other and from the nucleotide bound structures (dictated, in part, by unique crystal contacts) suggesting that in the nucleotide free state the kinase is conformationally flexible and that the presence of ATP or ADP stabilizes the domain. This is in agreement with the observation that the apo-GRK1 crystals diffract poorly. Even though the apo structure of GRK1 is a low resolution structure it is still informative when considering the differences in the relative orientation of the two lobes of the kinase domain. The superposition of the small lobes of various ATP and ADP bound forms with those of the apo-GRK1 reveal that nucleotide binding leads to a ~ 8° (Fig. 21a) closure of the kinase domain but even so, the active site catalytic machinery is still not properly aligned. The catalytic base Asp314 is ~3 Å away from the γ-phosphate when compared to the structure of ADP·AlF_3 bound transition state complex of PKA [96]. Thus, nucleotide binding alone is not sufficient to provide the free energy required for domain closure. Superposition of the small lobes reveals that an additional ~13-15° rotation of large lobe is required (along an axis running roughly parallel to and between the αD and αE helices) to attain the "closed" active conformation (Fig. 21b) (Table 5). The required domain closure leading to activation of the kinase could be achieved when GRKs dock to an activated GPCR.

Structural Comparison of the Kinase Peptide-Binding Channel

By analogy to the AGC kinases, the peptide-binding surface lies on the large lobe adjacent to the nucleotide-binding site with αD-αE and αF-αG loops forming the walls of the channel. Comparison with PKA structure reveals that both these loops are longer in GRKs (a 4-residues insertion in GRK1) and hence adopt distinct conformations. The binding of Glycogen Synthase Kinase 3β (GSK3β) peptide to the large lobe of PKB

(PDB 1O6L) reveals that the peptide-binding channel is wider in GRK1, reflecting its more "open" conformation (Fig. 21e,f). The phosphoacceptor oxygen is > 4 Å away from the γ-phosphate of ATP, which is too far to achieve catalysis. In addition, the N-terminus of the modeled peptide is obstructed by the αF-αG loop. This was also observed in the GRK6 structure. Thus, either the peptide substrates bind GRKs in a distinct manner or the channel might assume a different conformation when docked to a receptor. The electrostatic surface representation reveals that the channel bears an overall basic character, which may explain why GRK1 prefers acidic substrates.

Figure 21. The structural comparison of the GRK1 kinase domain.

(a) The kinase domain adopts a similar conformation in the various nucleotide-bound ligand states of GRK1. The kinase C-terminal extension is not modeled in this figure, for clarity. **(b)** The small lobe of the transition state PKA complex (magenta) was aligned with that of the GRK1·$(Mg^{2+})_2$·ADP (green) complex to compare the relative orientations of their large lobes. The brown circle indicates the position of the rotation axis (coming directly out of the figure) around which the large lobe of GRK1 would have to rotate 15˚ to assume the same conformation as PKA. **(c)** A rotation of ~ 8° is associated with nucleotide-binding in GRK1. **(d)** The conformation of the apo GRK1 (chain A) structure (orange) is more similar to the GRK6·Mg^{2+}·AMPPNP (cyan). **(e)** The peptide binding channel of GRK1. The channel has a strikingly basic character, explaining why GRK1 prefers acidic substrates [102, 103] and how it can phosphorylate multiple closely spaced Ser and Thr residues at the C-terminus of Rho*. The channel is also wider in GRK1 than in nucleotide-bound PKB (see panel f). A model of residues 332-345 from the C-terminus of Rho*, is shown as a stick model docked to the large lobe with Ser338 in position to be phosphorylated (position "+0"). The molecular surface of GRK1 is colored by its electrostatic potential from -7 (red, acidic) to +7 (blue, basic) kT/e^-. **(f)** The GSK3b peptide bound to PKB. The PKB kinase domain (PDB code 1O6L) is in its closed conformation and thus the channel is much narrower. The channel is acidic and the kinase has a preference for basic substrates.

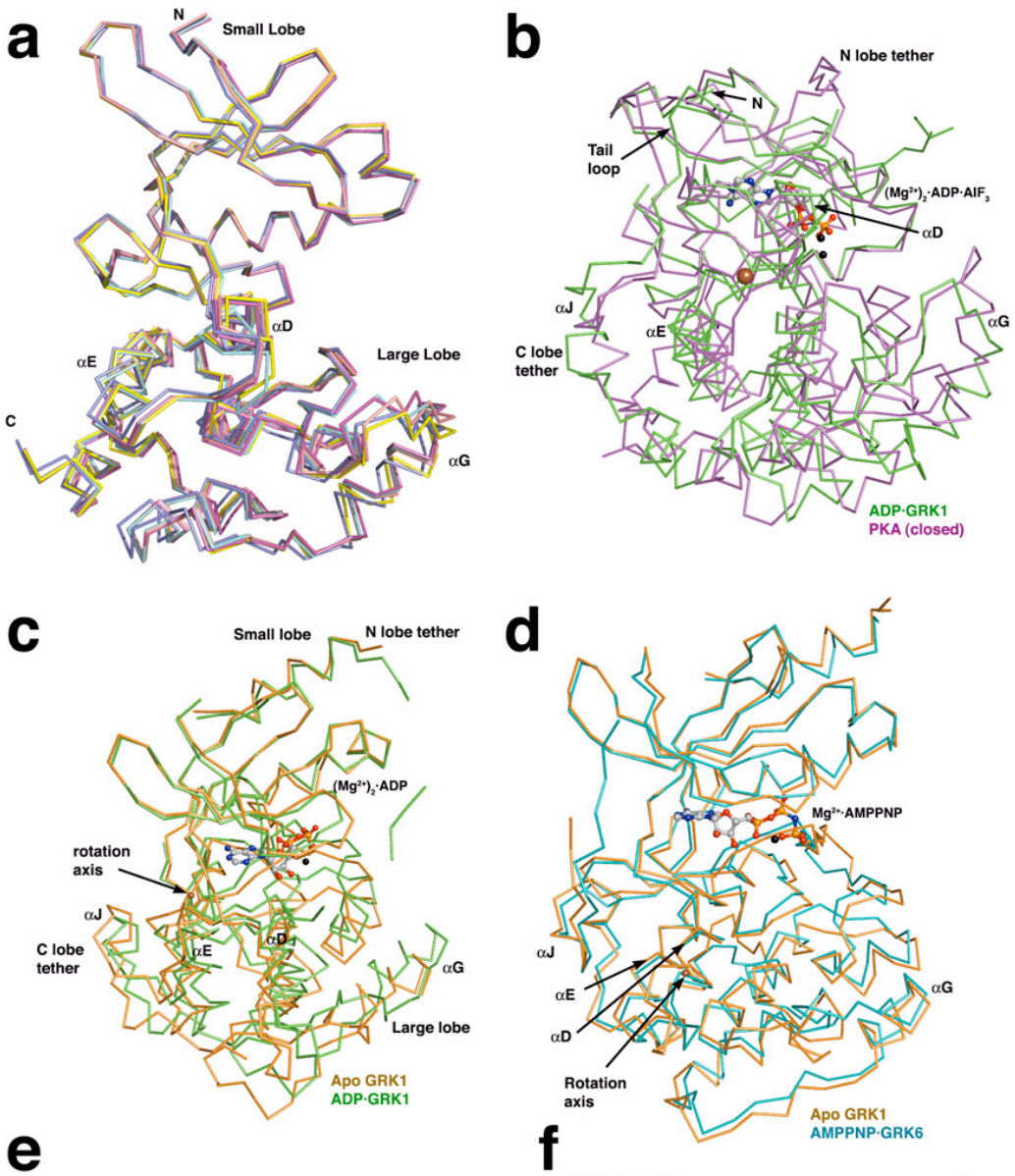
a
N
Small Lobe
αD
αE
Large Lobe
C
αG
b
N lobe tether
N
Tail loop
(Mg2+)2·ADP·AlF3
αD
αJ
αE
αG
C lobe tether
ADP·GRK1
PKA (closed)
c
Small lobe
N lobe tether
(Mg2+)2·ADP
rotation axis
αJ
C lobe tether
αE
αD
αG
Large lobe
Apo GRK1
ADP·GRK1
d
Mg2+·AMPPNP
αJ
αE
αD
αG
Rotation axis
Apo GRK1
AMPPNP·GRK6
e
Small Lobe
Rhodopsin C-tail peptide
GRK1
αF-αG loop
Large Lobe
f
PKB
GSK3β
+3
+2
+1
+0
-1
-2
-3
-4
-5
-6

Table 5. Comparison of kinase domains.

Rotation of large lobe relative to small lobe required to achieve a conformation similar to the closed state of PKA.

	PKA_c	PKB_c	PKA_o	PKB_o	I	II	IIIa	IIIb	IV	V	VI	GRK2	GRK6
PKA_c	**0**	**4**	**13**	**13**	**14**	**13**	**20**	**12**	**15**	**13**	**15**	**20**	**17**
PKB_c		0	129	29	110	108	130	132	103	107	109	97	120
PKA_o			0	100	20	24	8	20	29	26	24	32	14
PKB_o				0	81	79	101	103	74	78	81	68	91
I					0	5	20	27	10	8	8	13	11
II						0	22	26	5	3	4	14	12
IIIa							0	12	27	23	21	33	10
IIIb								0	31	26	23	39	15
IV									0	4	7	11	17
V										0	3	15	13
VI											0	17	11
GRK2												0	24
GRK6													0

The "c" and "o" subscripts refer to the "closed" (catalytic) and "open" conformations of PKA and PKB. PKA_c = PDB code 1L3R; PKA_o = 1CMK; PKB_c = 1O6K; PKB_o = 1MVR. I-VI refer to the different crystal forms of GRK1. For GRK1 and GRK6, the sequence analyzed corresponds to the "A" chain of their structures unless otherwise specified. Red numbers are the degrees required to superimpose the kinase large lobe of each of these structures with that of PKA_c. All other values indicate the difference in degrees between the rotation axes required to superimpose the large lobes, as determined by the direction cosines of each of the rotation axes. Hence, small values indicate that the rotation axes are similarly oriented, and large values indicate large discrepancies (e.g. 90° indicates they are orthogonal). Not all the rotation axes intersect. The GRK rotation axes required to achieve the closed conformation are quite similar and intersect (with the exception of crystal form III) while those required to close the domains of PKA and PKB are unique. Note that among the GRK1 rotation axes, those of the apo-GRK1 (crystal form III) are the most divergent (yellow highlights). They are most similar to, although significantly different from, each other (blue highlight), indicating not only a large degree of flexibility in apo-GRK1, but also a discrete conformational state. The conformation of the apo-GRK1 domains are most similar to those of GRK6 (2ACX, grey highlights).

GRK1 Kinase C-terminal Extension

The residues 455-511 span the kinase C-terminal extension of GRK1, a region that plays a regulatory role in non-GRK AGC kinases. The kinase extension has been divided into three different elements: the C-terminal (large) lobe tether (CLT; residues 455-471 in GRK1), an active site tether (AST; residues 472-480) and N-terminal (small) lobe tether (NLT; residues 498-511). While the CLT and the NLT were observed in GRK2 and GRK6, no structural information is available for AST of GRKs. Together with other elements of the C-terminal extension, the AST is thought to coordinate the nucleotide and peptide binding with domain closure thereby activating the kinase [64].

The GRK CLT is structurally analogous to those of PKA and PKB, but uniquely interacts with the adjacent RH domain. The AST contributes residues to the nucleotide binding site and is disordered in structures of PKA that lack ligands in the active site. This is true for GRK1 structures, as the AST was observed in only the ATP or ADP bound structures, except when displaced by crystal contacts (in one chain of crystal forms I, II and VI) (Fig. 22b). The GRK1 AST begins with the "tail loop" (residues Asp472-Tyr477), which is 4 residues shorter than the analogous loops of PKA and PKB (Fig. 2b). The tail loop lies in close proximity to the active site and packs adjacent to the hinge connecting the two lobes of the kinase domain. The side chain of GRK1-Tyr477 (Tyr473 in GRK6, Tyr438 in PKB, Asn478 in GRK2 and Asn326 in PKA) forms a hydrogen bond with the backbone nitrogen of the first residue of the tail loop (Fig. 22a). The next residue, Ala478, is conserved as phenylalanine in all non-GRK AGC kinases, wherein the aromatic side chain contributes to the adenine binding pocket. Interestingly, whereas mutation of this residue in PKA (F327A) has been shown to render the kinase catalytically inactive [104], in GRKs this residue is conserved as either an alanine or a cysteine. The striking lack of a phenylalanine at this position may help render GRKs

catalytically silent until receptor binding. The side chain of the next residue, Lys479 (GRK1), extends towards the peptide-binding channel where it could interact with an acidic peptide substrate. These features suggest that the GRK1 AST will be one of the key elements involved in receptor-mediated activation and the phosphorylation of polypeptide substrates.

Residues 481-489 of GRK1, which connect the AST to the NLT, wander over the surface of the β1-β2 strands and αB helix of the small lobe. This region, however, follows several distinct paths among GRK1 structures that are, at least in part, dictated by unique crystal contacts. However, in every case the path is distinct from those of PKA and PKB, consistent with this region being poorly conserved among AGC kinases. Although the backbones of Ser488 and Thr489 (autophosphorylation sites) are visible in some structures, high temperature factors (Fig. 15) prevent interpretation as to whether they are phosphorylated in the crystal, even though the presence of phosphorylation at both sites was detected by mass spectrometry in ATP-treated $GRK1_{535}$-His_6 (Fig. 17d). These residues map to the "turn motif" of AGC kinases. Phosphorylation of this site in PKC stabilizes the kinase and enhances activity. Indeed, given their location on the surface of GRK1, Ser488 and Thr489 phosphorylation may permit stabilizing electrostatic interactions with Arg222 and Lys221, respectively in the αB helix (Fig. 16a inset).

The last element of the kinase extension, the NLT (residues 490-511 in GRK1, (Fig. 22b) follows a common path in all GRKs, and its extreme C-terminus (502-511) is structurally analogous to those of PKA and PKB with the motif contributing a final, short β10 strand to the small lobe of the kinase domain in both GRKs and PKB. The GRK1 NLT contains the hallmark hydrophobic motif, but lacks the phosphorylation site characteristic of PKB and PKC, presumably because the immediate re-entry of the

polypeptide chain to begin α10 of the RH domain keeps this motif fixed in place in lieu of phosphorylation.

Figure 22. The kinase C-terminal extension of GRK1.

(a) The AST regions of GRK1 and PKB. For this comparison, the coordinates of the various GRK1 crystal forms were merged to generate a composite structure of GRK1 that spans residues 5-533 (out of 558), and the large lobe was rotated to generate the expected closed, active state. The kinase C-terminal extension of PKB is grey, and the GSK3β peptide bound to PKB is cyan. The "tail-loop" of GRKs is 4 residues shorter than those of either PKB or PKA, resulting in formation of a shallow canyon with the hinge of the kinase domain at the bottom. This region forms a putative receptor-docking site (transparent ellipse). **(b)** Structural alignment of the kinase C-terminal extension of GRKs with PKA and PKB. The alignment was carried out using ClustalW followed by manual alignment of the residues corresponding to the active site and the C-lobe tether. The region immediately following the AST is structurally divergent among GRKs, PKA and PKB and thus no alignment is attempted. The numbers above the alignment refer to the sequence of bovine GRK1. The different segments of the C-terminal extension that were observed in each of our crystal forms are indicated below the alignment, with the black regions corresponding to structurally heterogeneous portions in each structure that appear influenced by crystal contacts. Accession codes for the protein sequences are: GRK1, P28327; GRK2, NP_777135.1; GRK3, P26818; GRK4, AAI17321.1; GRK5, P43249; GRK6, P43250; GRK7, NP_776757.1; PKA, 1L3R; PKB, 1O6L.

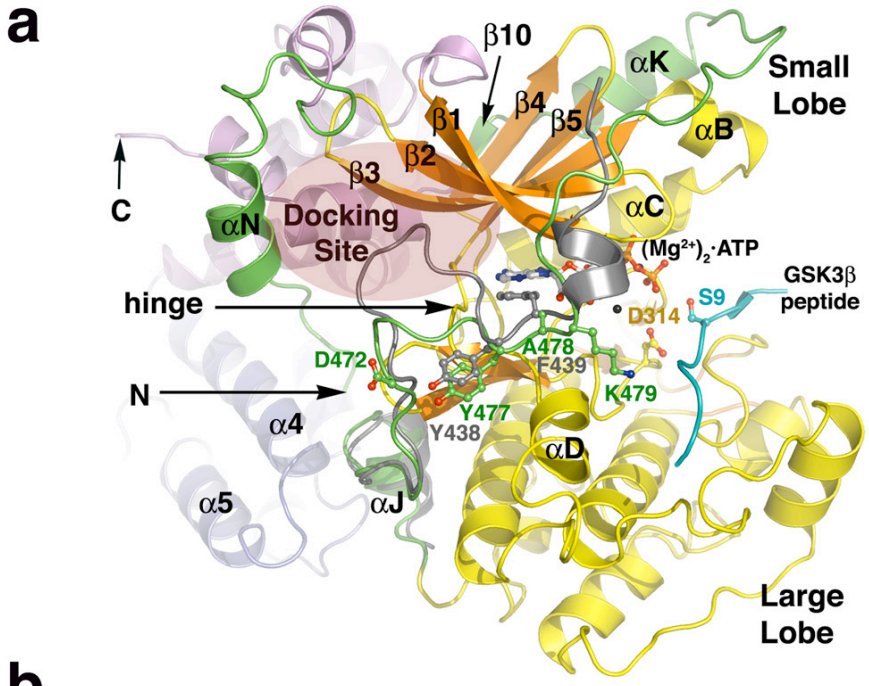
a
β10
αK
Small
Lobe
β1
β4
β5
αB
β2
β3
C
αN
Docking
Site
αC
(Mg2+)2·ATP
GSK3β
peptide
hinge
S9
D314
A478
F439
D472
K479
N
Y477
Y438
α4
αD
α5
αJ
Large
Lobe

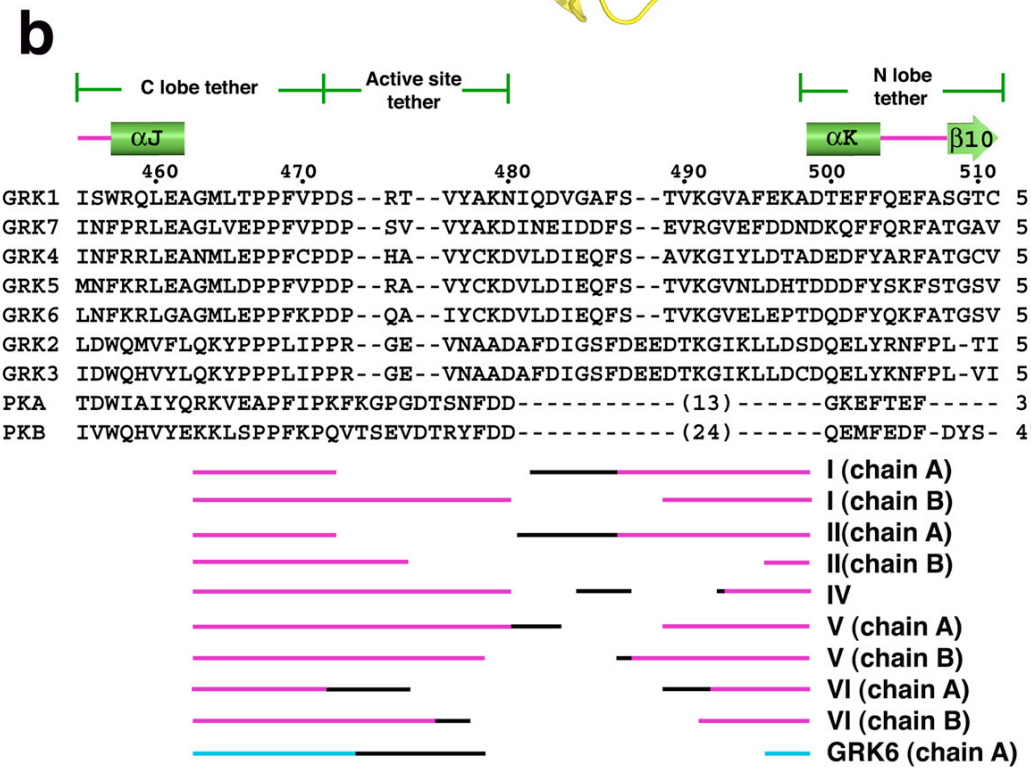
b
C lobe tether
Active site
tether
N lobe
tether
αJ
αK
β10
460
470
480
490
500
510
GRK1 ISWRQLEAGMLTPPFVPDS--RT--VYAKNIQDVGAFS--TVKGVAFEKADTEFFQEFASGTC 511
GRK7 INFPRLEAGLVEPPFVPDP--SV--VYAKDINEIDDFS--EVRGVEFDDNDKQFFQRFATGAV 511
GRK4 INFRRLEANMLEPPFCPDP--HA--VYCKDVLDIEQFS--AVKGIYLDTADEDFYARFATGCV 508
GRK5 MNFKRLEAGMLDPPFVPDP--RA--VYCKDVLDIEQFS--TVKGVNLDHTDDDFYSKFSTGSV 507
GRK6 LNFKRLGAGMLEPPFKPDP--QA--IYCKDVLDIEQFS--TVKGVELEPTDQDFYQKFATGSV 507
GRK2 LDWQMVFLQKYPPPLIPPR--GE--VNAADAFDIGSFDEEDTKGIKLLDSDQELYRNFPL-TI 513
GRK3 IDWQHVYLQKYPPPLIPPR--GE--VNAADAFDIGSFDEEDTKGIKLLDCDQELYKNFPL-VI 513
PKA TDWIAIYQRKVEAPFIPKFKGPGDTSNFDD----------(13)------GKEFTEF----- 351
PKB IVWQHVYEKKLSPPFKPQVTSEVDTRYFDD----------(24)------QEMFEDF-DYS- 476
I (chain A)
I (chain B)
II(chain A)
II(chain B)
IV
V (chain A)
V (chain B)
VI (chain A)
VI (chain B)
GRK6 (chain A)

AIM 2: FUNCTIONAL ANALYSIS OF GRK1

The structures of GRK1 along with mass spectral analysis identified phosphorylation of GRK1 at several previously unidentified sites (Ser5 and Thr8). In addition, the RH domain was observed to form a dimer interface in all the six crystal forms. Using site-directed mutagenesis, roles of the N-terminal residues (Ser5 and Thr8) and the residues at the dimer interface were tested in the steady state kinetics assays in context of the full-length protein. The soluble fraction of wild-type GRK1 was chosen for the initial studies, as there was sufficient amount of material available. Based on the time course of Rho* phosphorylation, a 10 minute end point was chosen so that the rhodopsin phosphorylation was in a linear range (Fig. 23a). Initially, GRK1 wild-type and mutant proteins were purified in separate soluble and the membrane fractions, as the latter is expected to be farnesylated at the C-terminus. However, the steady state kinetics revealed that the K_m for Rho* were similar (2-4 μM) for both fractions of the protein. Thus, some of the proteins used in the assays were purified as a mixture. Based on the kinase titrations, the assays were conducted using either 18 nM soluble fraction of GRK1 (Fig. 23b) or 8 nM membrane fraction or a mixture of both (Fig. 23c).

Phosphorylated N-terminus

Evidence for phosphorylation at Ser5 and Thr8 sites has not been reported so far, although it has been suggested that GRK1 can incorporate 3-4 phosphates by autophosphorylation [25]. Because these sites were in the critical N-terminus of GRKs, we investigated whether the activity of GRK1 would be affected if these residues were mutated to an alanine or aspartate/glutamate (to mimic constitutively phosphorylated residues) by site-directed mutagenesis. The expression of T8D mutant was poor and the S5D mutant was unstable when purified. This was observed even when different batches

of baculoviruses were used for protein expression. As a result, the effect of these mutants could not be tested. The S5A, T8A and T8E mutants phosphorylated Rho* similarly to the wild-type GRK1 (Table 6). Thus, these *in vitro* assays did not reveal any significant effects of the N-terminal phosphorylations.

Analysis of the crystalline dimer interface

Although GRK1 is monomeric in solution based on size exclusion chromatography and analytical ultracentrifugation, we tried to assess the physiological significance of the interface as all the six crystal forms of GRK1 were observed to be dimers analogous to that formed by GRK6 [63]. Interestingly, rhodopsin is also predicted to form dimers and higher oligomers [105]. Using site-directed mutagenesis, single (D164A, L166K and W531A) and double mutations (D164A/L166K, D164A/W531A and L166K/W531A) were introduced in wild-type GRK1, all of which disrupt the key interacting residues in the dimer interface. The kinetic properties of D164A and L166K mutants alone and in combination towards Rho* were similar to those of wild-type GRK1 (Table 6). All the W531A-containing single and double mutants were however, unstable and could not be purified to homogeneity suggesting that this residue plays a structural role.

Figure 23. Steady state kinetics.

(a) The time course assay using 50 nM wild-type GRK1 (soluble fractions) and 20 μM ROS. Based on this curve, a 10 minute end point was picked as rhodopsin phosphorylation remains in the linear range. **(b)** The kinase titration using varying amounts of soluble wild-type GRK1 and 20 μM ROS as a substrate. Based on this curve, we picked 125 ng kinase (~18 nM) for assays. **(c)** Similar assays as in (b) but for membrane fraction of wild-type GRK1. Similar curves were obtained when a mixture of soluble and membrane fraction of GRK1 was used. **(d)** A plot of a reaction using GRK1 wild-type in the assays as a reference. The data for wild-type GRK1 and the mutants has been summarized in Table 5. Two measurements were taken for each concentration of ROS in 2-3 independent assays. The signal from GRK1 autophosphorylation is negligible because of the low amounts of kinase used in these assays.

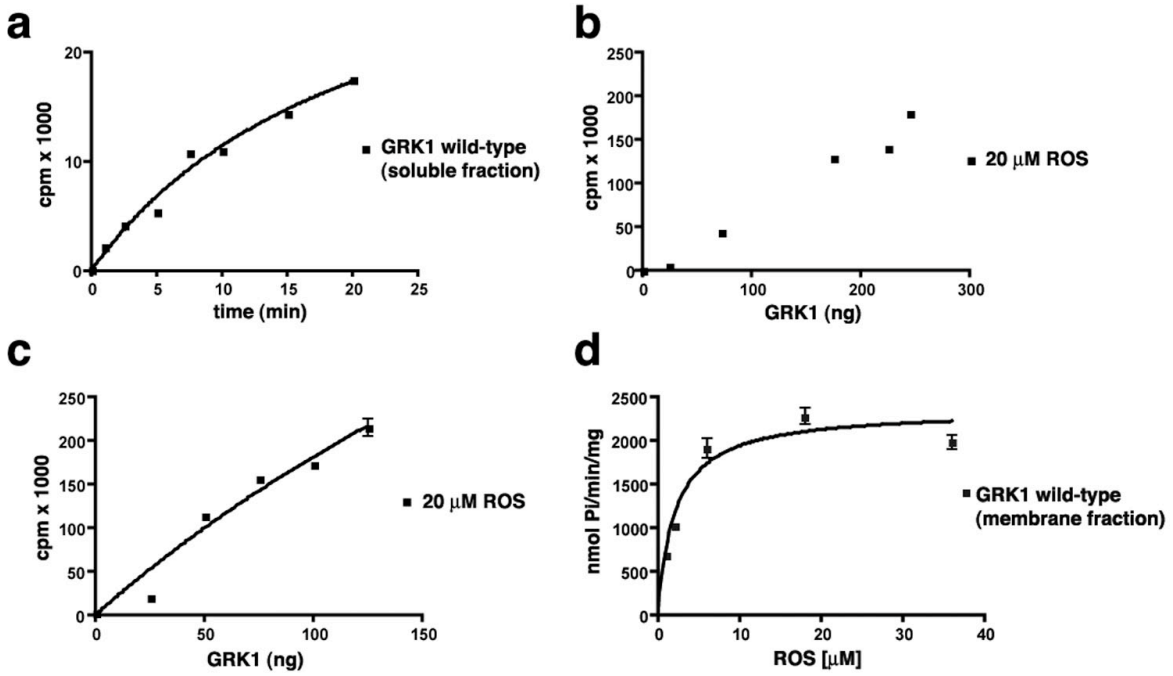

Table 6. Kinetic Analysis of GRK1

$GRK1_{535}$-His_6	K_m (μM)[†]	V_{max} (nmol P_i/min/mg)[†]
Pool A	12±1.5	1100±46
Pool B	5.5±1.0	16±0.80
Pool C	inactive*	inactive*
GRK1		
Wild-type	2.1±0.40	2300±110
Amino-terminal mutants		
S5A	5.1±1.0	1600±69
S5D	ND[‡]	ND
T8A	1.5±0.30	1200±78
T8E	4.8±1.5	1700±130
T8D	ND	ND
Dimer interface mutants		
D164A	3.8±0.7	2300±160
L166K	6.7±0.40	2400±56
W531A	ND	ND
D164A/L166K	3.1±0.60	1100±44
D164A/W531A	ND	ND
L166K/W531A	ND	ND

[†] Results are listed as means ± S.D for two to three independent experiments, with two measurements for each concentration of ROS (1-40 μM). The kinase was assayed at 18 nM (soluble fraction) or 8 nM (membrane fractions and protein purified as a mixture) in 100 μl reactions. The protein amounts were normalized by SDS-PAGE and A_{280} measurements (>95% homogenous). The data was analyzed using non-linear analysis and curve-fitting programs of GraphPad Prism version 4.0a for Macintosh.

[‡] ND = not determined. These mutants either did not express or were unstable.

* These steady-state kinetic parameters could not be estimated owing to poor Rho* phosphorylation. However, the initial rate of Pool C was estimated to be ~20-fold lower than Pool A under similar assay conditions.

Chapter 2. GRKs and Calcium Sensing proteins

INTRODUCTION

Calmodulin and recoverin belong to a class of proteins called calcium sensor proteins (CSP) that undergo a conformational change upon binding calcium and have regulatory functions. Recoverin, a 23 kDa myristoylated protein with four "EF hands", is localized to the vertebrate photoreceptor cells and is highly selective for GRK1 [29]. In the calcium-bound state, recoverin undergoes a conformational change that forms a hydrophobic cleft on the surface of the protein that can bind residue 1-15 of GRK1 [58, 106] (Fig. 24). Recoverin modulates GRK1 activity *in vitro*, in a calcium dependent manner [30], although the affinity for calcium is low (K_d = 2-13 μM) [107, 108]. It was proposed that this interaction prolongs the photoresponse by preventing the phosphorylation of Rho* by GRK1 without affecting the intrinsic kinase activity of GRK1 [58, 109]. The physiological significance of this interaction *in vivo* is not clear as the phosphorylation of Rho* in permeabilized rods and intact retina is not affected by the levels of calcium [110, 111]. It is now believed that recoverin plays a major role at the synapse where Ca^{2+} is a known regulator of the release of neurotransmitters [112].

Calmodulin is a ubiquitous protein and a universal regulator of GRKs. GRK5 is very sensitive to Ca^{2+}·CaM (IC_{50} in nM range) while GRK2 and GRK1 are affected at high concentrations (IC_{50} in μM range or higher) [113]. Interaction with calcium bound CaM appears to block membrane binding and this leads to inhibition of receptor phosphorylation by GRK5. This hypothesis is supported by the observation that the CaM binding site on GRK5 overlaps with the PIP_2 binding site. The CaM binding site have been mapped to both the N- and the C-terminus of GRKs and are not been well-defined for GRK6 [109].

Figure 24. NMR structure of GRK1 peptide bound to Ca^{2+}·recoverin.

Recoverin, a calcium sensing protein, contains four helix-loop-helix motifs (four EF hands) with EF-1 (wheat) and EF-2 (slate) forming the N-domain and EF-3 (green) and EF-4 (salmon) forming the C-domain. The calcium ions are shown as orange colored spheres. Compared to calmodulin and other calcium-binding proteins, recoverin contains extra residues at the N- and C-terminus and an insertion (yellow and grey helices) between the EF-3 and EF-4 hands. In addition, recoverin lacks an extended α-helical insertion between the N- and C-domain and hence forms a more compact structure as opposed to a dumbbell (as seen in calmodulin). The N-terminal helix (yellow) is usually disordered or is sequestered in a calcium free state. In calcium-bound state the helix is extruded (calcium-myristoyl switch) and recruits recoverin to the membrane. This also exposes a hydrophobic surface on the protein in the N-domain that binds GRK1 (magenta). (PDB accession code: 2I94).

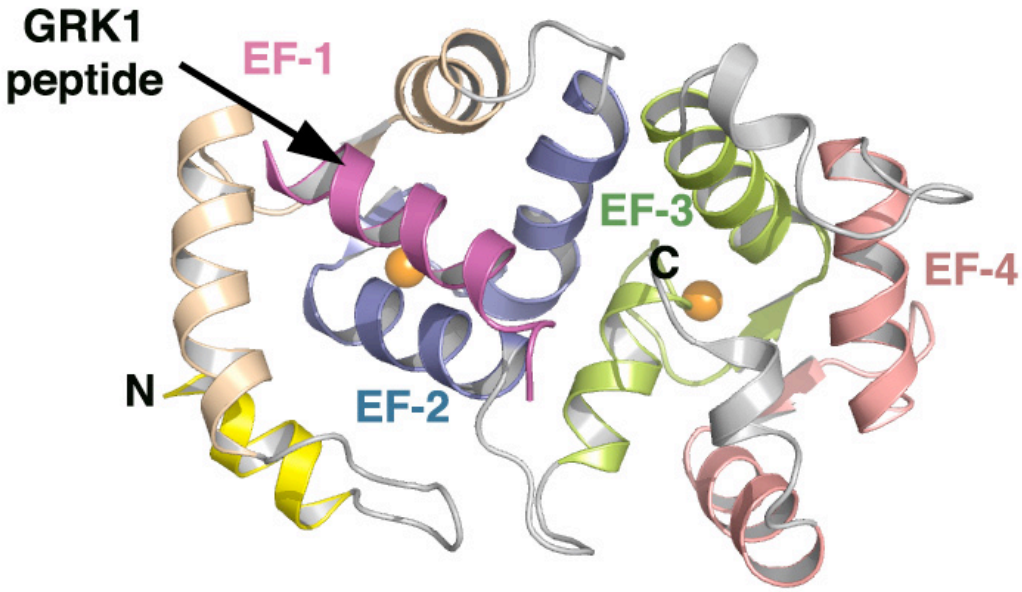

Project Goals

Determine the structure of Ca^{2+}·calmodulin·GRK6

The amino-terminus of GRKs has been implicated in receptor recognition and/or activation [45, 49, 57]. In the crystal structure of human GRK6 (PDB code 2ACX) this region of the protein was disordered. The aim of this project was to isolate and crystallize a complex of GRK6 with calmodulin. The crystal structure of GRK6·calmodulin complex would help in predicting the structure of the N-terminus of GRK6 and would also help map the calmodulin-binding sites on GRK6.

Determine the structure of Ca^{2+}·recoverin·GRK1

The second aim of this project was to isolate a complex of GRK1 ($GRK1_{1-535}$-His_6 construct) and recoverin for structural studies. The structure of this complex would reveal the structure of the amino-terminus of GRK1 in the context of the full-length modular protein and would reveal additional sites of interaction. This would help us gain insights into the physiological significance of this interaction *in vivo*, which is currently debated.

METHODS

Purification of Soluble Mutant (Pal$^-$) of GRK6

The soluble mutant of human GRK6, which lacks all the palmitoylation sites (soluble GRK6 or sGRK6) was expressed and purified as described earlier [63] with the only difference being that the last ion-exchange purification step was carried out on SP Sepharose (Pharmacia) column instead of Source 15S.

Attempts to Isolate a Complex of sGRK6 with Ca^{2+}·calmodulin

Lyophilized bovine calmodulin (Calbiochem) was reconstituted in 1 ml buffer consisting of 20 mM Na-HEPES, pH 7.0, 100 mM NaCl, and 100 μM $CaCl_2$ and stored at –20 ºC. Calmodulin and sGRK6 (20 mM Na-HEPES, pH 8.0, 200 mM NaCl, 2 mM DTT) were mixed in 2:1 molar ratio and the reaction mixture was supplemented with $CaCl_2$ to a 1 mM final concentration. The protein mixture was incubated on ice for an hour before loading onto two tandem Superdex 200 HR 10/30 columns (Pharmacia) pre-equilibrated with 20 mM Na-HEPES, pH 8.0, 100 mM NaCl, 1 mM $CaCl_2$, and 1 mM DTT. Under these conditions, we were not able to demonstrate that GRK6 binds Ca^{2+}·calmodulin (Fig. 25).

Figure 25. Attempts to isolate a potential complex of sGRK6 with Ca^{2+}·calmodulin using size-exclusion chromatography.

A mixture of 1:2 molar ratio of the two proteins was loaded onto two tandem Superdex 200 columns in a running buffer containing 1 m*M* $CaCl_2$. Calmodulin did not associate detectably with sGRK6 as the two proteins elute in two separate peak fractions.

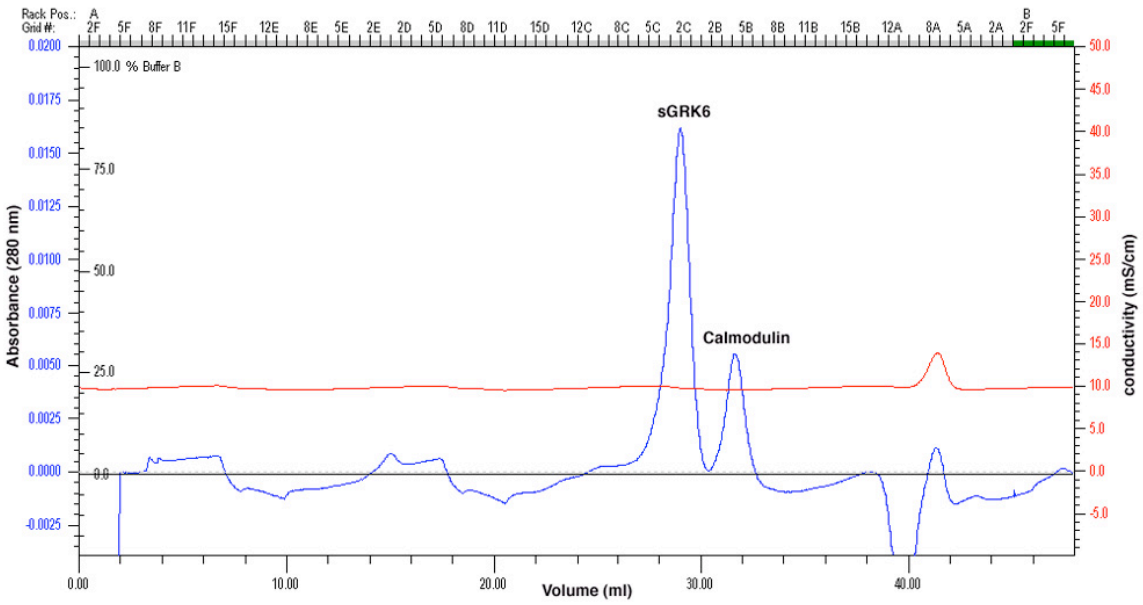

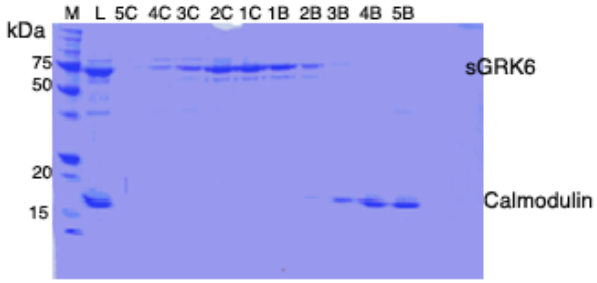

Expression and Purification of Ca^{2+}·Recoverin

The pTrec2 expression vector encoding bovine non-acylated (NA) recoverin was purchased from American Type Culture Collection (ATCC). The expression and purification of NA-recoverin was carried out as described earlier [114] with a few modifications in the protocol. Recoverin expression was enhanced when 250 ml DH5α cells (100 μg/ml ampicillin) in Terrific broth (EMD) were grown (30 °C) in 2 L flasks (instead of 1 L per flask) as this helps with efficient and uniform heating of the culture during heat induction. After 4-5 hours of induction at 42-45 °C, cells were harvested by centrifugation. The cell pellet was resuspended in ice-cold lysis buffer (10 ml/L of culture) containing 50 mM Na-HEPES, pH 8.0, 10% glycerol, 5 mM EDTA, 1 mM DTT and 0.1 mM PMSF (phenylmethanesulfonylfluoride) and was frozen in liquid nitrogen.

Thawed cell slurry was diluted in twice the volume of cold lysis buffer containing 0.1 mM PMSF. Cells were lysed by a single pass through Avestin C3 high pressure homogenizer at 20,000 psi. The first centrifugation was carried out for 20 minutes at 10,000 X g in a Beckman JA-17 rotor (4 ºC). Solid ammonium sulfate was added to the supernatant to 65 % saturation while stirring the solution on an ice-bath. The solution was stirred for one hour and the precipitated proteins were removed by centrifugation at 10,000 X g for 20 minutes in JA-17 rotor. The supernatant was collected and filtered using a glass filter (Fisherbrand). Purification using Phenyl-Sepharose column (Pharmacia) was skipped, as no significant purification was achieved using this column in our hands. The filtered supernatant was dialyzed against 2 L dialysis buffer (20 mM Na-HEPES, pH 8.0, 10% glycerol, 2 mM $MgCl_2$, and 1 mM DTT) for a few hours and then overnight against fresh 4 L dialysis buffer at 4 ºC (Fig 15A). The dialyzed sample (volume doubles during dialysis) was diluted 3-4 fold with fresh dialysis buffer to ensure that conductivity of the solution was close to 5 mS/cm. The protein solution was loaded

onto 7.85 ml Source Q column (Pharmacia) pre-equilibrated with dialysis buffer. Majority of the contaminating proteins but not recoverin bind the Q column (Fig. 15B). Amicon stirred cell (Millipore) with 10 kDa MWCO filter (Millipore) was used for concentrating 600 ml of protein solution to about 50 ml which, was further concentrated using a 30 kDa MWCO centriprep (Millipore) to about 10 ml. Protein was flash-frozen as 50 μl pellets in liquid nitrogen.

NA-recoverin was purified in batches (~ 1 ml at a time) on two tandem Superdex 75 HR 10/30 columns (Pharmacia) pre-equilibrated with NA-recoverin gel filtration buffer (20 mM Na-HEPES, pH 8.0, 100 mM NaCl, 5% glycerol, 2 mM $MgCl_2$, 1 mM $CaCl_2$, and 1 mM DTT). The molecular weight of the unmyristoylated recoverin was estimated to be 28 kDa (calculated mass is 23.3 kDa) based on the elution of standard proteins of known molecular weights (Bio-Rad) (Fig. 15C). Protein concentration was quantified by Bradford (Bio-Rad) assay and 12% gels were used to assess the purity of protein at various stages of purification. The yield of pure protein varied from 10 - 15 mg/L of culture.

Figure 26. Purification of Ca^{2+}·recoverin

(A) Gel representing purification by ammonium sulfate salting-out procedure. Samples have been labeled from left to right as; (M) protein standards, (P1) pellet fraction after lysis, (S1) supernatant fraction containing soluble protein after lysis, (P2) pellet fraction from ammonium sulfate fractionation step, (S2) supernatant fraction post-ammonium sulfate fractionation, (D) protein sample after extensive overnight dialysis.

(B) - (C) Purification of NA-recoverin on Source Q column. Even after extensive dialysis and dilution of protein to lower the ionic strength of the solution, NA-recoverin does not bind the column. The contaminating proteins are eluted in a 100 ml gradient of 0-200 mM NaCl (shown in green box, panel C). Samples have been labeled as: (M) protein standards, (L) dialyzed and diluted protein loaded onto 7.85 ml Source Q column, (FT) Flow-through of loading protein on Source Q column, (Fractions) fractions eluted with a NaCl gradient (shown in green box in panel C).

D) Purification of NA-recoverin on gel filtration column. 1-2 ml of concentrated and filtered protein (flow-through of loading on Source Q column) was loaded (labeled 'L' on the gel) on two tandem Superdex 75 columns and eluted in running buffer containing 1 mM $CaCl_2$. The peak fractions containing NA-recoverin have been marked with magenta colored box.

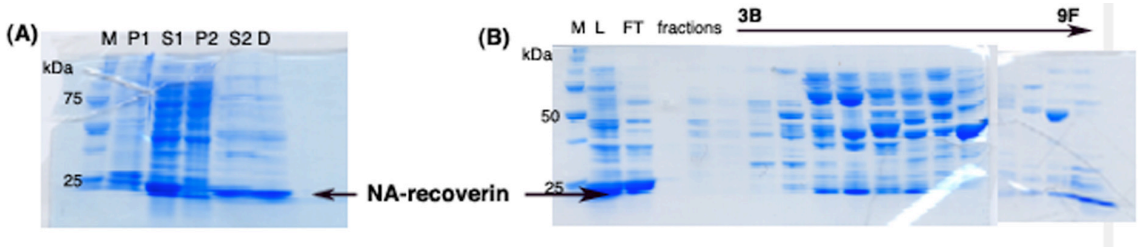
(A)
M P1 S1 P2 S2 D
kDa
75
25
NA-recoverin
(B)
M L FT fractions
3B
9F
kDa
50
25

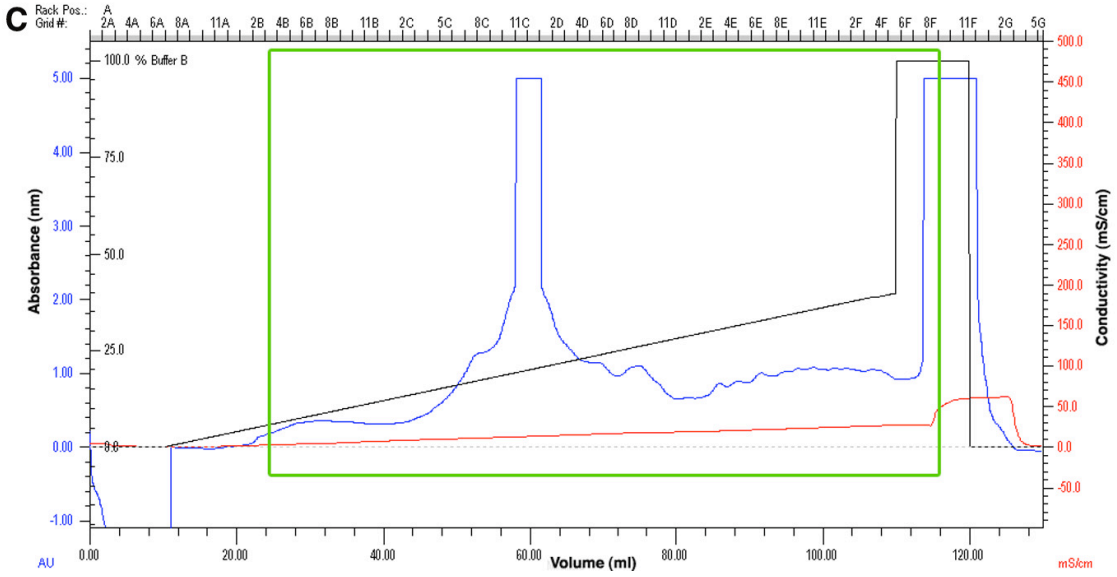
C
Rack Pos.:
Grid #:
100.0 % Buffer B
Absorbance (nm)
Conductivity (mS/cm)
Volume (ml)
AU
mS/cm

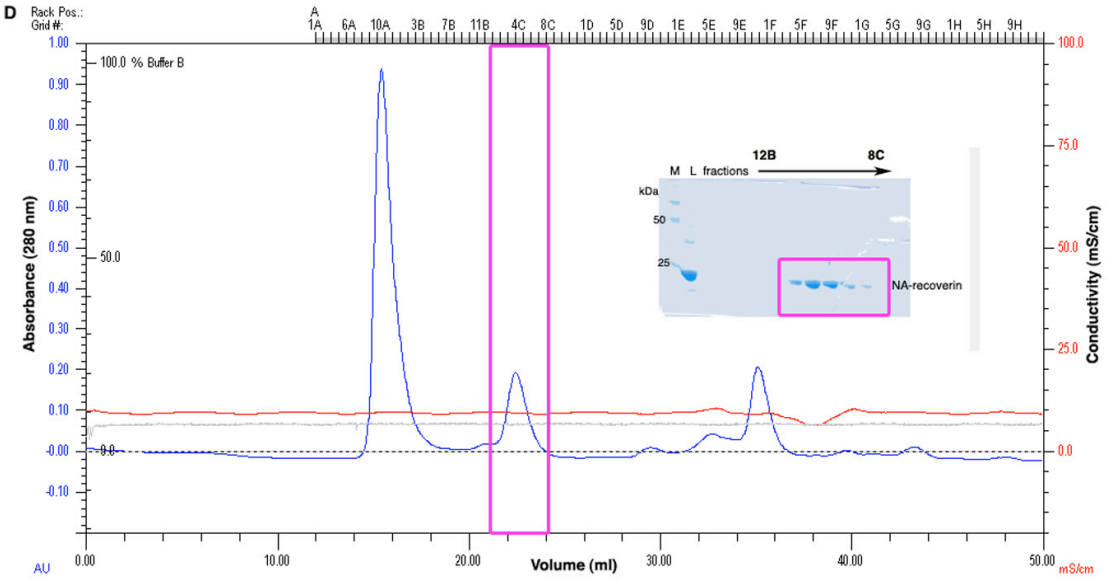
D
Rack Pos.:
Grid #:
100.0 % Buffer B
Absorbance (280 nm)
Conductivity (mS/cm)
Volume (ml)
AU
mS/cm
12B
8C
M L fractions
kDa
50
25
NA-recoverin

Isolation of Ca^{2+}·recoverin·$GRK1_{535}$-His_6 Complex

$GRK1_{535}$-His_6 (Pool A) in 20 mM Na-HEPES, pH 7.5, 120 mM NaCl, and 1 mM DTT was mixed with NA-recoverin (post size exclusion chromatography) in a 1:1.5 molar ratio. The protein mixture was incubated on ice for 30-60 minutes and then loaded onto two tandem Superdex 200 HR 10/30 columns (Pharmacia) pre-equilibrated with NA-recoverin gel filtration buffer (Fig. 16). Peak fractions containing Ca^{2+}·recoverin·$GRK1_{535}$-His_6 were pooled and concentrated using a 50 kDa MWCO centricon to 10 mg/ml and used for crystallization trials. The molecular weight of the peak containing the complex is 80.5 kDa, which corresponds to a 1:1 complex of the two proteins. Excess Ca^{2+}·recoverin (NA-recoverin) elutes as a 28 kDa protein under the conditions used (Fig. 27). To demonstrate calcium dependence, the complex could not be isolated in the absence of $CaCl_2$ (data not shown).

Figure 27. Isolation of Ca^{2+}·recoverin·$GRK1_{535}$-His_6 complex on gel filtration column.

A 1:1 complex (based on a standard run of proteins of known molecular weights) of the two proteins was isolated by size exclusion chromatography (peak 1 on the chromatogram). The fractions containing the complex that were pooled are marked with a magenta colored box. The second peak contains excess recoverin.

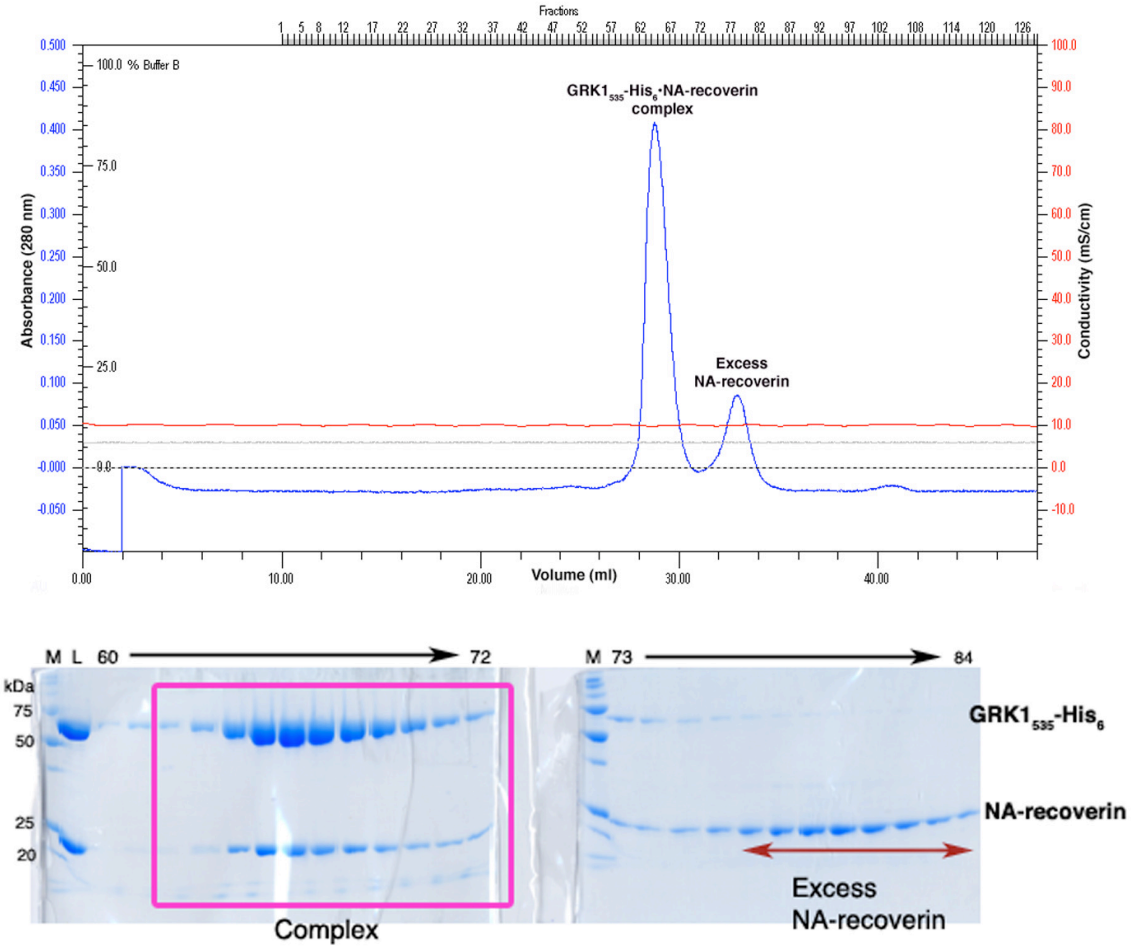

Attempts to Crystallize Ca^{2+}·recoverin· $GRK1_{535}$-His_6 Complex

The protein complex was screened for crystallization at 4 ºC using commercial screens (Hampton Research) in the presence of 2 mM $MgCl_2$ and either 4 mM ATP or 4 mM AMPPNP or in the absence of any nucleotide ligands. No crystal hits were obtained under any of the crystallization conditions. Additional trays were set up to screen different precipitating agents (polyethylene glycols, ammonium sulfate etc) under varying range of pH, both at high (1 M) and low (200 mM) salt (NaCl). To ensure that the complex does not dissociate during crystallization, 1 mM $CaCl_2$ was also included in the well solution. Thin, needle-like crystals appeared after 4 months and were grown using protein pre-mixed with 4 mM ATP, pH 7.5 and 2 mM $MgCl_2$ with the well solution containing 15% PEG 8000, 200 mM NaCl, and either 100 mM Na-HEPES, pH 7.5 or 100 mM Tris-base, pH 8.0-8.5. These crystals were tiny and not harvested (Fig. 28).

Figure 28. Crystals grown from drops containing Ca^{2+}·recoverin·$GRK1_{535}$-His_6.

Tiny crystals nucleated in this drop after ~ 4 months and were not harvested.

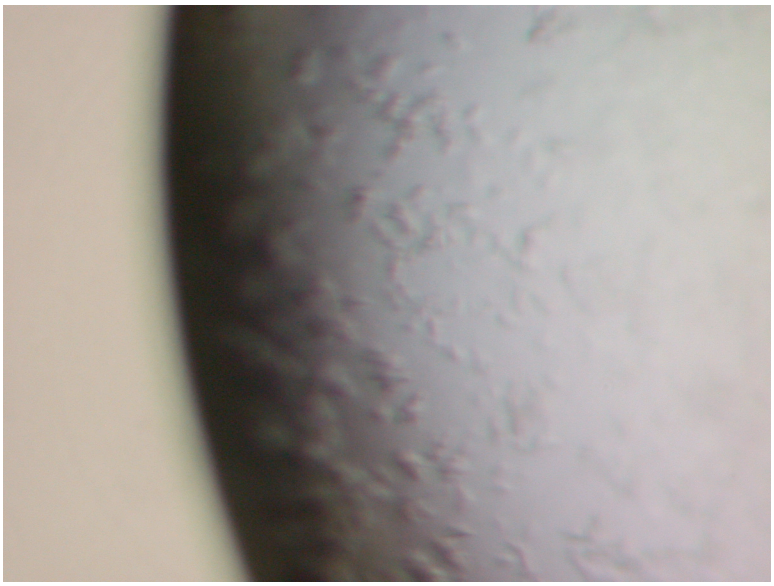

RESULTS

AIM 1. DETERMINE THE STRUCTURE OF Ca^{2+}· CALMODULIN·GRK6

Attempts to isolate a complex of GRK6 with Ca^{2+}·calmodulin

The calmodulin binding sites has been mapped to both the N- and the C-terminus based on studies with GRK1, GRK2 and GRK5. In GRK5, the disruption of the C-terminal site (site 2) lowers the sensitivity of the kinase whereas mutation of the N-terminal site (site 1) alone has no significant effect on the IC_{50} of calmodulin [109]. The binding sites for GRK6 have not been well characterized however based on the sequence alignment it appears that it would bind calmodulin at structurally analogous sites to GRK5 (Fig. 29). To try and isolate a complex of GRK6 with calmodulin, reactions were set up such that there was 2-5 fold molar excess of calmodulin in the to reaction buffer. The amount of calcium in different experiments was varied from 100 μM to 1 mM to ensure that all the four Ca^{2+}-binding sites were occupied. The same amount of calcium was also included in the gel filtration buffer. Under these conditions, the two proteins did not associate and eluted in two different peaks on a gel filtration column (Fig. 25). The mass of the first peak was estimated to be 62.4 kDa (GRK6 is ~67 kDa) while the calmodulin elutes in the second peak as a ~ 34 kDa protein (known mass of calmodulin is 16 kDa). GRK6 used was a soluble mutant of GRK6 wherein the three palmitoylation sites at the C-terminus (Cys561, Cys562 and Cys565) were mutated to serine. Considering the importance of site 2 in GRK5, it remains a possibility that palmitoylation of the C-terminus of GRK6 could favor the binding to calmodulin. Also, because GRK5 has been used for most of the binding studies, in the future GRK5 should be tested for calmodulin binding.

Figure 29. Mapping of calmodulin binding sites in the GRK4 sub-family.

The GRK4 subfamily (GRK4, 5 and 6) is more potently inhibited by the calmodulin (IC_{50} is in nM range) compared to other GRKs [109, 115]. The N- (Site 1) and the C-terminal (Site 2) calmodulin binding sites identified in GRK5 are colored green. The potential palmitoylation sites mutated in the soluble mutant of GRK6 used in this study are colored pink. The residues disordered in GRK6 structure [63] are colored grey, which also includes C-terminal region spanning the "Site 2". The accession codes for the protein sequences are: GRK4, AAI17321.1; GRK5, P43249; GRK6, P43250. The sequence alignments were performed using the ClustalW program.

AIM 2. DETERMINE THE STRUCTURE OF Ca^{2+}·RECOVERIN·GRK1

Attempts to crystallize Ca^{2+}·Recoverin·$GRK1_{535}$ complex

Since the affinity of recoverin for GRK1 is not regulated by the presence of the myristoyl group [82], the unmyristoylated recoverin was picked for structural studies as it increases the solubility of the protein. A stoichiometric complex of $GRK1_{535}$ (Pool A) and non-myristoylated recoverin was isolated by size-exclusion chromatography in a Ca^{2+}-dependent manner (Fig. 27). Since GRK1 crystallization was facilitated by the addition of nucleotides (apo form of the protein diffracts poorly and takes much longer to nucleate) the complex was pre-incubated with 4 mM ATP or ADP or AMPPNP, pH 7.5 and 2 mM $MgCl_2$ prior to setting up the protein in trays. Trays were also set up in the absence of any nucleotide ligand. Thin needle-like crystals appeared after ~4 months in drops containing ATP (Fig. 28). These crystals were tiny and not harvested. Since autophosphorylation of GRK1 has been suggested to weaken the interaction [82], it is possible that the complex dissociates over time. The conditions need to be optimized to grow thicker crystals. This could include varying the temperature, using a mutant of $GRK1_{535}$ lacking all the potential autophosphorylation sites and, use of a pure form of ADP, free of contaminating amounts of ATP.

Chapter 3. GRK6 and the $G\alpha_{16}$ subunit

INTRODUCTION

GRKs can regulate G protein coupled signaling at the level of Gα subunits, in addition to phosphorylating and thereby inhibiting the GPCRs. GRK2 is known to bind $G\alpha_q$, $G\alpha_{11}$ and $G\alpha_{14}$ subunits to block their interactions with the downstream effectors [116-118] [61]. Pull-down assays using COS-1 cell lysates (unpublished data, Jeff Benovic Lab, Thomas Jefferson University) suggested that GRK6 could bind the $G\alpha_{16}$ subunit (another member of the $G\alpha_q$ family).

Project Goals

Determine the structure of GRK6·$G\alpha_{16}$

The aim of this project was to isolate a complex of GRK6 and $G\alpha_{16}$ for structural studies. The first step was to overcome the problems associated with expression levels of $G\alpha_{16}$ [119]. A chimera of $G\alpha_{16}$ was thus designed the same way $G\alpha_{i/q}$ chimera was generated [61]. The amino-terminus comprises of residue 1-28 of rat $G\alpha_{q1}$ and the C-terminus contains residues 40-374 of human $G\alpha_{16}$. Since the expression of functional Gα subunits is enhanced in the presence of Gβγ, human $G\alpha i/_{16}$ chimera was expressed as a heterotrimer in insect cells.

METHODS

Cloning of $G\beta_1$ Subunit into a pFastBac Dual Vector

A DNA template encoding bovine $G\beta_1$ was prepared from the bovine $G\beta_1$ virus (a gift from Dr. Tohru Kozasa, University of Illinois at Chicago). The same $G\beta_1$ virus was earlier used for crystallization of GRK2 in complex with $G\beta_1\gamma_{C68S}$ [60]. The protocol (Novagen) for preparation of viral DNA template is briefly described here. To a 0.5 ml eppendorf tube containing 10 μl of high-titer $G\beta_1$ virus stock (> 1 x 10^8 pfu/ml), 89 μl of lysis buffer (10 mM Tris-HCl, pH 8.3, 0.45% Triton X-100, 0.45% Tween-20, 50 mM KCl) was added. After adding 1 μl of Proteinase K (6 mg/ml in water, Invitrogen), the reaction mixture was incubated at 60 ºC for an hour. This was followed by heat-inactivation of Proteinase K (95 ºC for 10 minutes). The concentration of viral DNA isolated is about 10 pg/μl. About 5 μl of $G\beta_1$ viral DNA isolated was used as a template in a 50 μl reaction to amplify $G\beta_1$ coding fragment using Gbeta1for and revGbeta1 primers (Table 1). Pfu polymerase (Invitrogen) was used for amplification (35 cycles) with the annealing temperature of 56 ºC.

$G\beta_1$ fragment was ligated into the Sal I/Hind III sites of pFastBac Dual vector downstream of the polyhedrin (PH) promoter of pFastBac Dual vector. Ampicillin-resistant (100 μg/ml) clones in DH5α were picked and DNA sequence was verified (DNA core facility, ICMB, University of Texas at Austin). Database search revealed that the DNA sequence was homologous to rat $G\beta_1$. A single point mutation in the rat coding sequence, which changes aspartate 307 to a valine residue, makes the expressed protein equivalent to the bovine sequence.

Cloning of $G\alpha_{i/16}$ Chimera into a pFastBac Dual Vector

$G\alpha_{i/q}$ viral DNA was first isolated from the $G\alpha_{i/q}$ virus (a gift from Dr. Tohru Kozasa, University of Illinois at Chicago) following the protocol used to prepare $G\beta_1$ viral DNA, and then used as a template to amplify a fragment encoding residues 1-28 of rat $G\alpha_{i1}$. The mutGi1forXmaI and rev28Gi1BglII primers (Table 1) were used for PCR amplification with an annealing temperature of 60 ºC. The mutGi1forXmaI primer carries a point mutation that changes glycine at position two in rat $G\alpha_{i1}$ to alanine so that the protein expressed does not undergo myristoylation.

Residues 37-359 of mouse $G\alpha_q$ in the $G\alpha_{i/q}$ chimera correspond to the residues 40-374 of human $G\alpha_{16}$. This fragment was amplified from the $G\alpha_{16}$ cDNA (a gift from Dr. Tohru Kozasa, University of Illinois at Chicago) using G16for40BglII and revG16KpnI primers (Table 1). Annealing temperature used was 60 ºC.

$G\alpha_{i1}$ (residues 1-28) and $G\alpha_{16}$ (residues 40-374) fragments were both digested with BglII and then ligated to generate a $G\alpha_{i/16}$ chimera with BglII sequence at the junction, which was also present in the functional $G\alpha_{i/q}$ chimera. The $G\alpha_{i/16}$ chimera was then ligated into the pFastBac Dual vector (encoding $G\beta_1$ sequence) at the Sma I and Kpn I sites downstream of the p10 promoter.

The recombinant pFastBac Dual vector has $G\beta_1$ coding sequence downstream of the PH promoter and $G\alpha_{i/16}$ chimera cloned downstream of the p10 promoter (Fig. 30). DNA sequencing revealed that the $G\alpha_{i/16}$ chimera encodes a point mutation changing glutamate residue 172 to alanine in the $G\alpha_{16}$ sequence (E172A mutation was present in the $G\alpha_{16}$ cDNA). The $G\alpha_{i/16}\beta_1\gamma_{sol}$ heterotrimer expressed using these clones will carry E172A mutation in $G\alpha_{i/16}$ subunit, which will be henceforth labeled as $G\alpha_{i/16}^{E172A}$.

Figure 30. Cloning of $G\alpha_{i1/16}$ chimera and $G\beta_1$ into the pFastBac Dual vector.

The recombinant vector encodes $G\beta_1$ and $G\alpha_{i1/16}$ sequences downstream of the PH and p10 promoters respectively. The numbers (bottom panel) indicate the start of the restriction site sequence (italicized and colored blue). $G\alpha_{i1/16}$ chimera lacks a myristoylation site (G2A mutation in $G\alpha_{i1}$, shown in magenta). The vector sequence is in lower case.

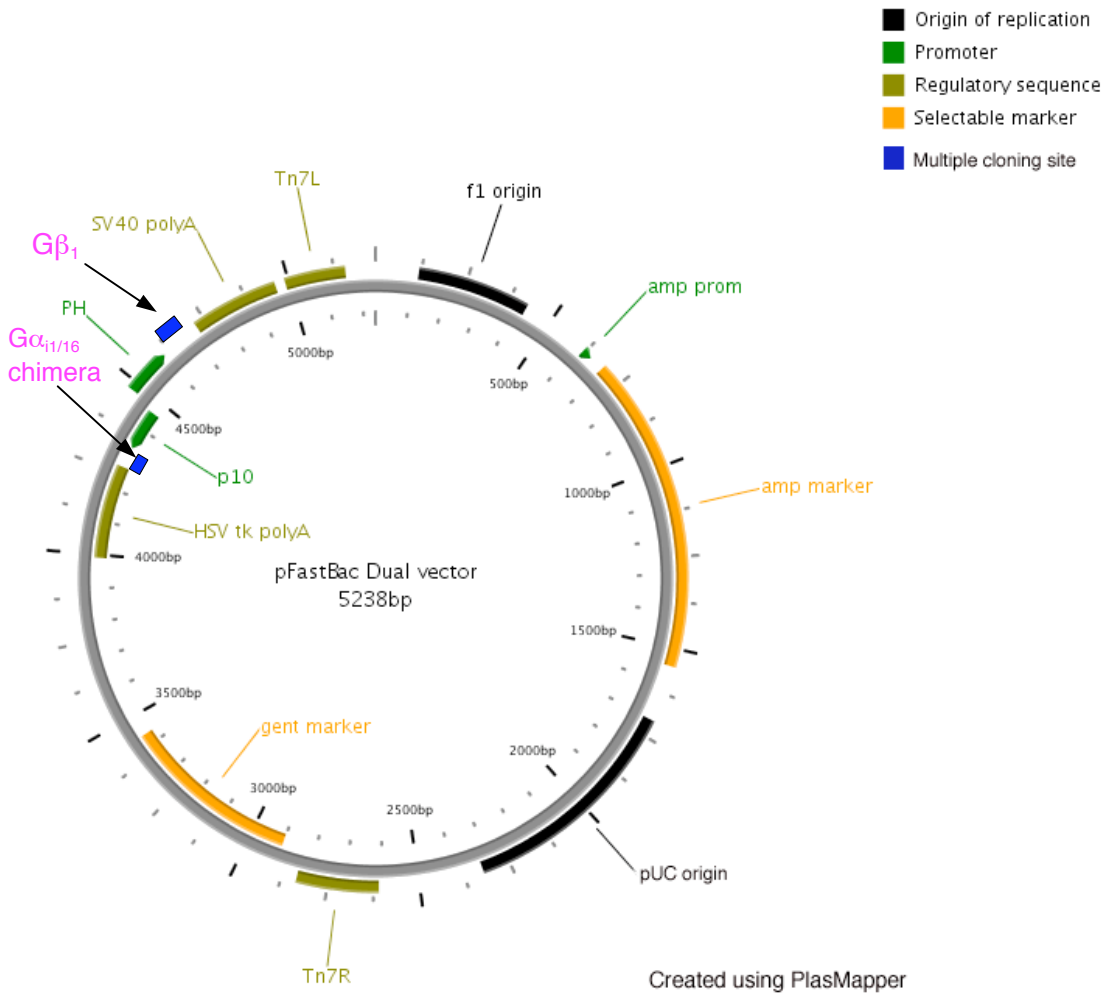

PH promoter... gcctac ^{4644}*gtcgac* ATGAGTGAA ...AAGATCTGGAACTAA^{4699}*aagctt* gtcgagaag ...

Sal I — $G\beta_1$ sequence — stop codon — Hind III

p10 promoter... tgatca ^{4324}*cccggg*ATGGCCTGCACA ...AACCTGCTGTGA ^{4279}*ggtacc* gggagatgg ...

Sma I — $G\alpha_{i1/16}$ chimera — stop codon — Kpn I

Expression and Purification of $G\alpha_{i/16}^{E172A}\beta_1\gamma_{C68S}$ Heterotrimer

Recombinant $G\alpha_{i/16}^{E172A}\beta_1\gamma_{C68S}$ protein was generated similarly to $GRK1_{535}$-His_6. Six liters (8 x 750 ml) of High Five cells (2 x 10^6 cells/ml) in 2 L baffled flasks were co-infected with 20 ml of $G\alpha_{i/16}^{E172A}\beta_1$ and 15 ml of His_6-$G\gamma_2$ viruses. The His_6-$G\gamma_2$ virus contains a C68S mutation [120] that encodes a soluble mutant of $G\gamma_2$ ($G\gamma_{C68S}$). Cells were incubated in a 28 ºC shaker at 140 rpm and harvested approximately 36 hours after viral addition by centrifugation at 1000 X g for 15 minutes at 4 °C in a Beckman JLA 8.1000 rotor. Cell pellet was flash-frozen in liquid nitrogen and stored at -80 °C. The heterotrimer was purified on a Ni^{2+}-NTA (Qiagen) column as described earlier [61]. The samples were visualized on SDS-PAGE and fractions containing the $G\alpha_{i/16}^{E172A}\beta_1\gamma_{C68S}$ heterotrimer were pooled and concentrated using 50 kDa MWCO centriprep.

Activation of $G\alpha_{i/16}^{E172A}$ Subunit and Complex Studies With sGRK6

The alpha subunit was first activated before incubating it with GRK6. About 2 mg of dialyzed $G\alpha_{i/16}^{E172A}\beta_1\gamma_{C68S}$ (in 20 mM Na-HEPES, pH 8.0, 100 mM NaCl, 1 mM $MgCl_2$, 50 μM GDP, pH 8.0, and 5 mM DTT) was mixed with activation buffer containing 20 mM Na-HEPES, pH 8.0, 100 mM NaCl, 25 mM $MgCl_2$, 1.5 mM EDTA, pH 8.0, 500 μM GTPγS, pH 8.0, and 1% cholate in a 100 μl reaction. Unlike $G\alpha_q$, $G\alpha_{16}$ cannot be activated by addition of GDP and Al^{3+}, Mg^{2+} and F^-. Instead, it needs GTPγS, as shown for its ability to activate PLC-β_1 [119]. The heterotrimer was incubated at 30 ºC for 30 minutes. Assuming that about one-third of the heterotrimer solution is activated $G\alpha_{i/16}^{E172A}$ subunit, an equimolar amount of sGRK6 (1.27 mg in 20 mM Na-HEPES, pH 8.0, 200 mM NaCl and 2 mM DTT) was added and the reaction mixture was incubated for 15 minutes at 30 ºC. The final concentrations of $MgCl_2$, EDTA, GTPγS and cholate in approximately 500 μl reaction volume were 5 mM, 0.3 mM, 100 μM and 0.2%

respectively. The protein mixture was loaded onto a single Superdex 200 HR 10/30 column (Pharmacia) pre-equilibrated with $G\alpha_{i/16}^{E172A}$ gel filtration buffer (20 mM Na-HEPES, pH 8.0, 100 mM NaCl, 5 mM $MgCl_2$, 10 μM GTPγS, and 1 mM DTT). Under these conditions, $G\alpha_{i/16}^{E172A}$ did not associate with sGRK6. The potential problems were the presence of significant amounts of contaminating $\beta_1\gamma_{C68S}$ subunits and 0.2% cholate in the final reaction mixture. Hence, the protocol to purify $G\alpha_{i/16}^{E172A}$ was modified to address these problems.

Isolation of Activated $G\alpha_{i/16}^{E172A}$ Subunit on Ni^{2+}-NTA Column

The goal was to first isolate pure and activated form of $G\alpha_{i/16}^{E172A}$ subunit and then use it for complex formation. The High Five cell pellet infected with the heterotrimer was lysed as described above and loaded onto a 10 ml Ni^{2+}-NTA drip column. After washing the column with 20 column volumes each of $G\alpha_{i/16}^{E172A}\beta_1\gamma_{C68S}$ Buffer A (20 mM Na-HEPES, pH 8.0, 100 mM NaCl, 1 mM $MgCl_2$, 50 μM GDP, pH 8.0, and 10 mM β-mercaptoethanol) and Buffer B (Buffer A containing 300 mM NaCl, and 10 mM Imidazole, pH 8.0), the column was incubated at room temperature for about 15 minutes in $G\alpha_{i/16}^{E172A}$ elution buffer (20 mM Na-HEPES, pH 8.0, 300 mM NaCl, 50 mM $MgCl_2$, 50 μM GTPγS, 10 mM CHAPS, and 10 mM β-mercaptoethanol). Activated $G\alpha_{i/16}^{E172A}$ was eluted in 1 ml fractions with 10 ml of room temperature $G\alpha_{i/16}^{E172A}$ elution buffer. Bound $G\beta_1\gamma_{C68S}$ was eluted with a buffer containing 20 mM Na-HEPES, pH 8.0, 300 mM NaCl, 50 mM $MgCl_2$, 50 μM GDP, 150 mM Imidazole, pH 8.0, and 10 mM β-mercaptoethanol (Fig. 31A). Fractions containing activated $G\alpha_{i/16}^{E172A}$ were pooled and concentrated to about 4 mg/ml using 50 kDa MWCO centricon (Millipore) and loaded onto a single Superdex 200 HR 10/30 column (Pharmacia) pre-equilibrated with $G\alpha_{i/16}^{E172A}$ gel filtration buffer (20 mM Na-HEPES, pH 8.0, 100 mM NaCl, 5 mM $MgCl_2$,

10 μM GTPγS, and 1 mM DTT). $G\alpha_{i/16}^{E172A}$ elutes in a single sharp peak as a ~52 kDa protein (Fig. 31B)

Purified $G\alpha_{i/16}^{E172A}$ (490 μg) and sGRK6 (770 μg) were mixed in $G\alpha_{i/16}^{E172A}$ gel filtration buffer containing 50 μM GTPγS. The mixture was incubated on ice for 30 minutes and loaded onto a single Superdex 200 HR 10/30 column (Pharmacia) pre-equilibrated with $G\alpha_{i/16}^{E172A}$ gel filtration buffer. The two proteins elute in two overlapping peaks and attempts to isolate a complex under these conditions were not successful (Fig. 31C).

Figure 31. Purification of activated $G\alpha_{i/16}^{E172A}$ from the heterotrimer and the complex formation with sGRK6.

(A) Ni^{2+}-NTA affinity purification. The $G\gamma_{sol}$ subunit is expressed as a His_6-tagged protein. The samples have been labeled from left to right as: (M) protein standards, (1) pellet fraction after lysis, (2) supernatant fraction containing soluble protein after lysis, (3) flow-through of supernatant loaded onto nickel column, (4) column wash with Buffer A, (5) column wash with Buffer B, (6)-(17) $G\alpha_{i/16}^{E172A}$ protein eluted with $G\alpha_{i/16}^{E172A}$ elution (activation) buffer, and (18) bound $G\beta_1\gamma_{C68S}$ eluted with the elution buffer containing 150 mM imidazole.

(B) Size-exclusion chromatography of activated $G\alpha_{i/16}^{E172A}$. Fractions (lanes labeled 6-14) from step (A) containing activated $G\alpha_{i/16}^{E172A}$ were pooled and concentrated and purified on a single Superdex 200 HR 10/30 column (Pharmacia) pre-equilibrated with $G\alpha_{i/16}^{E172A}$ gel filtration buffer

(20 mM Na-HEPES, pH 8.0, 100 mM NaCl, 5 mM $MgCl_2$, 10 μM GTPγS, and 1 mM DTT). Samples on the gel have been labeled as: (M) protein standards, (L) pooled and concentrated sample of activated $G\alpha_{i/16}^{E172A}$ loaded onto the column, and the peak fractions.

(C) Attempts to isolate a complex of $G\alpha_{i/16}^{E172A}$ and sGRK6. Activated $G\alpha_{i/16}^{E172A}$ subunit from step (B) was concentrated and mixed with sGRK6 in a 1.5:1 molar ratio. The protein solution was supplemented with GTPγS to a final concentration of about 50 μM. The samples have been labeled as: (M) protein standards, (L) mixture of $G\alpha_{i/16}^{E172A}$ and sGRK6 loaded onto a single Superdex S200 HR 10/30 column and, the fraction numbers.

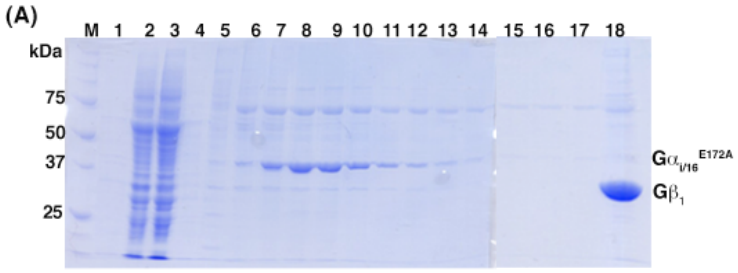
(A)
M 1 2 3 4 5 6 7 8 9 10 11 12 13 14 15 16 17 18
kDa
75
50
37
25
$G\alpha_{i/16}^{E172A}$
$G\beta_1$

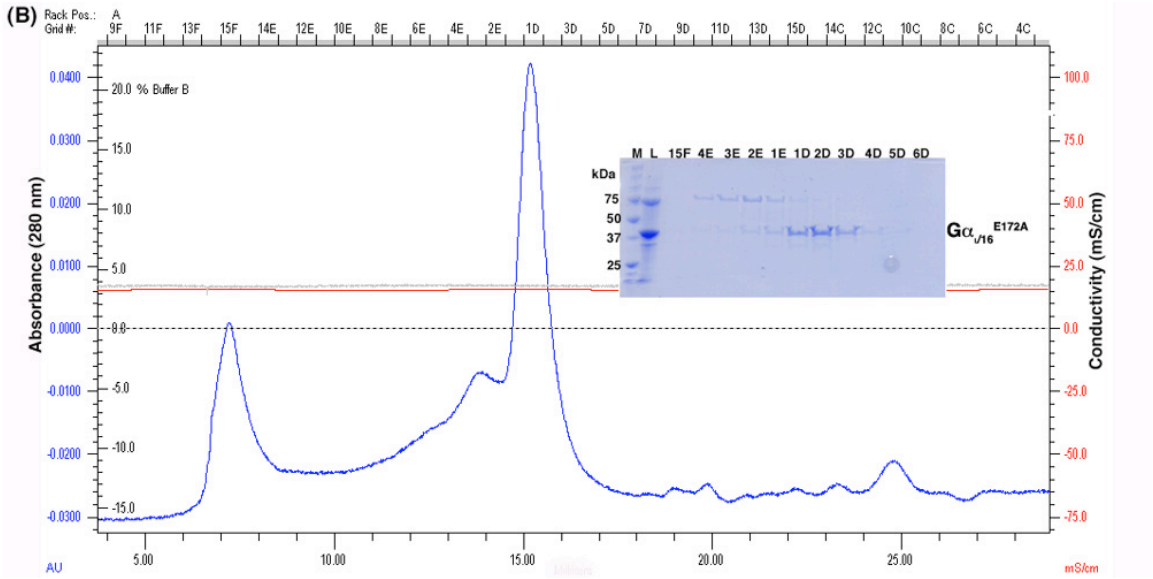
(B)
Rack Pos.: A
Grid #:
20.0 % Buffer B
Absorbance (280 nm)
Conductivity (mS/cm)
AU
mS/cm
M L 15F 4E 3E 2E 1E 1D 2D 3D 4D 5D 6D
kDa
75
50
37
25
$G\alpha_{i/16}^{E172A}$

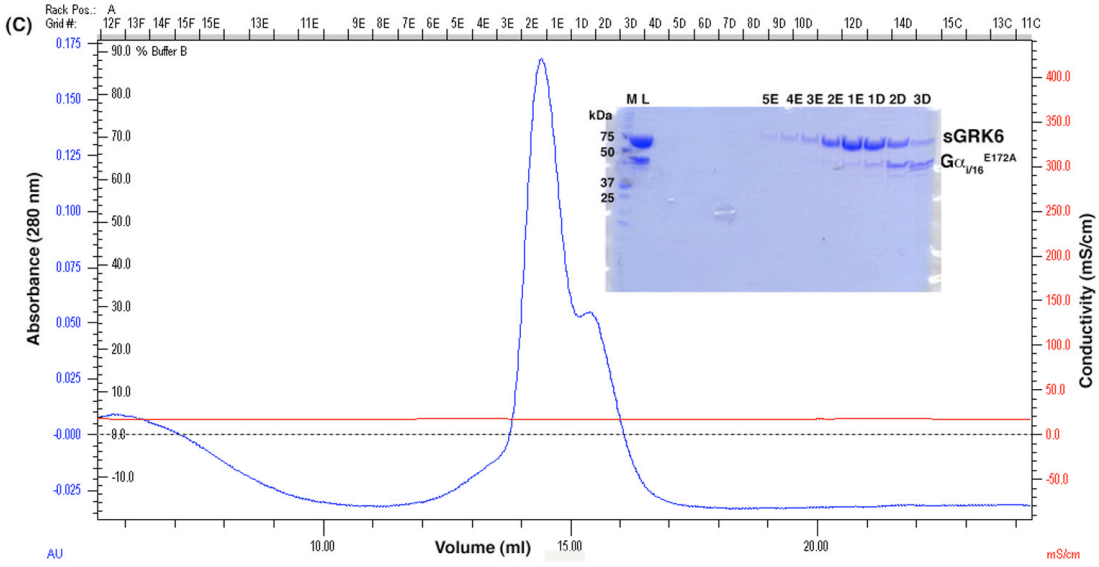
(C)
Rack Pos.: A
Grid #:
90.0 % Buffer B
Absorbance (280 nm)
Conductivity (mS/cm)
Volume (ml)
AU
mS/cm
M L 5E 4E 3E 2E 1E 1D 2D 3D
kDa
75
50
37
25
sGRK6
$G\alpha_{i/16}^{E172A}$

RESULTS

AIM 1. DETERMINE THE STRUCTURE OF GRK6·$G\alpha_{16}$

The $G\alpha_{16}$ subunit used in these studies was a chimera ($G\alpha_{i/16}$) wherein the N-terminus of $G\alpha_{16}$ was replaced with that of $G\alpha_{i1}$. The yield of $G\alpha_{16}$ chimera was enhanced over that of wild-type protein expressed in baculovirus-infected insect cells, and was estimated to be about 750 μg/L of cell culture. This is significantly higher than the published expression levels of a non-chimeric $G\alpha_{16}$ subunit (~18 μg from six liters of insect cells) [119]. We were also able to modify the purification protocol to generate the activated form of the $G\alpha_{16}$ subunit (Fig. 31), free from contaminating amounts of Gβγ subunits. However, the attempts to isolate a complex of activated $G\alpha_{16}$ and GRK6 by size exclusion chromatography were not successful. The project was initiated taking the lead from the lab of Jeff Benovic (Thomas Jefferson University; unpublished data) who provided preliminary evidence for the two proteins to associate based on pull-down assays using crude COS-1 cell lysates. We were using purified proteins and the fact that they did not associate in our assays suggests that the interaction could be indirect, or in fact an artifact.

DNA sequencing revealed that the $G\alpha_{16}$ subunit carries a point mutation (E172A). This residue is either glutamate or aspartate in all the other $G\alpha_{16}$ sequences. Structural comparison with $G\alpha_q$ suggests that the mutation lies in a solvent exposed αE-αF loop and would not affect the folding of $G\alpha_{16}$ (Fig. 32). Size exclusion chromatography confirms that the protein ($G\alpha_{16}^{E172A}$) is not misfolded (Fig. 31B). The mutation does not overlap with the GRK2 binding site mapped on $G\alpha_q$, which involves α2, α3 and α3-β5 loop.

Figure 32. Structural alignment of the $G\alpha_q$ family members.

The numbers on top of the sequence alignment indicate residue numbers in the $G\alpha_q$ sequence. The secondary structure assignment (yellow bars represent α-helices and orange arrows for β-sheets) is based on the $G\alpha_q$ structure (PDB code 2BCJ) [61]. The blue boxes represent the three switch regions in the Gα subunits. The E172 residue mutated in the $G\alpha_{16}$ chimera is colored red. All the sequences are mouse except $G\alpha_{16}$, which is human. The accession codes for the protein sequences are: $G\alpha_q$, AAA63306.1; $G\alpha_{11}$, NP_034431.1; $G\alpha_{14}$, NP_032163.2; $G\alpha_{16}$, AAA35860.1. The sequence alignments were performed using the ClustalW program.

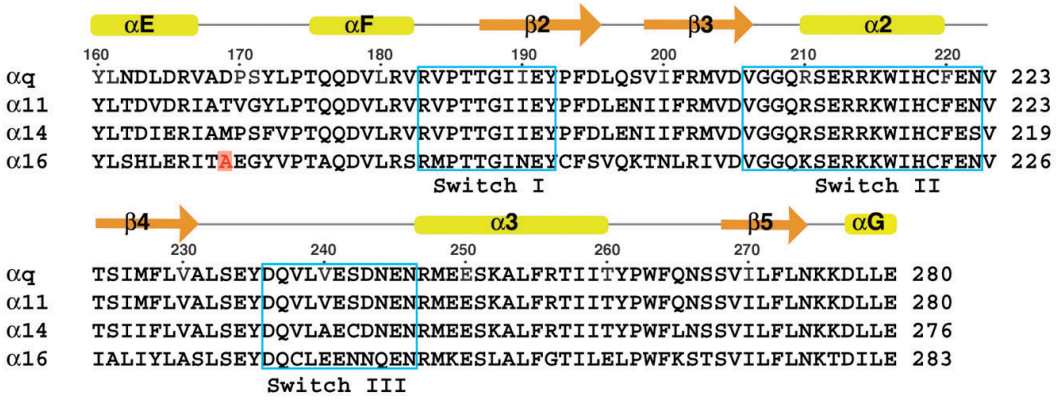

Chapter 4. Discussion

A model for Rho* Docking

Peptides derived from the cytoplasmic tail (C-tail) of rhodopsin are poor substrates and their phosphorylation by GRK1 is enhanced in the presence of Rho* by ~ 100-fold [40, 76, 77] suggesting that receptor docks at site(s) other than the C-tail. In addition, peptides derived from various cytosolic loops compete with rhodopsin for GRK1 suggesting that the cytoplasmic loops of Rho* are involved in binding [41, 52]. The rhodopsin binding surface on GRKs, however, is not well characterized but is thought to involve the amino-terminus of GRKs [45, 49, 57], which is revealed in one of the structures of GRK1. The conformation of the N-terminus appears to be stabilized by the crystal contacts mediated by the loop connecting the αN and α0 helices (Fig. 14c). The symmetry related loop docks in the canyon lined by the αN helix, the small lobe and the "tail-loop" of the C-terminal extension and could mimic the interactions between receptor and GRK1 during signaling events. Comparison of GRK1 structure with those of PKA and PKB reveals that the "tail-loop" in GRKs is 4 residues shorter (Fig. 22b) forming a solvent exposed canyon. The αN helix of the N-terminus and the active site tether of the C-terminal extension form the walls of this canyon, with the hinge of the kinase domain resting at the bottom (Fig. 33a). The canyon is lined by several hydrophobic residues that are conserved in all the GRKs. We expect Rho* to dock at this site. In our model (Fig. 33b), the third cytoplasmic loop of Rho* is modeled to engage the docking site as site-directed mutants in this loop have been shown to affect transducin activation and phosphorylation [52, 79]. The C-tail of Rho* was modeled that such it binds to the large lobe of the kinase domain in a manner similar to the way peptides bind PKB [121]. In this model, the membrane proximal surface of GRK1 is relatively flat and

is lined by both positively charged and hydrophobic residues. Similar orientation has been predicted for other GRKs [60, 61, 63]. In this orientation, the GRK1 active site is accessible to other molecules of Rho or Rho* in the same membrane plane, allowing high-gain phosphorylation [122, 123] and would allow for multiple rounds of nucleotide exchange on GRK1 while Rho* is engaged in the docking site.

Rho*-meditated Activation of GRK1

The binding of nucleotide ligands stabilizes the kinase domain of GRK1 [52] as is evidenced by the conformational flexibility of the kinase domain in apo-GRK1 structure. Nucleotide-binding is associated with the ordering of different elements of the kinase C-terminal extension that packs adjacent to the nucleotide-binding pocket. However, even though nucleotide binding induces a ~8° closure of the kinase domain, an additional closure of ~15° is still needed to properly align the two lobes of the kinase domain to resemble the active PKA structure [96] (Table 5) The glycine-rich P-loop, which makes contact with the phosphate tail of the nucleotide is shifted up from the nucleotide-binding pocket and resembles the structure of P-loop in the apo structure of PKA [101]. Since the kinase C-terminal extensions lies close to the P-loop in the structure and also contributes to the putative receptor docking site, we hypothesize that receptor binding might induce the additional domain closure needed along with the reorientation of the P-loop to resemble the activated structure of PKA [96, 99] (Fig. 34).

Figure 33. A model of Rhodopsin docked to GRK1.

(a) A close-up of the proposed receptor docking canyon (see Fig. 22b). The conserved hydrophobic residues forming the walls of the canyon are indicated. **(b)** GRK1 is rendered as spheres and the view is rotated 180° around the vertical axis from panel (a). The RH domain is colored magenta, the kinase domain yellow, and the N-terminus and kinase C-terminal extension are green. A model of an array of rhodopsin molecules (PDB 1N3M) was docked such that loop 3 of Rho* (red) lies in the proposed "docking canyon". Only two rhodopsin molecules from this array have been shown for clarity. Using PKB peptide (PDB 1O6L) as a guide, the C-tail Rho peptide (cyan) was modeled such that the Ser338 residue is close to the γ-phosphate of ATP in the active site. With these constraints, the active site is accessible to the C-tail of either Rho* or a neighboring inactive Rho (brown) in the same membrane plane.

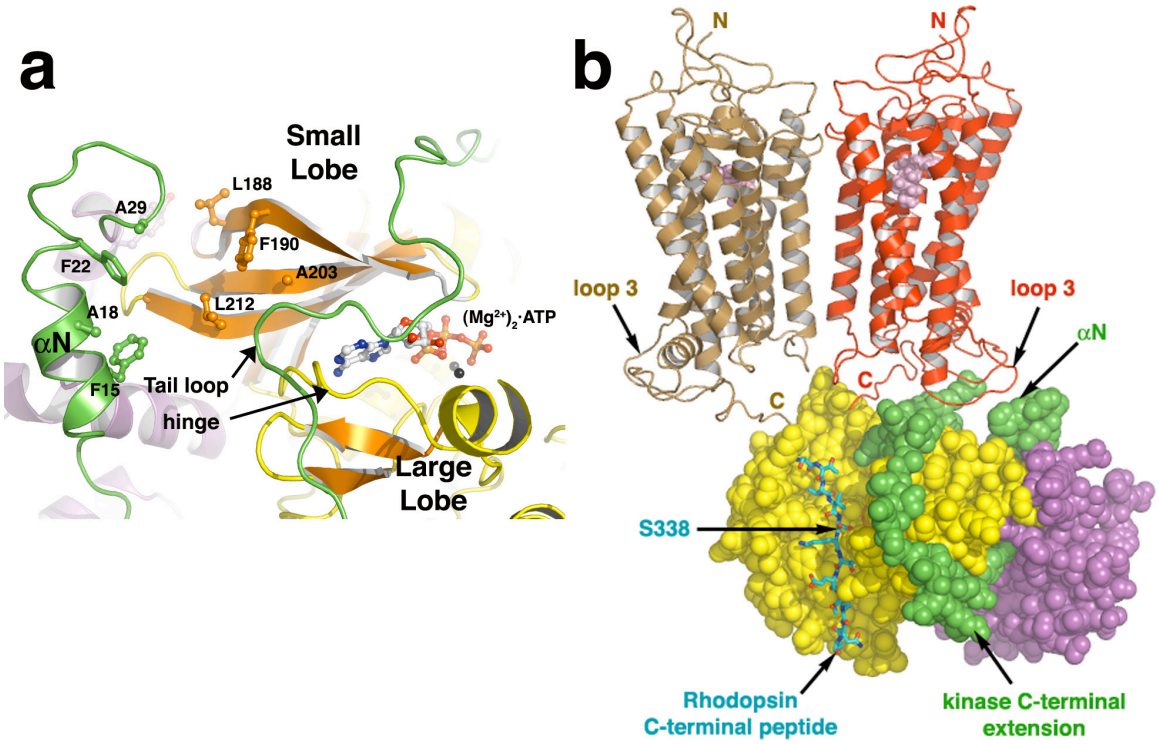

Figure 34. A schematic representation of Rho*-mediated activation of GRK1.

Upon light stimulation, the chromophore 11-cis-retinal is isomerized to all-trans-retinal resulting in an active conformation of rhodopsin (Rho*), which stimulates transducin activation. The RH domain of GRK1 is colored violet and the kinase domain is yellow. The N-terminus of GRK1 in the apo state is disordered in this model and we predict that it becomes ordered (dark green helix) when bound to Rho*/lipid-bilayer or Ca2+·recoverin. The nucleotide-binding induces a 8° closure of the kinase domain, but additional closure is expected when the third cytosolic loop of Rho* docks in the putative docking canyon. The C-tail of Rho* or a neighboring inactive Rho is phosphorylated creating a binding site for arrestin. The retinal molecule is recycled and binds to the opsin moiety to regenerate Rho.

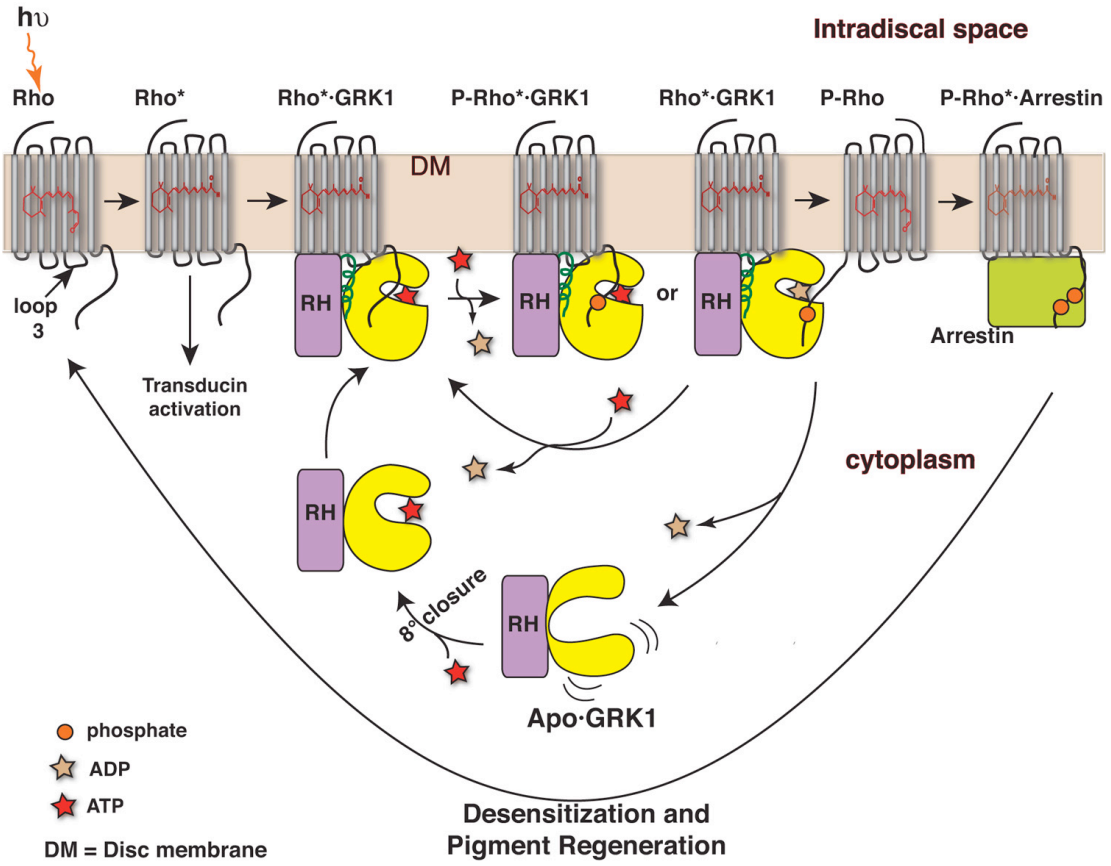

Mutagenesis Studies

GRK1 structure and mass spectral analysis revealed that the N-terminus of GRK1 was phosphorylated at several previously unidentified sites (Ser5 and Thr8). Our *in vitro* assays suggest that phosphorylation at these sites is not required for rhodopsin phosphorylation. However, they could play a role in functions other than direct interaction with receptor, such as stability or the localization of the kinase in the rod cells. Phosphorylation has been shown to affect the activity, localization and protein-protein interactions in case of several proteins. For example, phosphorylation of nitrate reductase and cytosolic pyruvate kinase has been suggested to target them for degradation [124].

The dimerization mediated by the RH domain in crystals has been previously reported for GRK6, and, as for GRK6, the residues at this interface in GRK1 are not required for rhodopsin phosphorylation in our *in vitro* assays [63]. Modeling studies using a different rotamer of W531 residue suggests that dimerization could be resulting from a short domain-swap occurring at high protein concentrations during crystallization. However, considering the extent and the conservation of the interface and the role of RH domains serving as protein-binding surfaces in several other proteins [59, 61, 125], it remains possible that this interface could mediate interaction with as of yet unidentified protein target(s) *in vivo*.

Recoverin Binding

Although the physiological relevance of the recoverin-GRK1 interaction is debated [110, 112], comparison of our GRK1 structure with that of the recently determined N-terminal peptide of GRK1 (residues 1-25) in complex with Ca^{2+}·recoverin [126] suggests a mechanism by which recoverin can inhibit GRK1 function *in vitro*. The ordered portion of GRK1 in the recoverin bound structure extends from residue 4 through 16 with GRK1-Val9, Val10, Ala11, Ala14 and Phe15 binding to a hydrophobic surface

on recoverin. In our structure the αN forms a helix from residues 12-25, and both Val9 and Phe15 pack against the RH domain. This suggests that recoverin binding would inhibit receptor phosphorylation by sterically blocking the interaction of N-terminus of GRK1 with the lipid-bilayer/micelles or the receptor itself.

Molecular basis of Oguchi Disease

Defects in rhodopsin kinase can lead to Oguchi disease in humans (Fig. 35). A number of mutations have been identified in several patients that suffer abnormal recovery kinetics of rod photoreceptors [84]. Patient with heterozygous mutations in the two alleles bearing a point mutation V380D in exon 5 (Val377 in bovine GRK1) and a Ser-536 (4-bp del) suffers prolonged dark adaptation. The Val377 residue is a buried residue in the αF helix, and mutation to negatively charged Asp would likely destabilize the fold of the kinase domain. The frameshift mutation Ser-536 (4-bp del) resembles the soluble bovine GRK1 (spanning residues 1-535) we used for structural studies and is two amino acids longer. The unaffected family members of the patient were found to be carriers of one of the two mutations and were normal. Another patient was found to be homozygous for deletion of residues 357-398 (residues 354-395 in bovine GRK1) in the exon 5 that would result in a loss of αEF1, αEF2 and αF helices and the αF-αG loop in the large lobe of kinase domain. These regions help constitute the peptide-binding channel. In addition, a frameshift mutation results in a premature truncation 18 codons downstream leading to a more lethal disruption of the kinase domain. Recently, a missense mutation P391H [86] in GRK1 affecting the cone recovery kinetics was reported in two Japanese siblings. The Pro391 residue (Pro388 in bovine sequence) in the αF-αG loop of the kinase domain is conserved in all the GRK sub-families. The substitution of proline by histidine would introduce polarity and size differences that are likely to result in steric clash with neighboring hydrophobic residues.

Figure 35. Mapping of Oguchi causing mutations on the GRK1 structure.

(a) Teal colored sphere represents the V377 residue (V380 in humans) in αF helix that is mutated to an aspartate residue. The frameshift mutation Ser536 (4-bp del) in the second allele results in a truncated protein that is 2 residues longer than $GRK1_{535}$ protein. **(b)** The residues 354-395 (357-398 in humans) deleted are colored teal and the region deleted as a result of the frameshift mutation is colored black. **(c)** Teal colored sphere represents the P388H mutation (P391 in humans).

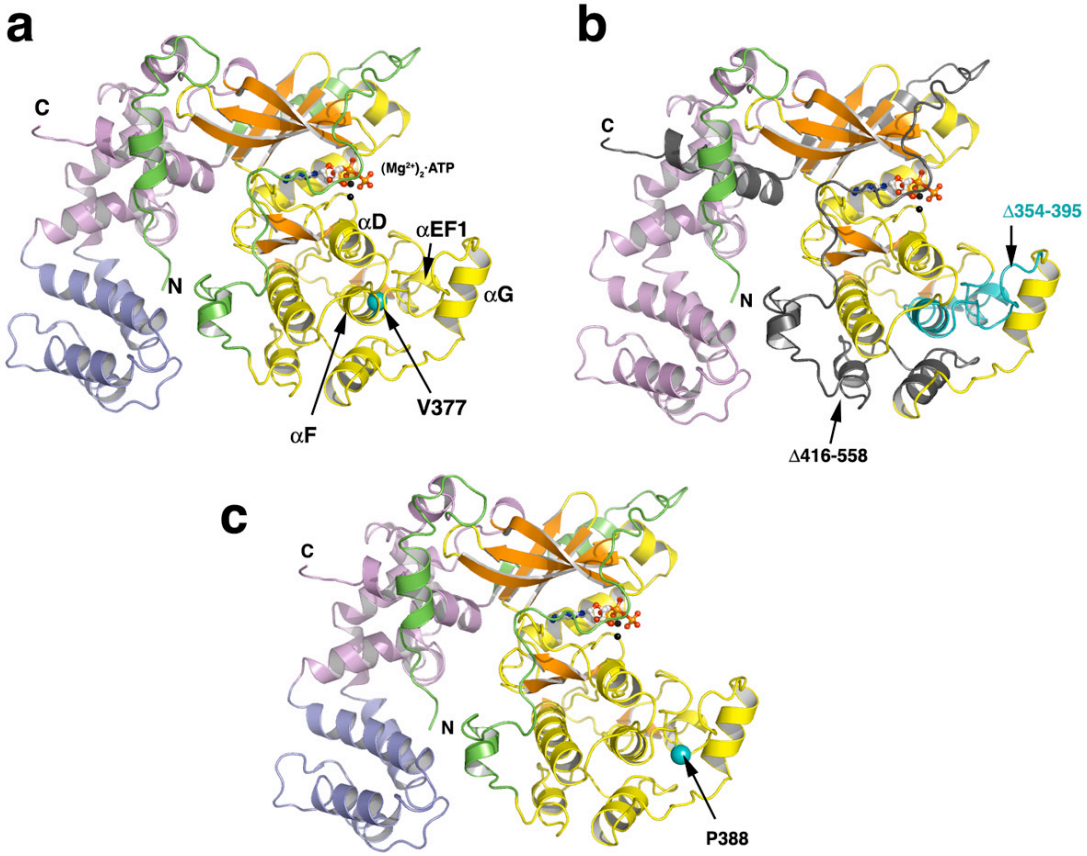

Future Directions

Based on the information revealed in different GRK1 structures we have proposed a testable hypothesis for receptor-mediated activation of GRKs. Mutational analysis of the putative docking canyon in GRK1 would confirm if the residues are implicated in receptor function. The studies could be translated to other GRK sub-families as well to reveal a conserved model of receptor-mediated activation. The structure of a complex of GRK1·recoverin could reveal additional sites of interaction that could include the surface on the RH domain that mediates dimerization. This would lend further insights into the physiological significance of this interaction, which is currently debated. Even though it may need different crystallization conditions, the structural analysis of L166K mutant of GRK1 would confirm if dimerization at higher concentrations in crystals is resulting from a domain-swap. Finally, the structure of Rho* bound to GRK1 would reveal the mechanism by which GRKs recognize activated GPCRs and are in turn activated.

Appendix

Attempts to Crystallize Components of the Mre11/Nbs1/Rad50 Complex

Spodoptera frugiperda sf21 insect cells were co-infected with baculoviruses encoding human Mre11 and Nbs1 in Dr. Tanya. Paull's laboratory (University of Texas at Austin). Several constructs of the two proteins were expressed and purified:

- Wild-type Nbs1 and His_6-human Mre11 (R633stop, ~70 kDa)
- FLAG-tagged Nbs1 and hMre11-His_6 (Δ376-708)
- Rad50 mutant, Rad50Δcc lacking all the coiled coil domains (residues 209-1117 are replaced with a seven amino acid insertion that forms a loop) with His_6 tag at the N- and C-terminus.

All the purified Mre11 and Nbs1 constructs used were not stable in solution. Inclusion of CHAPS and glycerol in the buffers did not keep the protein stable (precipitation of protein when at a concentration ~ 1 mg/ml). The Rad50Δcc construct was the only protein that could be concentrated to about 10.5 mg/ml but high salt (500 m*M* NaCl) conditions were needed to keep it in solution. The yield of this mutant was estimated to be about 1 mg/L of cell culture. Crystallization trays were set up screening different precipitating agents at varying range of pH. No protein crystals were observed. Further crystallization conditions were not explored.

To overcome protein solubility problems different domains of Mre11 and Nbs1 were expressed as Maltose Binding Protein (MBP) fusion proteins using the *E. coli* strain Rosetta (DE3) pLysS. These were the well-folded regions of the protein based on the sequence alignment of various eukaryotic proteins and included the catalytic domains of the protein.

The various hMre11 fragments expressed in Rosetta cells express in milligram quantities (2-4mg/L). However, post digestion with TEV protease the protein was not soluble even in the presence of 1 m*M* $MnCl_2$. Mn^{2+} is essential for the exonuclease activity of Mre11 [127] and was added to all the buffers to help stabilize the protein. Also, the purified Mre11 constructs could not be concentrated to 1 mg/ml. All the Nbs1 protein fragments expressed behaved in a similar manner. Various constructs expressed in *E.coli* were:

Mre11 (13-370)

Mre11 (13-469)

Nbs1 (1-374)

Nbs1 (1-186)

Nbs1 (620-754)

(The numbers in the parentheses indicate the length of the protein fragments cloned).

Another problem with the Mre11 constructs was that the fusion-protein could either not be cleaved with TEV protease or the protein underwent proteolysis from the C-terminus. The only construct that looked promising was Nbs1(620-754), but the yield of purified protein was only 200 μg from six liters of E. coli culture. Attempts to co-purify Mre11 and Nbs1 fragments in order to stabilize the individual protein components also failed.

One potential reason for TEV protease not cleaving the fusion protein efficiently was the presence of a bulky phenylalanine residue (residue 13 in Mre11 sequence) in the vicinity of the TEV recognition sequence. Hence, new Mre11 constructs were designed to contain the entire amino-terminus. The strategy was to co-express Mre11 and Nbs1 constructs in insect cells in order to keep the proteins stable. Based on sequence

alignments, two Mre11 constructs were designed: M489 (residues 1-489) and M402 (residues 1-402) which, encode the phosphodiesterase motif of the nuclease domain of Mre11. The two fragments were ligated into the EcoRI/SalI sites downstream of the Polyhedrin promoter of pFastBac Dual-His_6. Nbs1 fragment (residues 620-754, N620) was ligated into the NcoI/XhoI sites of p10 promoter of the same vector that encodes Mre11 fragment. Both the Mre11 fragments bear a non-cleavable C-terminal His_6-tag. Baculoviruses were generated using the Bac-to-Bac Baculovirus Expression System (Invitrogen).

For the purification of the two Mre11/Nbs1 constructs expressed in High Five cells, one liter of (2×10^6 cells/ml) insect cells were infected with 25-30 ml of either the M489/N620 or M402/N620 baculoviruses and harvested 36 hours post viral addition. Thawed cells pellets were resuspended in 40 ml lysis buffer (50 mM Na-HEPES, pH 8, 500 mM NaCl, 10% glycerol, 0.5% Tween 20, and 20 mM b-mercaptoethanol) containing EDTA-free protease inhibitor cocktail (Roche) per liter of cells. Cells were lysed the same way $GRK1_{535}$-His_6 infected cells were processed (refer to section XX). Clarified supernatant was loaded onto a 5 ml Ni^{2+}-NTA drip column (Qiagen) pre-equilibrated with lysis buffer. After washing the column with 10 column volumes each of lysis buffer and wash buffer (lysis buffer containing 20 mM imidazole), the bound protein was eluted as 1 ml fractions in elution buffer (lysis buffer containing 150 mM imidazole). Fractions containing M489/N620 or M402/N620 complex were pooled and dialyzed twice for one hour each time at 4 °C against a buffer containing 25 mM Na-HEPES, pH 8, 100 mM NaCl, 10% glycerol, and 1 mM DTT. A slight precipitation in the protein solution was observed during dialysis and it was removed by filtration. The filtered protein was then purified on a 7.85 ml Mono Q column (Pharmacia) pre-equilibrated with QA buffer (dialysis buffer). The complex elutes at an approximate ionic

strength of 200 mM NaCl in a 60 ml gradient of 0-60% QB buffer (QA buffer containing 1M NaCl) at a flow rate of 2 ml/min. The 1 ml fractions containing the protein complex were pooled and concentrated using a 50 kDa MWCO centricon (Millipore). The last purification step was gel filtration chromatography. The concentrated protein sample from the Mono Q purification step was filtered and loaded onto tandem Superdex 200 HR 10/30 columns (Pharmacia) pre-equilibrated with QA buffer at a flow rate of 0.3 ml/min. The protein complexes elute at 24-25.5 ml of buffer QA with an approximate molecular weight of 200 kDa as a higher order complex (the expected molecular weight of a 1:1 complex is ~72 kDa). A 12% gel was used to monitor the purity of protein at various stages of purification. The pooled protein fractions (75-80% pure) were concentrated to about 5 mg/ml with an estimated recovery of about 85%.

The protein complex (M489/N620) was functional in endonuclease assays using a hairpin DNA oligo as a substrate:

5’ CATCCATGCCTACCTGAGTACCAGTAG

3’CAGCTAGACCGTAGGTACGGATGGACTCATGGTCATC

Determine the Atomic Structure of human Mre11 (M/R/N) Complex

To gain further insight into the functioning of the human Mre11 complex, Mre11/Nbs1 complexes (from 1) were co-expressed in High Five cells along with deletion mutant(s) of Rad50. Active Rad50 mutants that also bind the wild-type Mre11/Nbs1 complex were picked. The complex was purified similarly to the purification of M/N constructs from High Five insect cells. The expression was poor and the protein complexes could not be purified to homogeneous levels. Several other combinations of various constructs of the three proteins were tested in High Five and sf21

cells but the levels of protein expression were low. Some of the combinations tested were:

- M489/N620/Rad50Δcc2 (mutant containing two copies of the seven amino acid insertion)
- M402/N620/ Rad50Δcc2
- His_6-human Mre11 (R633stop)/Nbs1/Rad50
- Mre11/Nbs1/ Rad50Δcc4 (contains four copies of the seven amino acid insertion)
- Mre11 (ATLD)/Rad50
- Human Mre11($ATLD_{1/2}$)/R
- Wt yeast Mre11/Rad50 complex
- Mre11 :221(5) human R633 stop mutant
  296(5) C-ter His tag Δ376-708
- Nbs1 40(2) human wt FLAG-tagged
  328(10)
- Rad50 543(15) Rad50Δcc2
  469 = Rad50Δcc

REFERENCES

1. Takeda, S., et al., *Identification of G protein-coupled receptor genes from the human genome sequence*. FEBS Lett, 2002. **520**(1-3): p. 97-101.
2. Wilson, S. and D. Bergsma, *Orphan G-protein coupled receptors: novel drug targets for the pharmaceutical industry*. Drug Des Discov, 2000. **17**(2): p. 105-14.
3. Ma, P. and R. Zemmel, *Value of novelty?* Nat Rev Drug Discov, 2002. **1**(8): p. 571-2.
4. Wise, A., K. Gearing, and S. Rees, *Target validation of G-protein coupled receptors*. Drug Discov Today, 2002. **7**(4): p. 235-46.
5. Hargrave, P.A., et al., *The structure of bovine rhodopsin*. Biophys Struct Mech, 1983. **9**(4): p. 235-44.
6. Ovchinnikov Yu, A., N.G. Abdulaev, and N.N. Modyanov, *Structural basis of proton-translocating protein function.* Annu Rev Biophys Bioeng, 1982. **11**: p. 445-63.
7. Okada, T., et al., *X-Ray diffraction analysis of three-dimensional crystals of bovine rhodopsin obtained from mixed micelles*. J Struct Biol, 2000. **130**(1): p. 73-80.
8. Salom, D., et al., *Crystal structure of a photoactivated deprotonated intermediate of rhodopsin*. Proc Natl Acad Sci U S A, 2006. **103**(44): p. 16123-8.
9. Palczewski, K., et al., *Crystal structure of rhodopsin: A G protein-coupled receptor*. Science, 2000. **289**(5480): p. 739-45.
10. Kuhn, H., et al., *Interactions between photoexcited rhodopsin and GTP-binding protein: kinetic and stoichiometric analyses from light-scattering changes*. Proc Natl Acad Sci U S A, 1981. **78**(11): p. 6873-7.
11. Gazi, L., J.F. Lopez-Gimenez, and P.G. Strange, *Formation of oligomers by G protein-coupled receptors*. Curr Opin Drug Discov Devel, 2002. **5**(5): p. 756-63.
12. Angers, S., A. Salahpour, and M. Bouvier, *Dimerization: an emerging concept for G protein-coupled receptor ontogeny and function.* Annu Rev Pharmacol Toxicol, 2002. **42**: p. 409-35.
13. Liang, Y., et al., *Organization of the G protein-coupled receptors rhodopsin and opsin in native membranes*. J Biol Chem, 2003. **278**(24): p. 21655-62.
14. Park, P.S., et al., *Oligomerization of G protein-coupled receptors: past, present, and future*. Biochemistry, 2004. **43**(50): p. 15643-56.
15. Guo, W., et al., *Crosstalk in G protein-coupled receptors: changes at the transmembrane homodimer interface determine activation*. Proc Natl Acad Sci U S A, 2005. **102**(48): p. 17495-500.
16. Park, P.S. and J.W. Wells, *Oligomeric potential of the M2 muscarinic cholinergic receptor*. J Neurochem, 2004. **90**(3): p. 537-48.
17. Kuhn, H. and W.J. Dreyer, *Light dependent phosphorylation of rhodopsin by ATP*. FEBS Letters, 1972. **20**(1): p. 1-6.

18. Kuhn, H., J.H. Cook, and W.J. Dreyer, *Phosphorylation of rhodopsin in bovine photoreceptor membranes. A dark reaction after illumination*. Biochemistry, 1973. **12**(13): p. 2495-502.
19. Miller, J.A. and R. Paulsen, *Phosphorylation and dephosphorylation of frog rod outer segment membranes as part of the visual process*. J Biol Chem, 1975. **250**(12): p. 4427-32.
20. Frank, R.N. and R.E. Bensinger, *Proceedings: Rhodopsin and light-sensitive kinase activity of retinal outer segments*. Exp Eye Res, 1974. **18**(3): p. 271-80.
21. Weller, M., N. Virmaux, and P. Mandel, *Light-stimulated phosphorylation of rhodopsin in the retina: the presence of a protein kinase that is specific for photobleached rhodopsin*. Proc Natl Acad Sci U S A, 1975. **72**(1): p. 381-5.
22. Frank, R.N. and S.M. Buzney, *Mechanism and specificity of rhodopsin phosphorylation*. Biochemistry, 1975. **14**(23): p. 5110-7.
23. Lorenz, W., et al., *The receptor kinase family: primary structure of rhodopsin kinase reveals similarities to the beta-adrenergic receptor kinase*. Proc Natl Acad Sci U S A, 1991. **88**(19): p. 8715-9.
24. Zhao, X., et al., *Molecular forms of human rhodopsin kinase (GRK1)*. J Biol Chem, 1998. **273**(9): p. 5124-31.
25. Buczylko, J., C. Gutmann, and K. Palczewski, *Regulation of rhodopsin kinase by autophosphorylation*. Proc Natl Acad Sci U S A, 1991. **88**(6): p. 2568-72.
26. Palczewski, K., J.H. McDowell, and P.A. Hargrave, *Purification and characterization of rhodopsin kinase*. J Biol Chem, 1988. **263**(28): p. 14067-73.
27. Bruel, C., et al., *Rhodopsin kinase: expression in mammalian cells and a two-step purification*. Proc Natl Acad Sci U S A, 2000. **97**(7): p. 3004-9.
28. Cha, K., et al., *Rhodopsin kinase: expression in baculovirus-infected insect cells, and characterization of post-translational modifications*. Proc Natl Acad Sci U S A, 1997. **94**(20): p. 10577-82.
29. Chen, C.K. and J.B. Hurley, *Purification of rhodopsin kinase by recoverin affinity chromatography*. Methods Enzymol, 2000. **315**: p. 404-10.
30. Chen, C.K., et al., *Ca(2+)-dependent interaction of recoverin with rhodopsin kinase*. J Biol Chem, 1995. **270**(30): p. 18060-6.
31. Okada, D. and A. Ikai, *Purification method of bovine rhodopsin kinase using regeneration of rhodopsin*. Anal Biochem, 1988. **169**(2): p. 428-31.
32. Shichi, H. and R.L. Somers, *Light-dependent phosphorylation of rhodopsin. Purification and properties of rhodopsin kinase*. J Biol Chem, 1978. **253**(19): p. 7040-6.
33. Anant, J.S. and B.K. Fung, *In vivo farnesylation of rat rhodopsin kinase*. Biochem Biophys Res Commun, 1992. **183**(2): p. 468-73.
34. Inglese, J., et al., *Isoprenylation of a protein kinase. Requirement of farnesylation/alpha-carboxyl methylation for full enzymatic activity of rhodopsin kinase*. J Biol Chem, 1992. **267**(3): p. 1422-5.
35. Inglese, J., et al., *Isoprenylation in regulation of signal transduction by G-protein-coupled receptor kinases*. Nature, 1992. **359**(6391): p. 147-50.

36. Zhao, X., et al., *A novel form of rhodopsin kinase from chicken retina and pineal gland*. FEBS Lett, 1999. **454**(1-2): p. 115-21.
37. Lee, R.H., B.M. Brown, and R.N. Lolley, *Autophosphorylation of rhodopsin kinase from retinal rod outer segments*. Biochemistry, 1982. **21**(14): p. 3303-7.
38. Palczewski, K., et al., *Identification of the autophosphorylation sites in rhodopsin kinase*. J Biol Chem, 1992. **267**(26): p. 18991-8.
39. Palczewski, K., et al., *Rhodopsin kinase autophosphorylation. Characterization of site-specific mutations*. J Biol Chem, 1995. **270**(25): p. 15294-8.
40. Brown, N.G., et al., *Mechanistic studies on rhodopsin kinase. Light-dependent phosphorylation of C-terminal peptides of rhodopsin*. Eur J Biochem, 1992. **208**(3): p. 659-67.
41. Kelleher, D.J. and G.L. Johnson, *Characterization of rhodopsin kinase purified from bovine rod outer segments*. J Biol Chem, 1990. **265**(5): p. 2632-9.
42. McCarthy, N.E. and M. Akhtar, *Activation of rhodopsin kinase*. Biochem J, 2002. **363**(Pt 2): p. 359-64.
43. Ohguro, H., et al., *Sequential phosphorylation of rhodopsin at multiple sites*. Biochemistry, 1993. **32**(21): p. 5718-24.
44. Ohguro, H., et al., *Structural and enzymatic aspects of rhodopsin phosphorylation*. J Biol Chem, 1996. **271**(9): p. 5215-24.
45. Palczewski, K., et al., *Identification of the N-terminal region in rhodopsin kinase involved in its interaction with rhodopsin*. J Biol Chem, 1993. **268**(8): p. 6004-13.
46. Pullen, N. and M. Akhtar, *Rhodopsin kinase: studies on the sequence of and the recognition motif for multiphosphorylations*. Biochemistry, 1994. **33**(48): p. 14536-42.
47. Pullen, N., et al., *Cooperativity during multiple phosphorylations catalyzed by rhodopsin kinase: supporting evidence using synthetic phosphopeptides*. Biochemistry, 1993. **32**(15): p. 3958-64.
48. Pulvermuller, A., K. Palczewski, and K.P. Hofmann, *Interaction between photoactivated rhodopsin and its kinase: stability and kinetics of complex formation*. Biochemistry, 1993. **32**(51): p. 14082-8.
49. Yu, Q.M., et al., *The amino terminus with a conserved glutamic acid of G protein-coupled receptor kinases is indispensable for their ability to phosphorylate photoactivated rhodopsin*. J Neurochem, 1999. **73**(3): p. 1222-7.
50. Yu, Q.M., et al., *Carboxyl terminal of rhodopsin kinase is required for the phosphorylation of photo-activated rhodopsin*. Cell Res, 1998. **8**(4): p. 303-10.
51. Zhao, X., K. Palczewski, and H. Ohguro, *Mechanism of rhodopsin phosphorylation*. Biophys Chem, 1995. **56**(1-2): p. 183-8.
52. Palczewski, K., J.H. McDowell, and P.A. Hargrave. *Rhodopsin kinase: substrate specificity and factors that influence activity*. in *Biochemistry*. 1988.
53. Pitcher, J.A., N.J. Freedman, and R.J. Lefkowitz, *G protein-coupled receptor kinases*. Annu Rev Biochem, 1998. **67**: p. 653-92.
54. Khani, S.C., et al., *Characterization and chromosomal localization of the gene for human rhodopsin kinase*. Genomics, 1996. **35**(3): p. 571-6.

55. Zhao, X., et al., *Molecular cloning and localization of rhodopsin kinase in the mammalian pineal*. Vis Neurosci, 1997. **14**(2): p. 225-32.
56. Somers, R.L. and D.C. Klein, *Rhodopsin kinase activity in the mammalian pineal gland and other tissues*. Science, 1984. **226**(4671): p. 182-4.
57. Noble, B., et al., *Development of a yeast bioassay to characterize G protein-coupled receptor kinases. Identification of an NH2-terminal region essential for receptor phosphorylation*. J Biol Chem, 2003. **278**(48): p. 47466-76.
58. Higgins, M.K., D.D. Oprian, and G.F. Schertler, *Recoverin binds exclusively to an amphipathic peptide at the N terminus of rhodopsin kinase, inhibiting rhodopsin phosphorylation without affecting catalytic activity of the kinase*. J Biol Chem, 2006. **281**(28): p. 19426-32.
59. Tesmer, J.J., et al., *Structure of RGS4 bound to AlF4--activated G(i alpha1): stabilization of the transition state for GTP hydrolysis*. Cell, 1997. **89**(2): p. 251-61.
60. Lodowski, D.T., et al., *Keeping G proteins at bay: a complex between G protein-coupled receptor kinase 2 and Gbetagamma*. Science, 2003. **300**(5623): p. 1256-62.
61. Tesmer, V.M., et al., *Snapshot of activated G proteins at the membrane: the Galphaq-GRK2-Gbetagamma complex*. Science, 2005. **310**(5754): p. 1686-90.
62. Spink, K.E., P. Polakis, and W.I. Weis, *Structural basis of the Axin-adenomatous polyposis coli interaction*. Embo J, 2000. **19**(10): p. 2270-9.
63. Lodowski, D.T., et al., *The structure of G protein-coupled receptor kinase (GRK)-6 defines a second lineage of GRKs*. J Biol Chem, 2006. **281**(24): p. 16785-93.
64. Kannan, N., et al., *The hallmark of AGC kinase functional divergence is its C-terminal tail, a cis-acting regulatory module*. Proc Natl Acad Sci U S A, 2007. **104**(4): p. 1272-7.
65. Cenni, V., et al., *Regulation of novel protein kinase C epsilon by phosphorylation*. Biochem J, 2002. **363**(Pt 3): p. 537-45.
66. Newton, A.C., *Regulation of the ABC kinases by phosphorylation: protein kinase C as a paradigm*. Biochem J, 2003. **370**(Pt 2): p. 361-71.
67. Yokoyama, S.Y., R., *Comparative molecular biology of visual pigments*. Handbook of Biological Physics: Molecular Mechanisms in Visual Transduction. Vol. 3. 2000: D.G. Stavenga, W.J. deGrip, E.N.l Pugh, Jr., Eds. 257-296.
68. Bownds, D., et al., *Characterization and analysis of frog photoreceptor membranes*. J Gen Physiol, 1971. **58**(3): p. 225-37.
69. Leskov, I.B., et al., *The gain of rod phototransduction: reconciliation of biochemical and electrophysiological measurements*. Neuron, 2000. **27**(3): p. 525-37.
70. Sachs, K., D. Maretzki, and K.P. Hofmann, *Assays for activation of opsin by all-trans-retinal*. Methods Enzymol, 2000. **315**: p. 238-51.
71. Vishnivetskiy, S.A., et al., *An additional phosphate-binding element in arrestin molecule. Implications for the mechanism of arrestin activation*. J Biol Chem, 2000. **275**(52): p. 41049-57.

72. Doan, T., et al., *Multiple phosphorylation sites confer reproducibility of the rod's single-photon responses*. Science, 2006. **313**(5786): p. 530-3.
73. Xue, L., et al., *A palmitoylation switch mechanism in the regulation of the visual cycle*. Cell, 2004. **117**(6): p. 761-71.
74. Burns, M.E. and V.Y. Arshavsky, *Beyond counting photons: trials and trends in vertebrate visual transduction*. Neuron, 2005. **48**(3): p. 387-401.
75. Krispel, C.M., et al., *RGS expression rate-limits recovery of rod photoresponses*. Neuron, 2006. **51**(4): p. 409-16.
76. Palczewski, K., et al., *Mechanism of rhodopsin kinase activation*. J Biol Chem, 1991. **266**(20): p. 12949-55.
77. Fowles, C., Sharma, R. and Akhtar, M., *Mechanistic studies on the phosphorylation of photoexcited rhodopsin*. FEBS Letters, 1988. **238**(1): p. 56-60.
78. Shi, G.W., et al., *Light causes phosphorylation of nonactivated visual pigments in intact mouse rod photoreceptor cells*. J Biol Chem, 2005. **280**(50): p. 41184-91.
79. Shi, W., et al., *Rhodopsin mutants discriminate sites important for the activation of rhodopsin kinase and Gt*. J Biol Chem, 1995. **270**(5): p. 2112-9.
80. Gan, X., et al., *Involvement of the C-terminal proline-rich motif of G protein-coupled receptor kinases in recognition of activated rhodopsin*. J Biol Chem, 2004. **279**(48): p. 49741-6.
81. Horner, T.J., et al., *Phosphorylation of GRK1 and GRK7 by cAMP-dependent protein kinase attenuates their enzymatic activities*. J Biol Chem, 2005. **280**(31): p. 28241-50.
82. Satpaev, D.K., et al., *Autophosphorylation and ADP regulate the Ca2+-dependent interaction of recoverin with rhodopsin kinase*. Biochemistry, 1998. **37**(28): p. 10256-62.
83. Chen, C.K., et al., *Abnormal photoresponses and light-induced apoptosis in rods lacking rhodopsin kinase*. Proc Natl Acad Sci U S A, 1999. **96**(7): p. 3718-22.
84. Yamamoto, S., et al. *Defects in the rhodopsin kinase gene in the Oguchi form of stationary night blindness*. in *Nat Genet*. 1997.
85. Zhang, Q., et al., *A variant form of Oguchi disease mapped to 13q34 associated with partial deletion of GRK1 gene*. Mol Vis, 2005. **11**: p. 977-85.
86. Hayashi, T., et al., *A novel homozygous GRK1 mutation (P391H) in 2 siblings with Oguchi disease with markedly reduced cone responses*. Ophthalmology, 2007. **114**(1): p. 134-41.
87. Benovic, J.L., et al., *Purification and characterization of the beta-adrenergic receptor kinase*. J Biol Chem, 1987. **262**(19): p. 9026-32.
88. Pronin, A.N., R.P. Loudon, and J.L. Benovic, *Characterization of G protein-coupled receptor kinases*. Methods Enzymol, 2002. **343**: p. 547-59.
89. Chervenka, C.H., *A Manual of Methods for the Analytical Ultracentrifuge*. 1969: Palo Alto; Spinco Divison of Beckamn Instruments. 100 pp.
90. Otwinowski, Z.a.M., W., *Processing of X-ray diffraction data collexted in oscillation mode*. 1997, New York Academic Press.

91. Collaborative, *The CCP4i suite:programs for protein crystallography*. Acta Crystallographica Section D, 1994. **50**(5): p. 760-763.
92. Matthews, B.W., *Solvent content of protein crystals*. J Mol Biol, 1968. **33**(2): p. 491-497.
93. Jones, T.A., Zou, J. Y. , *Improved methods for building protein models in electron density maps and the location of error in these models*. Acta Crystallographica Section A, 1991. **2**(2): p. 195-197.
94. Sitaramayya, A., et al., *Contribution of the guanosinetriphosphatase activity of G-protein to termination of light-activated guanosine cyclic 3',5'-phosphate hydrolysis in retinal rod outer segments*. Biochemistry, 1988. **27**(13): p. 4880-7.
95. Sicheri, F., I. Moarefi, and J. Kuriyan, *Crystal structure of the Src family tyrosine kinase Hck*. Nature, 1997. **385**(6617): p. 602-9.
96. Madhusudan, et al., *Crystal structure of a transition state mimic of the catalytic subunit of cAMP-dependent protein kinase*. Nat Struct Biol, 2002. **9**(4): p. 273-7.
97. Lodowski, D.T., et al., *Purification, crystallization and preliminary X-ray diffraction studies of a complex between G protein-coupled receptor kinase 2 and Gbeta1gamma2*. Acta Crystallogr D Biol Crystallogr, 2003. **59**(Pt 5): p. 936-9.
98. Zheng, J., et al., *Crystal structures of the myristylated catalytic subunit of cAMP-dependent protein kinase reveal open and closed conformations*. Protein Sci, 1993. **2**(10): p. 1559-73.
99. Zheng, J., et al., *Crystal structure of the catalytic subunit of cAMP-dependent protein kinase complexed with MgATP and peptide inhibitor*. Biochemistry, 1993. **32**(9): p. 2154-61.
100. Nowakowski, J., et al., *Structures of the cancer-related Aurora-A, FAK, and EphA2 protein kinases from nanovolume crystallography*. Structure, 2002. **10**(12): p. 1659-67.
101. Akamine, P., et al., *Dynamic features of cAMP-dependent protein kinase revealed by apoenzyme crystal structure*. J Mol Biol, 2003. **327**(1): p. 159-71.
102. Palczewski, K., et al., *Substrate recognition determinants for rhodopsin kinase: studies with synthetic peptides, polyanions, and polycations*. Biochemistry, 1989. **28**(22): p. 8764-70.
103. Onorato, J.J., et al., *Role of acidic amino acids in peptide substrates of the beta-adrenergic receptor kinase and rhodopsin kinase*. Biochemistry, 1991. **30**(21): p. 5118-25.
104. Batkin, M., I. Schvartz, and S. Shaltiel, *Snapping of the carboxyl terminal tail of the catalytic subunit of PKA onto its core: characterization of the sites by mutagenesis*. Biochemistry, 2000. **39**(18): p. 5366-73.
105. Jastrzebska, B., et al., *Functional characterization of rhodopsin monomers and dimers in detergents*. J Biol Chem, 2004. **279**(52): p. 54663-75.
106. Flaherty, K.M., et al., *Three-dimensional structure of recoverin, a calcium sensor in vision*. Cell, 1993. **75**(4): p. 709-16.
107. Erickson, M.A., et al., *The effect of recombinant recoverin on the photoresponse of truncated rod photoreceptors*. Proc Natl Acad Sci U S A, 1998. **95**(11): p. 6474-9.

108. Klenchin, V.A., P.D. Calvert, and M.D. Bownds, *Inhibition of rhodopsin kinase by recoverin. Further evidence for a negative feedback system in phototransduction*. J Biol Chem, 1995. **270**(27): p. 16147-52.
109. Levay, K., et al., *Localization of the sites for Ca2+-binding proteins on G protein-coupled receptor kinases*. Biochemistry, 1998. **37**(39): p. 13650-9.
110. Otto-Bruc, A.E., et al., *Phosphorylation of photolyzed rhodopsin is calcium-insensitive in retina permeabilized by alpha-toxin*. Proc Natl Acad Sci U S A, 1998. **95**(25): p. 15014-9.
111. Hurley, J., Spencer, M., Nieme, G.A., and Chen, J., *Effects of calcium and recoverinn on rod photoreceptor function in intact retinas*. Invest Ophthalmol Visual Sci, 1999. **40**(S214).
112. Sampath, A.P., et al., *Recoverin improves rod-mediated vision by enhancing signal transmission in the mouse retina*. Neuron, 2005. **46**(3): p. 413-20.
113. Pronin, A.N., et al., *Regulation of G protein-coupled receptor kinases by calmodulin and localization of the calmodulin binding domain*. J Biol Chem, 1997. **272**(29): p. 18273-80.
114. Ray, S., et al., *Cloning, expression, and crystallization of recoverin, a calcium sensor in vision*. Proc Natl Acad Sci U S A, 1992. **89**(13): p. 5705-9.
115. Sallese, M., et al., *Regulation of G protein-coupled receptor kinase subtypes by calcium sensor proteins*. Biochim Biophys Acta, 2000. **1498**(2-3): p. 112-21.
116. Carman, C.V., et al., *Selective regulation of Galpha(q/11) by an RGS domain in the G protein-coupled receptor kinase, GRK2*. J Biol Chem, 1999. **274**(48): p. 34483-92.
117. Usui, H., et al., *RGS domain in the amino-terminus of G protein-coupled receptor kinase 2 inhibits Gq-mediated signaling*. Int J Mol Med, 2000. **5**(4): p. 335-40.
118. Sallese, M., et al., *Selective regulation of Gq signaling by G protein-coupled receptor kinase 2: direct interaction of kinase N terminus with activated galphaq*. Mol Pharmacol, 2000. **57**(4): p. 826-31.
119. Kozasa, T., et al., *Purification and characterization of recombinant G16 alpha from Sf9 cells: activation of purified phospholipase C isozymes by G-protein alpha subunits*. Proc Natl Acad Sci U S A, 1993. **90**(19): p. 9176-80.
120. Kozasa, T., *Purification of recombinant G protein alpha and beta gamma subunits from Sf9 cells*. G proteins: Techniques of Analysis, ed. D.R. Manning. 1999, Boca Raton, FL: CRC Press LLC 23-37.
121. Yang, J., et al., *Crystal structure of an activated Akt/protein kinase B ternary complex with GSK3-peptide and AMP-PNP*. Nat Struct Biol, 2002. **9**(12): p. 940-4.
122. Binder, B.M., M.S. Biernbaum, and M.D. Bownds, *Light activation of one rhodopsin molecule causes the phosphorylation of hundreds of others. A reaction observed in electropermeabilized frog rod outer segments exposed to dim illumination*. J Biol Chem, 1990. **265**(25): p. 15333-40.
123. Shi, G.W., et al., *Light causes phosphorylation of nonactivated visual pigments in intact mouse rod photoreceptor cells*. J Biol Chem, 2005. **280**(50): p. 41184-91.

124. Huber, S., *Phosphorylation of Metabolic Enzymes: Effects on Activity, Localization and Degradation*. Molecular and Cellular Proteomics, 2003. **679**(2).
125. Chen, Z., et al., *Structure of the p115RhoGEF rgRGS domain-Galpha13/i1 chimera complex suggests convergent evolution of a GTPase activator*. Nat Struct Mol Biol, 2005. **12**(2): p. 191-7.
126. Ames, J.B., et al., *Structural basis for calcium-induced inhibition of rhodopsin kinase by recoverin*. J Biol Chem, 2006. **281**(48): p. 37237-45.
127. Furuse, M., et al., *Distinct roles of two separable in vitro activities of yeast Mre11 in mitotic and meiotic recombination*. EMBO J, 1998. **17**(21): p. 6412-25.

Vita

Puja Singh was born in Karnal, Haryana (India) on December 20, 1979, the daughter of Urmila Singh and Kamla Singh. After completing her work at Kendriya Vidyalaya No. 1, Uppal in Hyderabad, Andhra Pradesh (India), in 1997 she entered Osmania University in Hyderabad. She received the degree of Bachelor of Science from Osmania University in April 2000. In June of 2000, she entered the Department of Biochemistry and received the degree of Master of Science from Osmania University in May 2002. In August of 2002, she entered The Graduate School of the University of Texas at Austin as a student in the molecular biology program.

Permanent address: 25/10 Indira Nagar, Lucknow, UP, India 226016

This dissertation was typed by the author.